UNIVERSIDADE DE BRASÍLIA
INSTITUTO DE GEOCIÊNCIAS

MINERALIZAÇÕES SULFETADAS DE Ni-Cu ASSOCIADAS AOS COMPLEXOS INTRUSIVOS ULTRAMÁFICOS DO LINEAMENTO GUAPORÉ, MATO GROSSO – BRASIL. CARACTERIZAÇÃO DE UMA JANELA EXPLORATÓRIA PARA SULFETOS MAGMÁTICOS NA MARGEM SUDOESTE DO CRATON AMAZÔNICO

Jomar Stabili de Farias

DISSERTAÇÃO DE MESTRADO N° 493

Brasília - DF

2022

UNIVERSIDADE DE BRASÍLIA – UnB

INSTITUTO DE GEOCIÊNCIAS – IG

MINERALIZAÇÕES SULFETADAS DE Ni-Cu ASSOCIADAS AOS COMPLEXOS INTRUSIVOS ULTRAMÁFICOS DO LINEAMENTO GUAPORÉ, MATO GROSSO – BRASIL. CARACTERIZAÇÃO DE UMA JANELA EXPLORATÓRIA PARA SULFETOS MAGMÁTICOS NA MARGEM SUDOESTE DO CRATON AMAZÔNICO

DISSERTAÇÃO DE MESTRADO

Autor: Jomar Stabili de Farias

Orientador: Prof. Dr. Cesar Fonseca Ferreira Filho

Brasília – DF

2022

MINERALIZAÇÕES SULFETADAS DE Ni-Cu ASSOCIADAS AOS COMPLEXOS INTRUSIVOS ULTRAMÁFICOS DO LINEAMENTO GUAPORÉ, MATO GROSSO – BRASIL. CARACTERIZAÇÃO DE UMA JANELA EXPLORATÓRIA PARA SULFETOS MAGMÁTICOS NA MARGEM SUDOESTE DO CRATON AMAZÔNICO

Autor: Jomar Stabili de Farias

Examinadores:

Prof. Prof. Dr. Cesar Fonseca Ferreira Filho (Orientador)

Prof. Dr. Valmir da Silva Souza (UnB)

Prof.ª. Dra. Juliana Charão Marques (UFRGS)

Prof.ª. Dra. Maria Emília Schuteski Della Giustina (Suplente - UnB)

Brasília, 09 de Junho de 2022

FICHA CATALOGRÁFICA

Stabili de Farias, Jomar
Sm MINERALIZAÇÕES SULFETADAS DE Ni-Cu ASSOCIADAS AOS COMPLEXOS INTRUSIVOS ULTRAMÁFICOS DO LINEAMENTO GUAPORÉ, MATO GROSSO - BRASIL. CARACTERIZAÇÃO DE UMA JANELA EXPLORATÓRIA PARA SULFETOS MAGMÁTICOS NA MARGEM SUDOESTE DO CRATON AMAZÔNICO / Jomar Stabili de Farias; orientador César Fonseca Ferreira Filho. -- Brasília, 2022.
76 p.

Dissertação (Mestrado - Mestrado em Geologia) -- Universidade de Brasília, 2022.

1. Discovery History. 2. Geological Setting. 3. Morro Sem Boné and Morro do Leme Intrusions. 4. Constraints for the Parental Magma of the Ultramafic Intrusions. 5. Tectonic Setting and Implications for Exploration. I. Fonseca Ferreira Filho, César, orient. II. Título.

AGRADECIMENTOS

O presente trabalho foi realizado com o apoio da Coordenação de Aperfeiçoamento de Pessoal de Nível Superior – Brasil (CAPES) – Código de Financiamento 001.

Os meus agradecimentos ao Instituto de Geociências tão bem representado por renomados professores, dedicados funcionários, e excelentes laboratórios, no qual tive a oportunidade de desenvolver parte desse trabalho, ao longo deste mestrado.

Dedico a todos os profissionais que passaram pelo Projeto Morro Sem Boné, e que contribuíram direta e indiretamente, para o apoio logístico, numa área remota, mas que tornaram o lugar cada vez mais aprazível, como se fosse a nossa casa. Além disso, durante mais de 25 anos, o Grupo pode desenvolver atividades de considerável risco, sem nenhum dano ambiental ou incidente com pessoas. Parabéns aos mais de 500 colaboradores que deram a sua contribuição ao Projeto e se mantiveram seguro.

Um especial agradecimento ao colega e geólogo José Elvir, parceiro de longas jornadas e de tantas discussões técnicas no Projeto Morro Sem Boné, bem como, aos Técnicos Manoel, Vinicius, Marcos Luz, Lavoisier, Gilvan, dentre outros, que se empenharam para fazer desse projeto um sucesso.

Aos colegas e geólogos de apoio do Escritório Sergio Machado, Giorgio Sartorato, Leonardo Souza, Roque Coelho, Fernando Duarte, Zé Matos, e aos novos contratados que contribuíram de forma positiva para que esse trabalho fosse concretizado, com suas discussões, contribuições e apoio.

Homenageio também o Romero Queiroz, que apoiou esse trabalho, e hoje desfruta de sua merecida aposentadoria. Também ao Gerente de Geologia da Unidade de Negócios da Anglo Geraldo Sarquis, que rimos de quando em vez relembrando sobre como deixamos parte de nossas vidas nas matas dessa Amazônia. Ele reabriu a exploração no Projeto Morro Sem Boné paralisado por mais de 10 anos, e me reinseriu nesse projeto.

Dedico também esse trabalho ao entusiasta Geólogo Vanderlei Farias, parceiro de mais de 4 anos de jornada, e por quem tenho um enorme apreço e admiração. Profissional dedicado e competente, e que me incentivou a reingressar e concluir esse mestrado, e que contribuiu enormemente para o desenvolvimento desse trabalho e do artigo técnico.

Ao meu orientador e Professor Cesar Ferreira, com seu exemplo de determinação, e dedicação, e que soube conduzir os trabalhos desse mestrado e artigo, de forma assertiva e dinâmica. Muito obrigado Professor! Aprendi muito com o senhor!

Aos meus pais, que me conduziram pelos caminhos da vida, me educaram, e me fizeram alcançar meus objetivos profissionais. Muito gratidão por vocês.

E por fim, a minha querida esposa Vanessa Machado, companheira, dedicada, e amiga, presente em todas as horas. Me apoiou quando esmoreci, me impulsionou nas horas mais difíceis, e me deu muita força, no momento mais frágil de minha vida, quando achei que iria perder a batalha pela vida. Ela apareceu em minha vida num encontro casual, e desse casual, se tornou uma realidade, e que se solidifica dia após dia. “Nossos destinos estavam traçados na maternidade”, já dizia o poeta! E assim, vamos conduzindo nossas vidas, com muita maestria, ao lado do nosso felino Pretinho! Muito obrigado meu amor, por você existir! Você é minha luz, minha vida. Te amo!

Ultramafic intrusions hosting Ni–Cu sulfide mineralization along a suture zone in the southwestern margin of the Amazonian craton, Brazil: Examples from Morro Sem Boné, Morro do Leme and their satellite intrusions.

ÍNDICE DE FIGURAS

ÍNDICE DE TABELAS

RESUMO

Este trabalho de pesquisa descreve e aborda várias intrusões ultramáficas de pequeno a médio porte localizadas ao longo do Zona de Sutura do Guaporé de idade Mesoproterozóico na margem sudoeste do Craton Amazônico. Com poucas deformações e esparsas zonas cisalhadas, as rochas ultramáficas exibem minerais ígneos e texturas amplamente preservadas. Paragêneses metamórficas compostas por metapelitos e anfibolitos das rochas encaixantes das intrusivas, bem como de zonas de cisalhamento nas intrusões ultramáficas, são indicativos da fácies anfibolito de metamorfismo regional. Interseções em intervalos de furos de sondagem com sulfetos disseminados a até sulfetos maciços nas rochas encaixantes, consistem principalmente de pirrotita e pirita. As intrusões ultramáficas consistem principalmente em cumulados de olivina com altos teores de MgO (até 45,9%) e Mg# (até 0,84), consistente com a composição de sua olivina mais primitiva (Fo93). A sequência de cristalização, dominada por olivina, ortopiroxênio e cromita, junto com razões e padrões de elementos traços incompatíveis de cumulados ultramáficos, apoiam a interpretação de que eles se originaram de um magma com alto teor de MgO parcialmente contaminado com rochas crustais. Mineralização de sulfetos nas intrusões ultramáficas compreende diferentes estilos de sulfetos magmáticos associados a rochas cumulática, incluindo mineralização do tipo contato, tipo *stratabound* e hospedada em *feeders*. Interseções significativas em furos de sondagem com presença de sulfetos intersticial a *net-textured* consistem em pirrotita, pentlandita e calcopirita, tem variável, mas geralmente baixo conteúdo de Ni-Cu-PGE (Ex.: 20 m@ 0.5% Ni, 0.1%Cu e 0.5 ppm Pt + Pd). A média de teores de Ni, Cu, Pt e Pd, de moderado a muito baixo, são interpretados como resultantes da variável eficiência de equilíbrio dos *xenomelts* de sulfetos, incorporados de rochas encaixantes ricas em sulfetos. As intrusões ultramáficas mineralizadas com Ni-Cu-PGE são interpretadas como pertencentes a uma rede de condutos de magma e câmaras de magma que intrudiram a sequência vulcano-sedimentar rica em sulfetos. Os resultados desta pesquisa indicam a existência de um *belt* com intrusões de alto MgO mineralizadas para Ni-Cu-PGE, localizado na margem sudoeste do Craton Amazônico, com alto potencial exploratório para depósitos magmáticos.

Palavras-Chave: Depósitos de Ni-Cu-PGE; Intrusões Ultramáfica; Dunito; Contaminação Crustal; Mesoproterozóico; Craton Amazônico; Olivina.

ABSTRACT

This research paper describes several medium-to small-sized ultramafic intrusions located along the Mesoproterozoic Guapore Suture Zone in the southwestern margin of the Amazonian craton. Apart from minor sheared zones, ultramafic rocks have igneous minerals and textures largely preserved. Metamorphic parageneses of metapelites and amphibolites of country rocks, as well as those from sheared zones of the ultramafic intrusions, are indicative of the amphibolite facies of regional metamorphism. Intersections of disseminated to massive sulfides consisting mainly of pyrrhotite and pyrite are common in the metamorphosed volcanic and sedimentary country rocks. The ultramafic intrusions consist mainly of olivine cumulates with high MgO contents (up to 45.9 wt.%) and Mg# (up to 0.84), consistent with the composition of their most primitive olivine (Fo93). The crystallization sequence, dominated by olivine, orthopyroxene, and chromite, together with ratios and patterns of incompatible trace elements of ultramafic cumulates, support the interpretation that they originated from a high-MgO magma partially contaminated with crustal rocks. Sulfide mineralization in the ultramafic intrusions comprises different styles of magmatic sulfides associated with cumulate rocks, including contact-type, stratabound-type and conduit hosted mineralization. Significant intersections of interstitial to net-textured sulfides consisting of pyrrhotite, pentlandite and chalcopyrite have variable but generally low Ni–Cu-PGE contents (e.g., ~20 m at 0.5 wt.% Ni, 0.1 wt.% Cu, and 0.5 ppm Pt+ Pd). The range of tenors of Ni, Cu, Pt and Pd, from moderate to very low, is interpreted as resulting from varying efficiency of equilibration of sulfide xenomelts incorporated from the sulfide-bearing country rocks. The Ni–Cu-PGE mineralized ultramafic intrusions are interpreted to belong to a network of magma conduits and staging magma chambers intruding the sulfide-bearing volcanic-sedimentary sequence. Our results indicate an additional prospective belt of high-MgO Ni–Cu-PGE sulfide mineralized intrusions located in a cratonic margin in Brazil.

Keywords: Ni-Cu-PGE deposit; Ultramafic intrusion; Dunite; Crustal contamination; Mesoproterozoic; Amazonian Craton; Olivine.

CONSIDERAÇÕES GERAIS

INTRODUÇÃO

Globalmente as ocorrências de níquel estão distribuídas em depósitos lateríticos (60%) e sulfetados (40%), e as reservas As reservas globais estimadas de atingem aproximadamente 74 milhões de toneladas de metal. O Brasil representa aproximadamente cerca de 16% dessas reservas mundiais de níquel, representado principalmente pelos Estados de Goiás (55,9%), Bahia (31,0 %), Pará (13,1 %).

Historicamente, a maioria dos depósitos de níquel sulfetados foi descoberta durante os trabalhos de prospecção regional, simplesmente pela identificação de gossans, e como exemplo, citam-se os depósitos de Noril'sk/Talnakh, Kambalda, Perserverance, Thompson, Raglan e Voisey's Bay, (Barnes, 2005). Esses depósitos sulfetados de Ni-Cu-PGE são encontrados associados aos complexos máficos e ultramáficos, e com raras exceções, todos eles foram formados a partir de magmas de origem mantélica, e formados pela segregação de um líquido sulfetado imiscível (Naldrett, 2004). Depósitos de Ni-Cu-PGE com reservas > 100.000 toneladas, e teores >0.2 % Ni apresentam uma larga distribuição temporal no mundo segundo Eckstrand et al 2007.

Os depósitos de níquel sulfetado em menor proporção, refletem custos de produção muito inferiores quando comparados aos depósitos lateríticos, entretanto as dificuldades de identificação de um depósito dessa natureza aliado à sua complexidade, como a dependência de um eficiente processo de transporte do líquido magmático pela crosta, e que tenha atuado de forma a reduzir a possibilidade de o elemento níquel ter participado na cristalização das olivinas, aliado a outros fatores importantes na formação dos depósitos sulfetados, representam custos elevados para as empresas de Exploração, e por consequência, algumas desistem e as descobertas desses tipos de depósitos estão cada vez mais raros.

As intrusões Máficas-Ultramáficas de Morro Sem Boné (MSB) e Morro do Leme (MDL) estão localizadas no extremo oeste do Estado do Mato Grosso, estão associadas ao extenso lineamento crustal de mais de 800 quilômetros de comprimento, entre as Províncias Rondônia Juruena (1.82-1.54 Ga) e Sunsás (1.47-1.10 Ga), às margens sudoeste do Craton Amazônico. Esta faixa conhecida como Zona de Sutura Guaporé, com reduzida carga de conhecimento e investigações para ocorrências de mineralizações polimetálicas associadas às MUM do belt, pode se tornar no futuro uma região com robustos investimentos para esse fim, já que reúnem importantes elementos contribuidores para formação desses tipos de depósitos. Esse estudo,

discute as intrusões MUM do MSB e MDL, e seus corpos satélites não aflorantes, e que abrem oportunidades sobre a vasta região de cobertura inconsolidada da região do Guaporé, que tem espessura média de 20 metros, e obscurece a identificação de outras intrusões ou associações com zonas mineralizadas Ni-Cu-PGE, senão por métodos geofísicos, seguido de sondagem. Os trabalhos desenvolvidos pela Anglo American nos anos 90 na região, possibilitou a identificação de depósito de Níquel Laterítico associado aos corpos MSB e MDL, com recursos >60 Mt @ 1.78% Ni, e com potencial para mineralizações associadas a intrusão de Ni-Cu-PGE (reportes interno do Grupo).

LOCALIZAÇÃO E FISIOGRAFIA

A área do depósito e de pesquisa localiza-se no extremo oeste do Estado de Mato Grosso, limite com Estado de Rondônia e fronteira com a Bolívia, na região do Vale do Rio Guaporé, município de Comodoro, distante cerca de 650 km da capital Cuiabá, Figura 001.

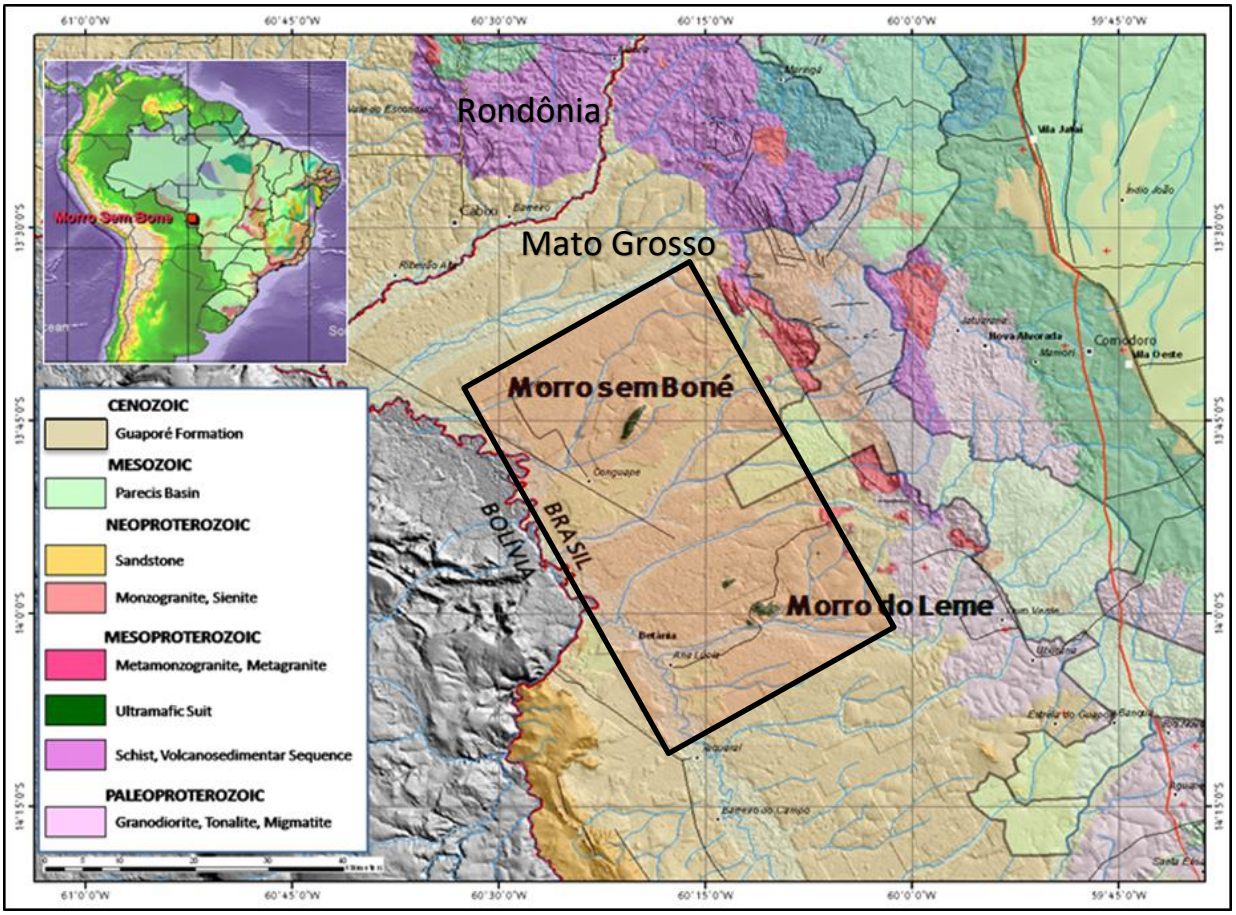

Figura 001 - Mapa de localização da área (retângulo preto) com destaque para os limites entre os Estados e países, e localização dos Morros Sem Boné e Morro do Leme no Mapa Geológico (CPRM, 2008) sobre imagem digital do terreno.

Os depósitos de Níquel Laterítico de Morro Sem Boné e Morro do Leme estão localizados na zona de transição entre o clima Equatorial e o Tropical, com estação seca bem-marcada, entre os meses de junho a setembro e período chuvoso, de outubro a março. A precipitação pluviométrica total anual está em torno de 2.150 mm, com uma média anual de umidade relativa do ar de 80% e temperatura de 24° a 26° C. A vegetação observada é também de transição entre a floresta úmida tropical e o cerrado (savanas), com árvores típicas da primeira, cujos representantes mais comuns são a sumaúma, palmeiras, cedro, peroba, faveiro, cerejeira, mogno e seringueiras, e da segunda, pau-terra, colher de vaqueiro, faveiro, lixeira, piqui e timbó. Os principais cursos d'água que drenam a região são os afluentes da margem direita da bacia hidrográfica do Rio Guaporé.

JUSTIFICATIVAS E OBJETIVO

As intrusões Máficas-Ultramáficas de Morro Sem Boné (MSB) e Morro do Leme (MDL) estão localizadas no extremo oeste do Estado do Mato Grosso, sendo associadas ao extenso lineamento crustal de mais de 800 quilômetros de extensão, entre as Províncias Rondônia Juruena (1.82-1.54 Ga) e Sunsás (1.47-1.10 Ga), às margens sudoeste do Craton Amazônico. Esta faixa conhecida como Zona de Sutura Guaporé, com reduzida carga de conhecimento e pouca exploração mineral para mineralizações polimetálicas associadas às MUM do belt, pode se tornar muito em breve, uma região bastante disputa pelas empresas de exploração mineral, já que reúne importantes elementos para formação desses tipos de depósitos, mas que, desafortunadamente, está obscurecida pela Formação Guaporé.

Esse trabalho, discute os Complexos máficos-ultramáficos conhecidos como Morro Sem Boné e Morro do Leme, seus corpos satélites, não aflorantes, identificados através de atividades de exploração mineral, por métodos geofísicos terrestres e aéreos, e sondagem. Essas intrusões MUM são bem definidas pela geofísica através de anomalias magnéticas, mascaradas sob a Formação Guaporé, uma faixa de sedimentos inconsolidados de espessura média de 20 metros, que cobre tanto as intrusões como todas as litologias encaixantes, numa superfície plana que se estende por centenas de quilômetros, conhecida como Faixa Guaporé. Essas anomalias magnéticas podem estar associadas a corpos intrusivos MUM com de Ni Laterítico de alto teor, e outros sugestivos para conter mineralizações sulfetadas de Ni-Cu-PGE, como é o caso que será discutido nesse trabalho, abrindo enorme potencial, e oportunidades para o imenso belt.

Os trabalhos desenvolvidos pela Anglo American nos anos 90 na região, possibilitou a identificação de depósito de Níquel Laterítico associado aos corpos MSB e MDL, com recursos >60 Mt @ 1.75% Ni, e com potencial para mineralizações associadas a intrusão de Ni-Cu-PGE (reportes interno do Grupo).

Este trabalho de pesquisa objetiva descrever, classificar e correlacionar as várias intrusões ultramáficas de médio a pequeno porte localizadas na margem Sudoeste do Craton Amazônico, na conhecida zona de sutura do Guaporé, divisa Brasil-Bolívia, buscando atrair investimentos para exploração de Ni-Cu-PGE e Níquel Laterítico, numa região considerada oportuna e desafiadora, e com enorme espaço para enriquecimento de conhecimentos geológicos. As rochas ultramáficas que compõem essas intrusões são caracterizadas pela preservação de texturas magmáticas, e minerais ígneos dominados por olivina, ortopiroxênio e cromita. Interseções significativas em furos de sondagem diamantada apontaram sulfetação intersticial de sulfetos consistindo em pirrotita, pentlandita e calcopirita. As mineralizações de Ni-Cu-PGE associados a sulfetos em corpos ultramáficos intrusivos pode compreender diferentes estilos: mineralização de contato com a country rock, tipo *stratabound*, tipo contato, e *feeder*. As rochas encaixantes das intrusões são principalmente metapelitos, metarcósios, anfibolitos, entre outras, todas com uma paragênese de metamorfismo regional fácies anfibolito, com sulfetação disseminada a massiva constituída por pirrotita e pirita.

METODOLOGIA

A caracterização geológica das intrusões ultramáficas vem sendo apoiada por dados do programa de exploração realizado pela Anglo American, incluindo projetos de mapeamento geológico, geoquímico e levantamentos geofísicos e sondagens diamantada profunda. Todos os dados geológicos, geofísicos e geoquímicos estão suportando o entendimento deste estudo. Os dados geoquímicos relatados neste estudo são derivados de análises químicas comerciais do banco de dados da Anglo American, baseado na análise multi-elementar dos testemunhos de sondagem de vários furos de sondagem diamantada do programa de exploração, em amostragem em intervalos contínuos de 1 metro, sempre respeitando os contatos litológicos. As análises químicas para a primeira fase do programa de exploração foram realizadas pela ACME Analytical Laboratories Ltd. em Vancouver e, para a segunda fase, pela ALS Chemex Ltd. em Toronto. Uma descrição completa dos métodos analíticos está disponível na página inicial da ACME Labs (www.acmelab.com) e na ALS Home Page da ALS Chemex (www.alsglobal.com).

Análises de elementos selecionados de furos (FD-01, 2A, 06, 11, 12, 14, 15, 17, 19, 22, 25 e FD-26) da primeira fase e reanálise parcial dos furos (FD-01, 02,02A, 04, 06 e FD-10) da segunda fase serão relatados neste estudo. O controle de qualidade foi mantido pela rotina de ambos os laboratórios, bem como os procedimentos da Anglo American do banco de dados analítico.

Os métodos usados pela ACME incluíram a preparação da amostra pela ACME código "R200-1000" (esmagar, dividir e pulverizar 1 kg de amostra para 200 malha), seque a 105 ◦C (polpas secas a 105 ◦C antes da análise), codifique"4A & 4B" e "AALitho" (fusão LiBO2 / LiB4O7 e análise por ICP-ES /ICP-MS), código "7TD" (digestão de Ni por ácido 4, análise por ICP-ES), LOI(perda por ignição), código "2A" (total C e S por LECO), código "1F" (1: 1: 1Digestão Aqua Regia; Análise Ultratrace ICP-MS), código "3BMS" (incêndio fusão de ensaio; Au Pt Pd por análise de ICP-MS). Os métodos usados pela ALS Chemex consistiram no "pacote de rocha inteira" (maior, menor e traço elementos), código "PGM-ICP23" (Pt, Pd, Au por ensaio de fogo de 30 g e ICP-MS análise) e código "ME-ICP81" (ICP Fusion - Ore Grade). Estudos petrográficos de 70 seções delgadas polidas foram realizados em Laboratório de Microscopia da Universidade de Brasília, Brasil. Microssonda análises de olivina de 16 amostras selecionadas (128 análises de olivina total) foram realizadas no Instituto de Geociências, Universidade de Brasília (Brasil) em um instrumento Cameca SX-50 totalmente automatizado. As análises dispersivas de comprimento de onda foram realizadas em uma tensão de operação de 15 kV e uma corrente de feixe de 40 nA. A contagem dos tempos foram de 20s para os elementos principais e 60s para o níquel. Padrões usados eram minerais de silicato naturais e óxidos sintéticos. Contagem de fundo o tempo foi definido para metade do tempo de contagem de pico. Os resultados são fornecidos em Material Suplementar Online.

ESCOPO DO ESTUDO

Conforme previsto no regulamento do Curso de Pós-graduação o reingresso na pós-Graduação do Curso de Geologia da Universidade de Brasília tem como parâmetro a apresentação de um artigo submetido e aprovado em revista periódica. Por sugestão do Orientador, esta dissertação de mestrado apresenta-se estruturada na forma deste artigo e foi submetido para publicação em periódico com corpo editorial.

O artigo, intitulado "**Ultramafic intrusions hosting Ni–Cu sulfide mineralization along a suture zone in the southwestern margin of the Amazonian craton, Brazil: Examples from Morro Sem Boné, Morro do Leme and their satellite intrusions**" foi elaborado durante o

ano de 2020, e submetido à revista Journal of South American Earth Science em novembro do mesmo ano, com publicação em fevereiro de 2021.

Este artigo tem como principal objetivo definir a gênese e os controles da mineralização de Ni-Cu-PGE do Morro Sem Boné, Morro do Leme e Corpos Satélites.

REFERÊNCIAS

Barnes, S.J., 1986. The effect of trapped liquid crystallization on cumulus mineral compositions in layered intrusions. Contrib. Mineral. Petrol. 93, 524–531.

Barnes, S.J., Cruden, A.R., Arndt, N., Saumur, B.R., 2016. The mineral system approach applied to magmatic Ni–Cu–PGE sulphide deposits. Ore Geol. Rev. 76, 296–316.

Barnes, S.J., Osborne, G.A., Cook, D., Barnes, L., Maier, W.D., Godel, B., 2011. The Santa Rita nickel sulfide deposit in the Fazenda Mirabela intrusion, Bahia, Brazil: geology, sulfide geochemistry, and genesis. Econ. Geol. 106, 1083–1110.

Barnes, S.J., Robertson, J.C., 2019. Time scales and length scales in magma flow pathways and the origin of magmatic Ni–Cu–PGE ore deposits. Geoscience Frontiers 10 (1), 77–87.

Barnes, S.-J., Lightfoot, P.C., 2005. Formation of magmatic nickel-sulfide ore deposits and processes affecting their copper and platinum-group element contents. In: Hedenquist, J.W., Thompson, J.F.H., Goldfarb, R.J., Richards, J.P. (Eds.), Economic Geology 100th Anniversary, ume, pp. 179–213.

Ferreira Filho, C.F., Nilson, A.A., Naldrett, A.J., 1992. The Niquelandia Mafic–Ultramafic Complex, Goias, Brazil: a contribution to the ophiolite X stratiform controversy based on new geological and structural data. Precambrian Res. 59, 125–143.

Ferreira Filho, C.F., Pimentel, M.M., Araujo, S.M., Laux, J.H., 2010. Layered intrusions and volcanic sequences in Central Brazil: geological and geochronological constraints for Mesoproterozoic (1.25 Ga) and Neoproterozoic (0.79 Ga) igneous associations. Precambrian Res. 183, 617–634.

Latypov, R.M., 2003. The origin of basic-ultrabasic sills with S-, D-, and I-shaped compositional profiles by in situ crystallization of a single input of phenocrystpoor parental magma. J. Petrol. 44 (9), 1619–1656.

Layton-Matthews, D., Lesher, C.M., Burnham, O.M., Hulbert, L., Peck, D.C., Golightly, J. P., et al., 2010. In: Exploration for Komatiite-Associated Ni–Cu–(PGE) Mineralization in the Thompson Nickel Belt, Manitoba, vol. 15. Special Publication Society of Economic Geologists (U.S.), pp. 513–538.

Lesher, C.M., 2007. In: Ni-Cu-(PGE) Deposits in the Raglan Area, Cape Smith Belt, New Qu´ebec, vol. 5. Geological Survey of Canada and Mineral Deposits Division of the Geological Association of Canada, Special Publication, pp. 351–386.

Lesher, C.M., 2017. Roles of residues/skarns, xenoliths, xenocrysts, xenomelts, and xenovolatiles in the genesis, transport, and localisation of magmatic Fe-Ni-Cu-PGE sulfides and chromite. Ore Geol. Rev. 90, 465–484.

Lesher, C.M., 2019. Up, down, or sideways: emplacement of magmatic Fe–Ni–Cu–PGE sulfide melts in large igneous provinces. Can. J. Earth Sci. 56, 756–773.

Lesher, C.M., Barnes, S.J., 2008. Komatiite-associated Ni-Cu-PGE deposits. In: Arndt, N. T. (Ed.), Komatiite: Cambridge. Cambridge University Press, pp. 295–327.

Lesher, C.M., Campbell, I.H., 1993. Geochemical and fluid dynamic modeling of compositional variations in Archean komatiite-hosted nickel sulfide ores in Western Australia. Econ. Geol. 88, 804–816.

Mansur, E.T., Ferreira Filho, C.F., 2016. Magmatic structure and geochemistry of the Luanga Mafic-Ultramafic Complex: further constraints for the PGE-mineralized magmatism in Caraj´as, Brazil. Lithos 266, 28–43.

Mansur, E.T., Ferreira Filho, C.F., Oliveira, D.P.L., 2020. The Luanga deposit, Carajas Mineral Province, Brazil: different styles of PGE mineralization hosted in a medium size layered intrusion. Ore Geol. Rev. 118 https://doi.org/10.1016/j. oregeorev.2020.103340.

Marques, J.C., Ferreira Filho, C.F., 2003. The chromite deposits of the ipueira-medrado sill, Bahia, Brazil. Econ. Geol. 98, 87–108.

Matos, V.B.M., Ferreira Filho, C.F., 2018. The Caboclo dos Mangueiros deposit: Ni-Cu sulfide mineralization hosted by an ultramafic intrusion in the northern edge of the Sao Francisco craton, Brazil. Econ. Geol. 113, 1525–1552.

Matos, R., Teixeira, W., Geraldes, M.C., Bettencourt, J.S., 2009. Geochemistry Li, C.S., Zhang, M.J., Fu, P., Qian, Z., Hu, P.Q., Ripley, E.M., 2012. The Kalatongke magmatic Ni-Cu deposits in the Central Asian orogenic belt, NW China: product of slab window magmatism? Miner. Deposita 47, 51–67.

Maier, W.D., Groves, D.I., 2011. Temporal and spatial controls Begg, G.C., Hronsky, J.A.M., Arndt, N.T., Griffin, W.L., O'Reilly, S.Y., Hayward, N., 2010.Lithospheric, cratonic and geodynamic setting of Ni–Cu–PGE sulfide deposits. Econ. Geol. 105, 1057–1070.

Mota-e-Silva, J., Ferreira Filho, C.F., Della Giustina, M.E.S., 2013. The Limoeiro deposit: Ni–Cu–PGE sulfide mineralization hosted within an ultramafic tubular magma conduit in the Borborema Province: Northeast Brazil. Econ. Geol. 108, 1753–1771.

Mota-e-Silva, J., Prichard, H.M., Ferreira Filho, C.F., Fisher, P.C., McDonald, I., 2015. Platinum-group minerals in the Limoeiro Ni–Cu–(PGE) sulfide deposit, Brazil: the effect of magmatic and upper amphibolite to granulite metamorphic processes on PGM formation. Miner. Deposita 50 (8), 1007–1029.

Naldrett, A.J., 2004. Magmatic Sulphide Deposits: Geology, Geochemistry and Exploration. Springer-Verlag, Berlin, p. 728.

Rizzotto, G.J., Hartmann, L.A., 2012. Geological and geochemical evolution of the Trincheira Complex, a Mesoproterozoic ophiolite in the southwestern Amazon craton, Brazil. Lithos 148, 277–295.

Rizzotto, G.J., Santos, J.O.S., Hartmann, L.A., Tohver, E., Pimentel, M.M., McNaughton, N.J., 2013. The Mesoproterozoic Guapore suture in the SW Amazonian Craton: geotectonic implications based on field geology, zircon geochronology and Nd-Sr isotope geochemistry. J. S. Am. Earth Sci. 48, 271–295.

Paper published at the Journal of South American Earth Sciences

https://doi.org/10.1016/j.jsames.2021.103240

Received 7 November 2020; Received in revised form 12 February 2021; Accepted 16 February 2021

Available online 22 February 2021

Ultramafic intrusions hosting Ni–Cu sulfide mineralization along a suture zone in the southwestern margin of the Amazonian craton, Brazil: Examples from Morro Sem Boné, Morro do Leme and their satellite intrusions.

Jomar Stabili de Farias a, b, Cesar Fonseca Ferreira Filho a, *

a *Instituto de Geociências, Universidade de Brasília-UnB, Brasília, DF, 70910-900, Brazil*

* Corresponding author. *E-mail address:* cesarf@unb.br (C.F. Ferreira Filho).

b *Anglo American, Av. Interlândia, 578, Goiânia, GO, 74672-360, Brazil*

ABSTRACT

This research paper describes several medium-to small-sized ultramafic intrusions located along the Mesoproterozoic Guaporé Suture Zone in the southwestern margin of the Amazonian craton. Apart from minor sheared zones, ultramafic rocks have igneous minerals and textures largely preserved. Metamorphic parageneses of metapelites and amphibolites of country rocks, as well as those from sheared zones of the ultramafic intrusions, are indicative of the amphibolite facies of regional metamorphism. Intersections of disseminated to massive sulfides consisting mainly of pyrrhotite and pyrite are common in the metamorphosed volcanic and sedimentary country rocks. The ultramafic intrusions consist mainly of olivine cumulates with high MgO contents (up to 45.9 wt%) and Mg# (up to 0.84), consistent with the composition of their most primitive olivine (Fo93). The crystallization sequence, dominated by olivine, orthopyroxene and chromite, together with ratios and patterns of incompatible trace elements of ultramafic cumulates, support the interpretation that they originated from a high-MgO magma partially contaminated with crustal rocks. Sulfide mineralization in the ultramafic intrusions comprises different styles of magmatic sulfides associated with cumulate rocks, including contact-type, stratabound-type and conduit hosted mineralization. Significant intersections of interstitial to net-textured sulfides

consisting of pyrrhotite, pentlandite and chalcopyrite have variable but generally low Ni–Cu-PGE contents (e.g., ~20 m at 0.5 wt% Ni, 0.1 wt% Cu, and 0.5 ppm Pt+ Pd). The range of tenors of Ni, Cu, Pt and Pd, from moderate to very low, is interpreted as resulting from varying efficiency of equilibration of sulfide xenomelts incorporated from the sulfide-bearing country rocks. The Ni–Cu-PGE mineralized ultramafic intrusions are interpreted to belong to a network of magma conduits and staging magma chambers intruding the sulfide-bearing volcanic-sedimentary sequence. Our results indicate an additional prospective belt of high-MgO Ni–Cu-PGE sulfide mineralized intrusions located in a cratonic margin in Brazil.

Keywords: Ni-Cu-PGE deposit Ultramafic intrusion Dunite Crustal contamination Mesoproterozoic Amazonian craton Olivine

1. Introduction

The tectonic setting has long been accepted as a regional targeting criterion for Ni–Cu-PGE sulfide deposits (e.g., Naldrett and Cabri, 1976), emphasizing analogues with known major mining camps. This led to exploration focused on mafic-ultramafic intrusions associated with continental rifts, following the postulated tectonic setting of the Noril'sk-Talnakh deposits or komatiitic lavas and sills in greenstone belt terrains (e.g., Naldrett, 2004, and references therein). The recognition of the close spatial association of Ni–Cu-PGE sulfide deposits and the margins of ancient Archean cratons (e.g., Begg et al., 2010; Maier and Groves, 2011; Barnes et al., 2016), regardless of the specific tectônic setting, provided a predictive framework for mineral exploration. The "craton margin" model for the formation of magmatic sulfide deposits assumes that the transport of upwelling magmas to the crust occurs through large systems of translithospheric faults in craton margins (Begg et al., 2010). The architecture of the crust in craton margins controls the development of complex conduit systems, providing structures where large volumes of mantle-derived magma may interact with crustal rocks (Barnes et al., 2016). There is a concensus that Ni–Cu-PGE sulfide deposits form by the accumulation of immiscible sulfide liquid from coexisting silicate magmas (e.g., Naldrett, 2004; Barnes et al., 2016). The interaction of mantle-derived magmas with crustal rocks during dynamic emplacement is a key factor leading to the origin of economic Ni–Cu-PGE sulfide deposits (e.g., Naldrett, 2004; Barnes and Lightfoot, 2005; Barnes et al., 2016; Lesher, 2017). Maier and Groves (2011) have noticed that some craton margins are particularly well mineralized (e.g., Superior craton in North

America; Karelia and Kola cratons in Europe; Zimbabwe craton in Africa), while others appear to be unmineralized (e. g., West Africa craton; Amazonian craton in Brazil). Recent studies in Brazil indicate a close association of Ni–Cu-PGE sulfide deposits with craton margins, as illustrated by the Caboclo dos Mangueiros Ni–Cu sulfide deposit in the northern edge of the São Francisco craton (Matos and Ferreira Filho, 2018) and the Luanga PGE-Ni deposit in the eastern margin of the Amazonian Craton (Mansur et al., 2020). These discoveries suggest that under-exploration in remote and poorly exposed crustal margins in Brazil should be considered when their endowment for Ni–Cu-PGE sulfide deposits is compared with those from extensively explored terrains.

Several mafic-ultramafic complexes are located in a Mesoproterozoic paleo-plate boundary in the southwestern margin of the Amazonian craton, known as the Guaporé Suture Zone (e.g., Rizzotto et al., 2013). This ~800 km long arc-shaped suture zone includes ophiolitic mafic-ultramafic bodies obducted during the collision of the paleo-plates in the Mesoproterozoic (Rizzotto and Hartmann, 2012; Rizzotto et al., 2013). Although not investigated in detail in previous studies, the Morro Sem Boné and Morro do Leme intrusions were also considered as part of the ophiolitic sequence (Rizzotto and Hartmann, 2012). Both intrusions are best known for hosting Ni-laterite resources (60.7 Mt at 1.75 wt% Ni, from Guaporé Mineração, 2012, internal report) developed on weathered olivine cumulates. Although the Ni-laterite resources were known since the 1990s, additional exploration was hampered by the remote location of the deposit. Nevertheless, intermittent exploration for Ni–Cu-PGE magmatic deposits carried out in the nickel-laterite mineralized intrusions and associated satellite bodies intersected Ni–Cu-sulfide mineralization.

This paper is the first systematic study of the ultramafic rocks and Ni–Cu-PGE sulfide mineralizations of the Morro Sem Boné, Morro do Leme and satellite intrusions. Geological descriptions supported by exploration data (e.g., drill core, geophysical surveys and whole-rock assay results of drill cores), together with petrographic and geochemical data (whole-rock analyses, olivine compositions), provide constraints for the nature of the ultramafic magmatism, the architecture of intrusions and their relationship with country rocks, and the origin of Ni–Cu-PGE sulfide mineralization. Our results characterize a Ni–Cu-PGE mineralized mafic-ultramafic magmatism in Brazil and add new insights for mineral exploration in a major suture zone at the southwestern margin of the Amazonian Craton.

2. Discovery History

Exploration for nickel was carried out by Anglo American in the Morro do Leme and Morro Sem Boné ultramafic bodies since early 1990's. The first exploration phase in 1992–1993 by Mineração Tanagra LTDA (Anglo American Group), focused on Ni–Cu-PGE sulfide mineralization, included regional mapping and field recognition of the ultramafic rocks. This phase indicated the potential for Ni–Co lateritic deposits over both ultramafic bodies, shifting the main focus of exploration toward supergene deposits. At the end of 1998, a drilling program to evaluate the lateritic deposits resulted in a resource of 49 Mt at 1.78 wt% Ni (Mineração Tanagra LTDA). Although magmatic sulfides were not a priority during this exploration phase, three diamond bore holes targeting Ni–Cu-PGE sulfides drilled in the Morro do Leme body intersected up to 8 m at 0.55 wt% Ni, 0.14% wt.% Cu, 0.79 ppm Pt+ Pd. Exploration for Ni–Cu-PGE sulfides, resumed in 2006–2007 by Guaporé Mineração (Anglo American Group), consisted of detailed geophysical surveys (magnetic, induced polarization and time-domain electromagnetic – Spectrem System) over the Morro Sem Boné, Morro do Leme and surrounding areas. Geophysical results indicated several combined electromagnetic and magnetic anomalies to support a new drilling program for Ni–Cu-PGE sulfide deposits in 2008. The follow-up drilling program returned several intersections of massive to disseminated Ni–Cu-PGE sulfides in both ultramafic bodies and their newly discovered satellites (e.g., 8 m at 0.22 wt% Ni, 1.78 ppm Pt+ Pd; 8 m at 0.46 wt% Ni, 0.37 ppm Pt+ Pd; 5 m at 0.65 wt% Ni and 0.14 wt% Cu). In 2011, magnetic anomalies together with geological re-interpretation of the ultramafic bodies, including satellite bodies, increased the areas with potential to host lateritic resource. Additional drilling in some of these geological-magnetic targets raised the lateritic resources to 60 Mt at 1.78 wt% Ni (Guaporé Mineração) and highlighted the potential for additional resources of nickel laterite in satellite bodies under Quaternary sedimentary cover.

3. Geological Setting

The Morro Sem Boné and Morro do Leme intrusions are located in the southwest margin of the Amazonian Craton at the boundary between the Rondônia-Juruena (1.82–1.54 Ga) and Sunsás Provinces (1.47–1.10 Ga) (Santos et al., 2008) (Fig. 1). The Rondônia Juruena Province is the result of long-lived accretionary orogens. It is composed of three main tectonostratigraphic terranes, known as Juruena, Jamari and Alto Jauru (Santos et al., 2000; Scandolara et al., 2017), as well as the Quatro Cachoeiras and Cachoeirinha orogens, and anorogenic magmatism of ca

1.50–1.53 Ga. (Bettencourt et al., 1999). The Sunsás Province, an allochthonous collisional-type belt (Santos et al., 2008), is the youngest regional event recorded along the fringe of the Amazonian Craton. The Sunsás Province consists of basement rocks of the Paraguá Block, including the Lomas and Chiquitania Complex and San Ignacio Group (Santos et al., 2008; Matos et al., 2009).

The Mesoproterozoic Guaporé Suture Zone is located along the border between the Rondônia-Juruena and Sunsás Provinces (Fig. 1). This suture forms a ~800 km long arc-shaped structure interpreted as the result of an accretional-collisional orogeny by oceanic plate subduction between 1.47-1.43 Ga. (Rizzotto and Hartmann, 2012; Rizzotto et al., 2013). The WNW-ESE trending segment of the Guaporé Suture Zone is covered by Cenozoic sedimentary sequences of the Parecis and Guaporé Basins (Fig. 1). In this region the suture is defined by deep gravimetric and magnetic discontinuities, as well as several mafic-ultramafic complexes interpreted as tectonic slices of ophiolites (Rizzotto and Hartmann, 2012). The main units of the Guaporé Suture Zone (see Fig. 1) are summarized as follows:

Colorado Complex: It includes a metasedimentary sequence consisting of paragneiss, pelitic schist, calc-silicate gneiss, para-amphibolite and metamorphosed banded iron formation, associated with metamorphosed mafic-felsic intrusions (Rizzotto et al., 2002). The later includes syn-to late-tectonic rapakivi granites closely associated with dioritic gneiss and amphibolite, interpreted as originated in a forearc setting (Rizzotto et al., 2002). Zircon U–Pb isotopic data of a dioritic gneiss from a mafic intrusion indicate a crystallization age of 1469 ± 5 Ma for the intrusion, followed by metamorphism at 1434 ± 7 Ma (Rizzotto et al., 2013).

Rio Galera and São Felipe Complex: The Rio Galera Complex (Fig. 1) is a volcano-sedimentary complex metamorphosed to upper amphibolite facies, consisting of biotite-muscovite schist, biotite-hornblende gneiss, sillimanite-quartz schist and amphibolite (Ruiz, 2005). In addition, the Galera Complex comprises metamorphosed plutonic rocks consisting of metagabbro, amphibolite and metaperidotite (Ruiz, 2005). Metamorphosed granitic bodies with compositions ranging from tonalitic to monzogranitic crosscut the volcanic-sedimentary and plutonic mafic-ultramafic rocks of the Rio Galera Complex (Ruiz, 2005). Zircon U–Pb isotopic data of a tonalitic gneiss sample provides an age for the granitic magmatism (1459 ± 9 Ma) and metamorphism (1435 ± 2 Ma) (Rizzotto et al., 2013). The São Felipe Complex comprises calc-alkaline granitoids, described as tonalitic orthogneiss, and discontinuous bodies of mafic-ultramafic rocks (Scandolara et al., 1999).

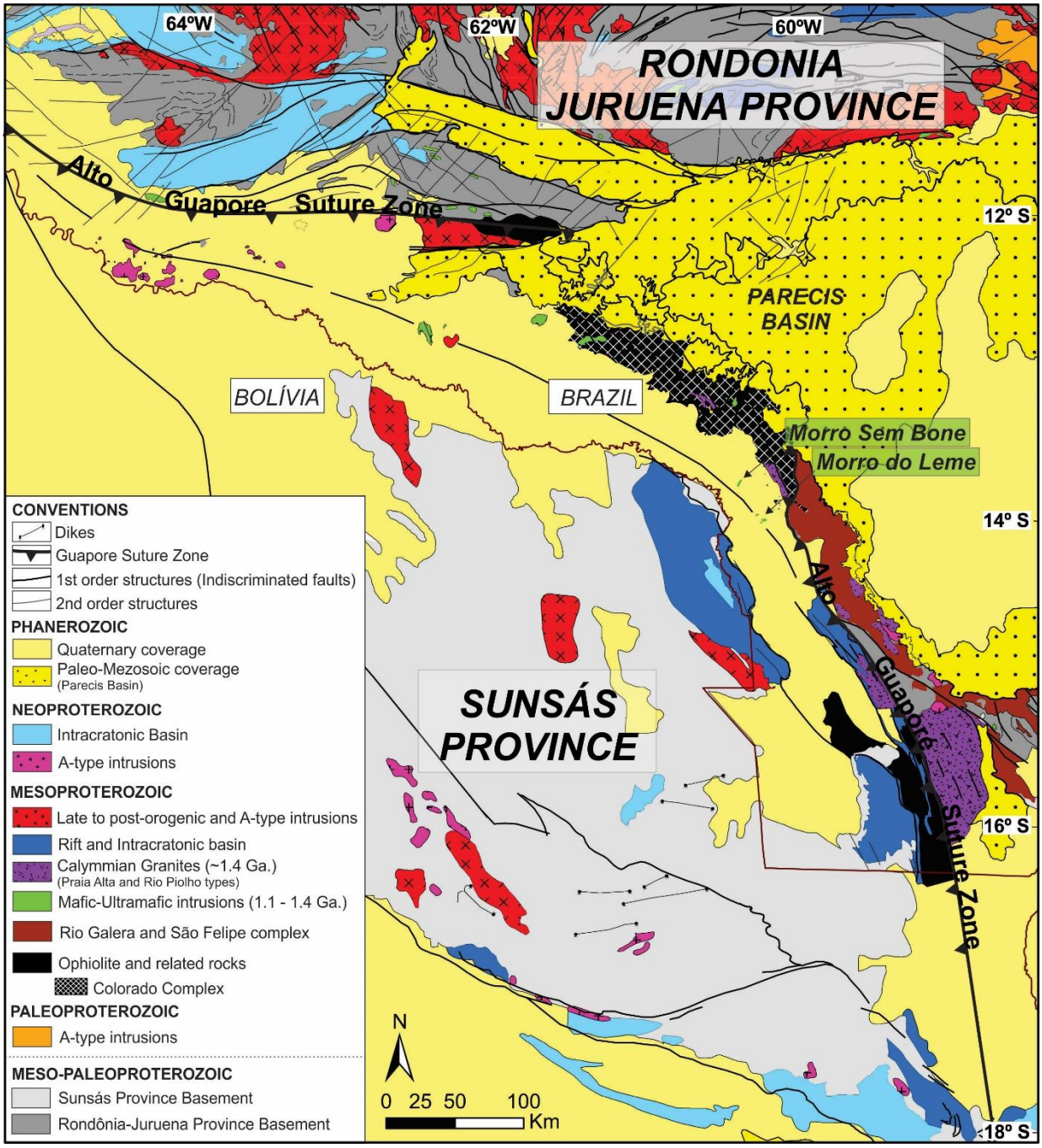

Figure 1. Regional geology of the western portion of the Amazonian Craton (modified from Rizzotto, 2010; Rizzotto and Hartmann, 2012). The dashed rectangle shows the location of. The insert shows the location of the regional map within the outline of the geochronological provinces of the Amazonian craton (modified from Santos et al., 2008).

Praia Alta and Rio Piolho granites: This group of evolved porphyritic to equigranular granitic rocks have compositions ranging from biotite syenogranite to syenogranite. Common primary magmatic features (e.g., microgranular enclaves, magmatic foliation) and the absence of tectonic textures led Rizzotto et al. (2013) to suggest that they are younger than the granitoids (orthogneiss) of the Rio Galera and São Felipe Complex. Zircon U–Pb isotopic data of syenogranites from the Praia Grande and Rio Piolho granites provide magmatic crystallization ages of 1436 ± 7 Ma and 1426 ± 5Ma, respectively (Rizzotto et al., 2013).

Trincheira Complex: It is interpreted as an ophiolite complex deformed and metamorphosed under granulite to amphibolite facies (Rizzotto and Hartmann, 2012). The ophiolite complex comprises fine-grained amphibolites (metabasalts) and metasediments (metachert, metamorphosed banded iron formation, metapelites, metapsamites and calc-silicate rocks), as well as metamorphosed melagabbro and gabbronorite (Rizzotto and Hartmann, 2012). According to these authors, this assemblage represents highly disrupted slices of an originally complete ophiolitic sequence, with primary magmatic structures and textures (e.g., pillow lavas, cumulate texture) locally preserved. Zircon U–Pb isotopic data of mafic granulite and amphibolite from the ophiolite complex indicate close ages for magmatism (1447 ± 12 Ma) and metamorphism (1435 ± 6 Ma) (Rizzotto et al., 2013). Although not investigated in detail in previous studies, the Morro Sem Boné and Morro do Leme intrusions were also considered as part of the ophiolitic sequence by Rizzotto and Hartmann (2012).

4. Materials and Methods

Geological characterization of the ultramafic intrusions was supported by data from the exploration program carried out by Anglo American, including geologic mapping projects, geochemical and geophysical surveys, and drill cores. All geochemical data reported in this study are derived from commercial chemical analyses from Anglo American database. We used systematic half diamond drill core whole-rock analyses of several drill holes from the exploration program. Drill cores were commonly sampled continuously at approximately 1-m intervals, respecting geologic contacts. Chemical analyses for the first phase of the exploration program were determined by ACME Analytical Laboratories Ltd. in Vancouver and, for the second phase, by ALS Chemex Ltd. in Toronto. A complete description of analytical methods is available in the ACME Labs Home Page (www.acmelab.com) and at ALS Chemex Home Page (www.alsglobal.com). Analyses of selected elements from drill holes (FD-01, 2A, 06, 11, 12, 14, 15, 17, 19, 22, 25 and FD-26) of the first phase and partial re-analysis of drill holes (FD-01, 02, 02A, 04, 06 and FD-10) of the second phase are reported for in this study. Quality control was maintained by the routine of both laboratories, as well as Anglo American procedures of the analytical database.

The methods used by ACME included sample preparation by ACME code "*R200-1000*" (crush, split and pulverize 1 kg of sample to 200 mesh), dry at 105 ◦C (dry pulps at 105 ◦C prior to analysis), code "*4A&4B*" and "AALitho" (LiBO2/LiB4O7 fusion and analysis by ICP-ES/

ICP-MS), code "*7TD*" (Ni by 4 acid digestion, analysis by ICP-ES), LOI (loss on ignition), code "2A" (total C and S by LECO), code "*1F*" (1:1:1 Aqua Regia digestion; Ultratrace ICP-MS analysis), code "*3BMS*" (fire assay fusion; Au Pt Pd by ICP-MS analysis). The methods used by ALS Chemex consisted of the "*whole rock package*" (major, minor and trace elements), code "*PGM-ICP23*" (Pt, Pd, Au by 30 g fire assay and ICP-MS analysis) and code "*ME-ICP81*" (ICP Fusion – Ore Grade). Representative strip logs with chemical results are provided for Drill Hole FD-01 (Appendix 1) and FD-15 (Appendix 2) in Online Supplementary Material.

Petrographic studies of 70 polished thin sections were carried out at the Microscopy Laboratory of the University of Brasília, Brazil. Microprobe analyses of olivine from 16 selected samples (128 olivine analyses altogether) were carried out at the Instituto de Geociências, Universidade de Brasília (Brazil) on a fully automated Cameca SX-50 instrument. The wavelength dispersive analyses were performed at an operating voltage of 15 kV and a beam current of 40 nA. The counting times were 20 s for major elements and 60 s for nickel. Standards used were natural silicate minerals and synthetic oxides. Background counting time was set to half of the peak counting time. The results are provided in Online Supplementary Material (Appendix 3).

5. Results

5.1 Local Geology

The Morro Sem Boné and Morro do Leme intrusions outcrop as isolated hills in plains consisting mainly of Quaternary sedimentary cover (Fig. 2). These hills are prominent features within a flat monotonous terrain, where the Morro Sem Boné intrusion stands up to 250 m higher than the surrounding sedimentary cover (Figures. 3 and 4a). The ultramafic rocks consist of partially to extensively weathered dunite and peridotite that host the nickel laterite deposits. The weathering profile is up to 70 m thick and commonly capped by an upper silica-rich crust. Several ultramafic bodies covered by sediments were also identified in drill core during the exploration program. The analytical signal magnetic image shows that ultramafic bodies are associated with magnetic anomalies (Fig. 2b) and suggests that abundant untested anomalies may indicate covered ultramafic intrusion. The sedimentary cover consists predominantly of clastic sediments and associated laterites from the Guaporé Basin (Pedreira and Bahia, 2000). These up to 60 m thick cover of unconsolidated sediments is a major challenge for geological studies and mineral exploration of the ultramafic targets in this region. Apart from the ultramafic rocks, scattered outcrops of partially weathered granitoids and metasedimentary rocks also occur

within the dominant Quaternary sedimentary cover. The metasedimentary rocks consist mainly of pelitic schists and metacherts of the Colorado Complex, a forearc sequence that extends more than 100 km to the north of the area investigated in this study (Rizzotto et al., 2002).

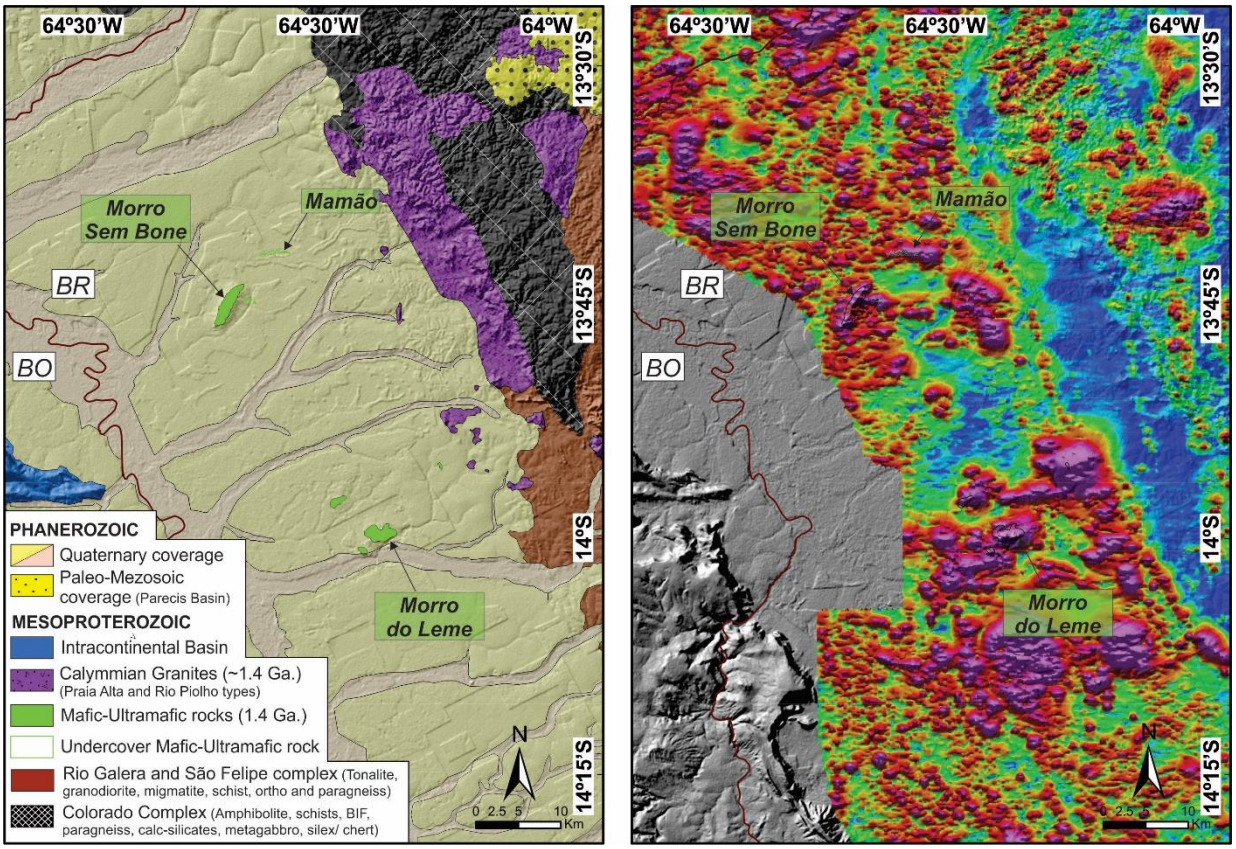

Figure 2. a) Geology of the area close to the Morro Sem Boné and Morro do Leme intrusions (modified from Rizzotto, 2010). b) Analytical signal amplitude image is shown for the same area. Geophysical data from the Brazilian Geological Survey open files.

In the following section we use exploration data, including drill core samples of unweathered rocks and geochemical analyses, to describe the ultramafic intrusions and their host rocks.

5.2 Morro Sem Boné Intrusion

The Morro Sem Boné intrusion (MSB) outcrops in a 6 km long NNE/ SSW hill (Figs. 3 and 4a) consisting of extensively weathered olivine cumulates of the lateritic profile associated with the Ni laterite deposit. Detailed geological map developed for Ni laterite exploration separates domains of silica-rich laterite, typical of the upper portions of the weathered profile, from domains of saprolite from ultramafic rocks in Brazil (Figs. 3 and 4a). The weathered profile, including the lower boulder zone where unweathered rocks eventually occur, is described in drilling logs of the exploration program of the MSB. The contact of the ultramafic intrusion with

country rocks are covered by sediments of the Guaporé Basin, including ferrigenous soils and laterites developed nearby the hill where weathered ultramafic rocks occur. The marginal country rocks are just exposed as rare, weathered domains of mica-quartz schist (Fig. 3).

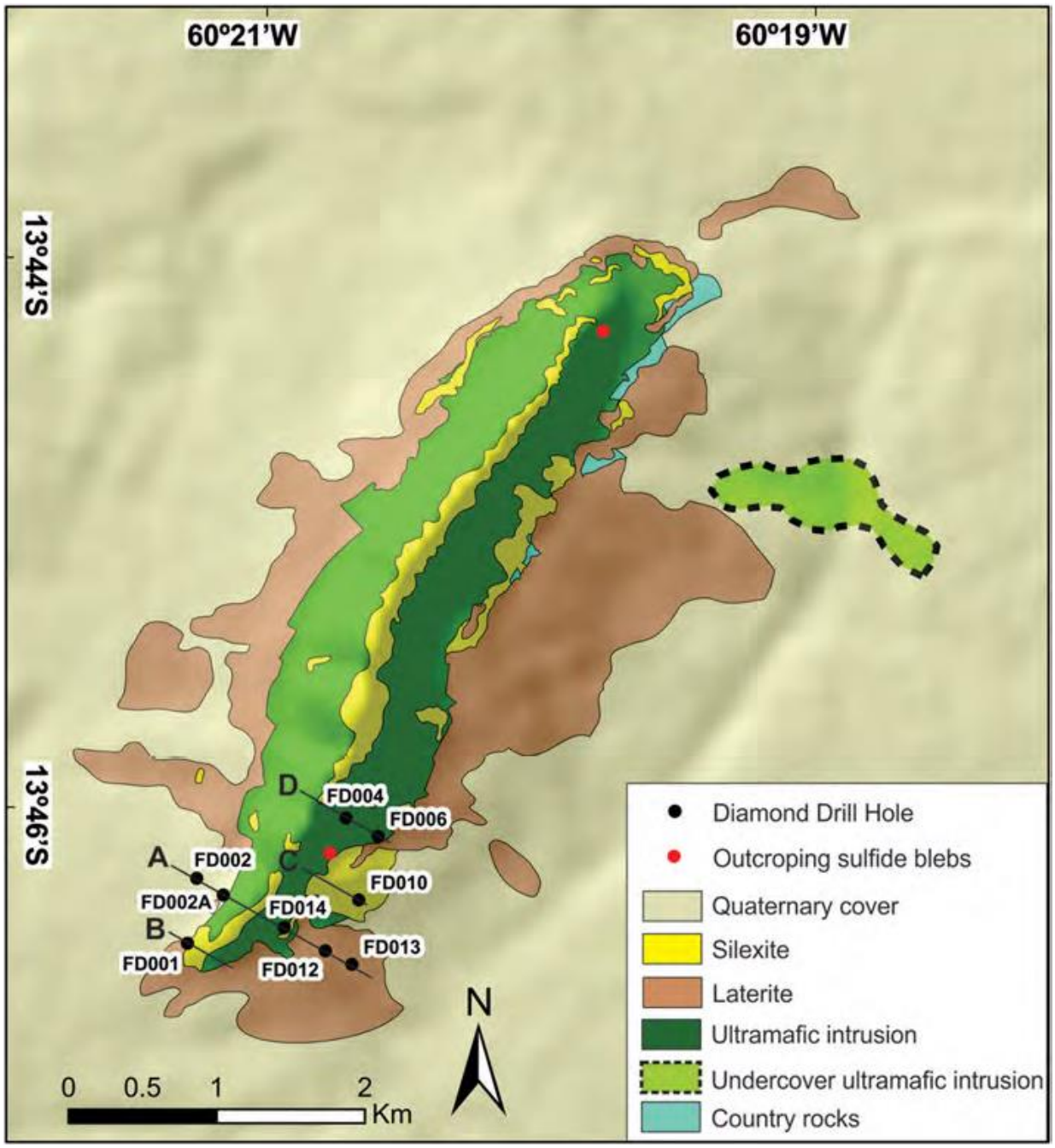

Figure 3. Geology of the Morro Sem Boné intrusion. The location of drill holes, geological sections and outcropping sulfide blebs are indicated. Modified from Anglo American Internal Report.

Although unweathered rocks are not preserved in outcrops, primary textures are commonly recognized and allow the identification of their protoliths throughout the MSB. They consist mainly of medium-sized olivine adcumulate (dunite) with interlayered medium-to coarse-

grained olivine + pyroxene cumulates (harzburgite) (Fig. 4c). Dunite and harzburgite have cumulus chromite pseudomorphs (2–4 vol%) indicated by black fine-grained euhedral crystals commonly enclosed in brownish weathered silicates. Orthopyroxenite is rare in the MSB and consists of medium-sized orthopyroxene cumulates with accessory chromite (1–2 vol%) (Fig. 4d). Weathered cumulates with primary preserved textures prevail in the MSB, but discrete domains of sheared ultramafic rocks also occur, where up to a few meters consist of weathered fine-grained foliated ultramafic rocks (Fig. 4e). These fine-grained ultramafic rocks at the intrusion margins or within shear zones have metamorphic assemblages consisting mainly of amphiboles (hornblende + cummingtonite), indicating their recrystallization under amphibolite facies of regional metamorphism. The predominance of primary igneous textures in the ultramafic rocks contrasts with the tectonic-metamorphic fabric of the country rocks. Although the regional tectonic compression from NNE to SSW is recognized in few outcrops of host rocks located close to the MSB, in the ultramafic cumulates this event is indicated by cleavage fractures on two main directions: NW-SE/ W-E, and NE-SW.

Drill core samples from exploration drill holes provide constraints for the magmatic structure, as well as unweathered rocks for petrological studies of the MSB. A geological section based on drill core logs across the southwestern portion of the MSB (Fig. 5 Section A), together with a section based on drill core log of FD-01 located at the southernmost tip of the intrusion (Fig. 5 Section B), indicate an apparent sequence of ultramafic cumulates and metasedimentary enclosing rocks. These features possibly result of magma injection and/or incorporation of xenoliths at the margin of the intrusion. Geological sections located in the wider portion of the intrusion (Fig. 5 Sections C and D) consist mainly of adcumulate dunite. The abundance of dunite in the main body of the intrusion is consistent with results from geological mapping and shallow drilling for nickel laterite deposits. The predominance of massive dunites without distinctive layering hampered the understanding of the primary magmatic structure of the intrusion. However, magmatic layering identified in few outcrops and drill core suggests variable primary layering (~15◦ and up to 70◦) but predominantly low angle dipping eastward.

Country rocks of the ultramafic intrusion consist of mica schists and associated amphibolites. Fine-grained biotite schist, consisting of variable amounts of quartz, biotite, muscovite, plagioclase and microcline, is the dominant rock type. Variable modal proportion of micas (biotite + muscovite) to feldspars (plagioclase + microcline) suggests that these rocks result from metamorphism of interlayered pelitic and immature psamitic sediments. Amphibolites are fine-grained rocks with nematoblastic texture consisting mainly of hornblende

and plagioclase, with accessory ilmenite and biotite. Amphibolites are interpreted as metamorphosed basalts interlayered in the metasedimentary sequence. Intersections of disseminated to massive sulfides are associated with the country rocks. These up to 2 m sufide-rich intersections consist mainly of pyrrhotite and pyrite with minor chalcopyrite and sphalerite. They occur within biotite schist and amphibolite, commonly hosted or enveloped by rocks with abundant garnet and/or quartz. Metamorphic assemblages of biotite schists (e.g., biotite + plagioclase + muscovite + quartz + microcline) and amphibolites (e.g., hornblende + plagioclase) are typical of amphibolite facies regional metamorphism (Bucher and Grapes, 2011). Massive medium to coarse-grained biotite granite bodies intrudes the ultramafic cumulates and their country rocks.

5.2.1 Ultramafic Rocks

Dunite with associated harzburgite and orthopyroxenite are the ultramafic rocks intersected in several drill holes in the MSB. Drill holes FD-01 and FD-06 (Figs. 5 and 6) were selected to illustrate petrographic, stratigraphic and geochemical features of the layered rocks of the MSB. Drill Hole FD-01 is representative of the southern portion of the intrusion where dunite and interlayered harzburgite and orthopyroxenite are closely associated with country rocks (Fig. 5 Section A and Fig. 6a), whereas drill hole FD-06 consists mainly of dunite (Fig. 5 Section D and Fig. 6b) and illustrates the most common intersected cumulate rock of the MSB. Dunite is a variably serpentinized olivine adcumulate with accessory euhedral chromite (Fig. 7). Olivine replacement by serpentine varies from moderate (~45–75%) to pervasive (Fig. 8) and decreases with depth in drill holes. Intercumulus minerals consist mainly of orthopyroxene (Opx) and minor phlogopite. Harzburgite and orthopyroxenite interlayered with dunite (Fig. 8) vary from few cm up to dozens of meters thick in drill core (i.e., apparent thickness), with both gradational and sharp contacts. Harzburgite (olivine + Opx + chromite cumulates; Fig. 8b, c and d) and orthopyroxenite (Opx + chromite cumulates; Fig. 8a, e and f) are medium-to coarse-grained adcumulates.

Orthopyroxenite is commonly unaltered, with just minor replacement of Opx by serpentine and talc along fractures. Chromite occurs as fine-grained euhedral crystals with 3–5 modal % in dunite, harzburgite and orthopyroxenite (Fig. 7).

Lithogeochemical results from the exploration database show the compositional differences expected for these cumulate rocks (Fig. 6). Dunite has higher MgO (~40 wt%) and lower SiO2

(~35 wt%) content than orthopyroxenite (~30 wt% and 50 wt% content of MgO and SiO2, respectively), as indicated in Fig. 6a. High Cr contents from 0.3 to 0.6 wt % in dunite, harzburgite and orthopyroxenite are consistent with the modal abundance of cumulus chromite (~3–5%) in these rocks. A few spikes in Cr contents (up to 1 wt%) are associated with chromitite pods, usually a few centimeters thick. Very low CaO contents (<2 wt%) in orthopyroxenite and harzburgite are consistent with Cpx being rarely described in the ultramafic rocks. Drill core intersections of sheared ultramafic rocks are indicated by higher contents of Al2O3 (see Fig. 6b).

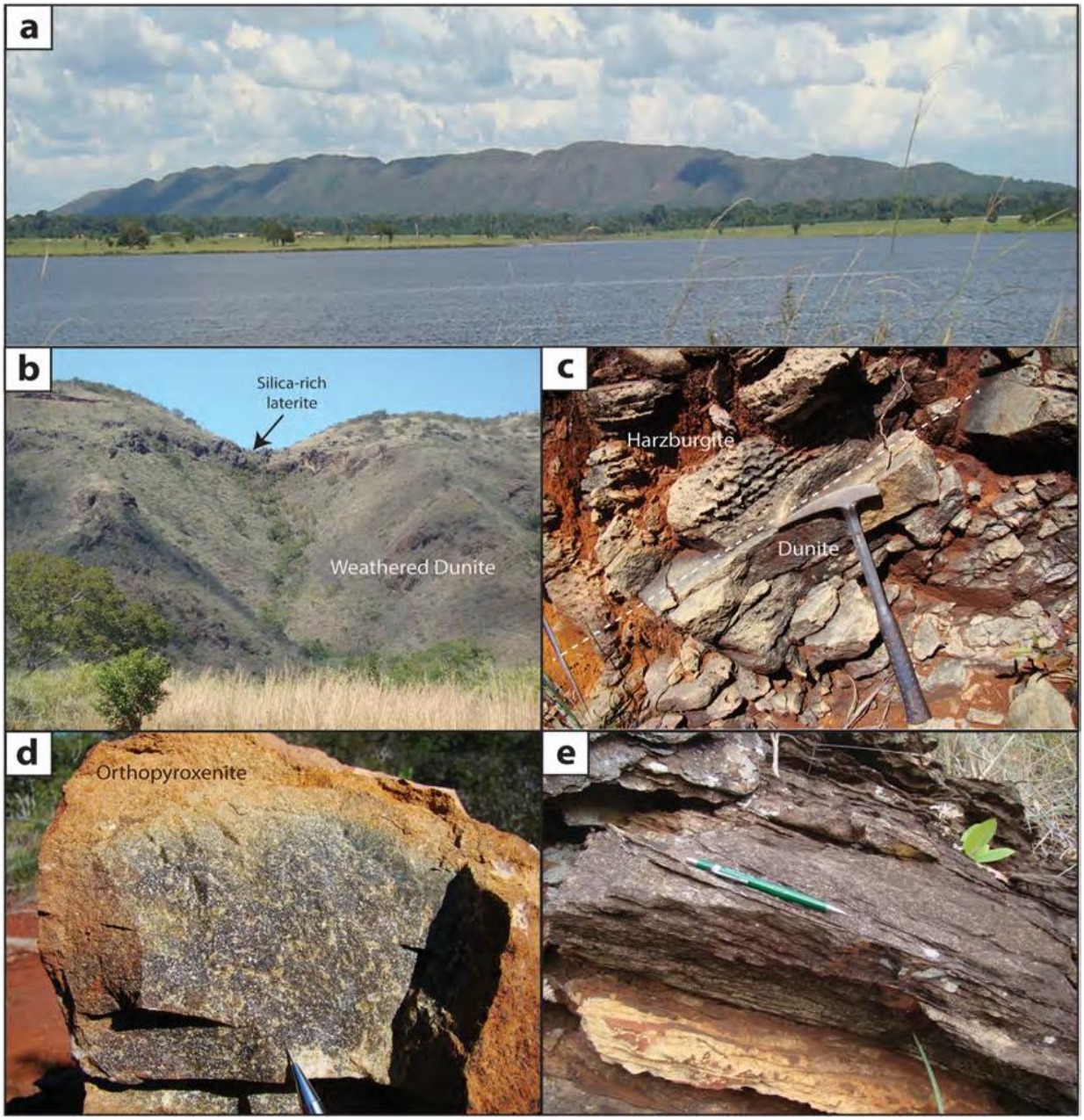

Figure 4. Photos of outcrops and rocks of the Morro Sem Boné intrusion. a) View from SW to NE of the 6 km long NNW trending Morro Sem Boné intrusion. Photos of outcrops and rocks of the Morro Sem Boné intrusion. a) View from SW to NE of the 6 km long NNW trending Morro Sem Boné intrusion. b) Outcrops of weathered dunite and silica-rich laterite in the southwestern side of the intrusion. c) Interlayered weathered dunite and coarse-grained harzburgite. d) Block of fresh orthopyroxenite taken from an exploration trench. e) Shearing overprinting of the ultramafic rock.

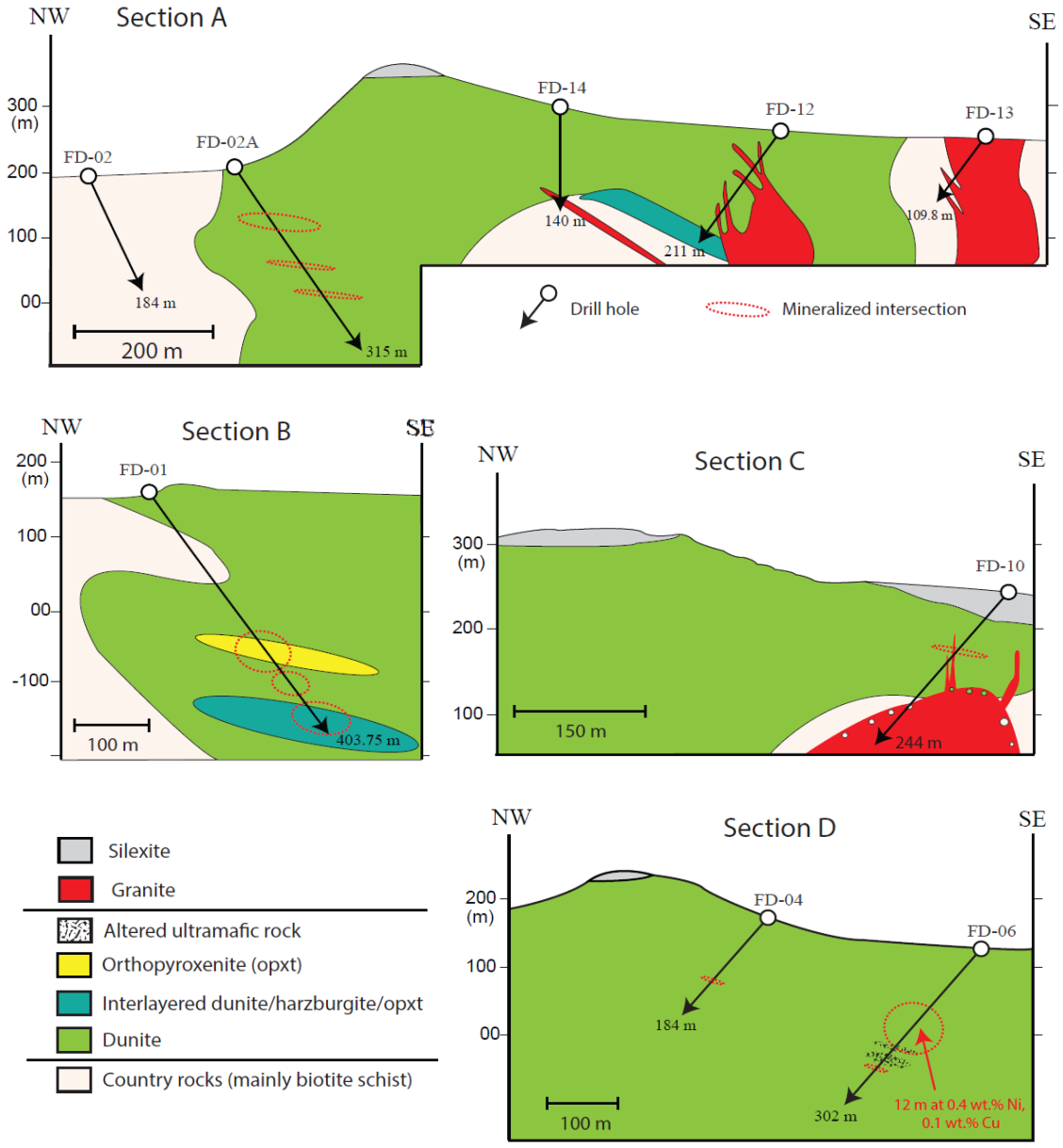

Figure 5. Geological sections of the Morro Sem Boné intrusion. See Fig. 3 for location of drill holes and sections. Modified from Anglo American internal reports.

5.2.2 Ni–Cu-PGE sulfide mineralization

Sulfide mineralization hosted in ultramafic rocks was identified in large outcrops located on top of the hill of the MSB (see Fig. 3 for location of outcrops). These outcrops are located within broad Cu anomalies identified in soil geochemical surveys and consist of weathered dunite with altered sulfide blebs with variable shapes and sizes. They occur as up to few centimeters weathered brownish spots (Fig. 9a and b) consisting of iron hydroxide and minor malachite.

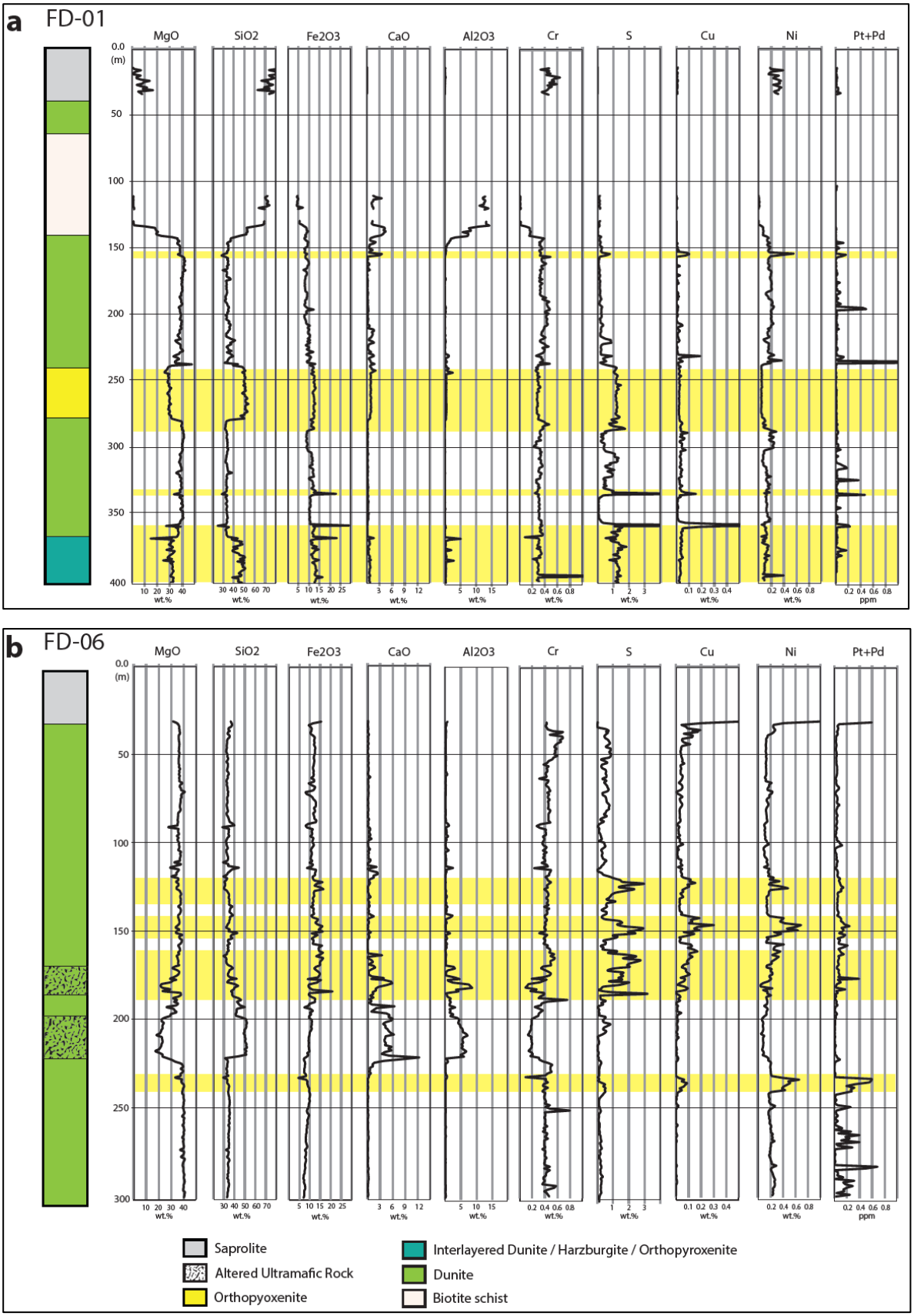

Figure 6. Strip logs of drill holes FD-01 (a) and FD-06 (b) of the Morro Sem Boné intrusion and its MgO, SiO2, Fe2O3, CaO, Al2O3, Cr, S, Cu, Ni and Pt + Pd geochemical results. Sulfide-rich zones are indicated by yellow shade. Data from Anglo American internal reports. See Figs. 3 and 5 for location of drill holes.

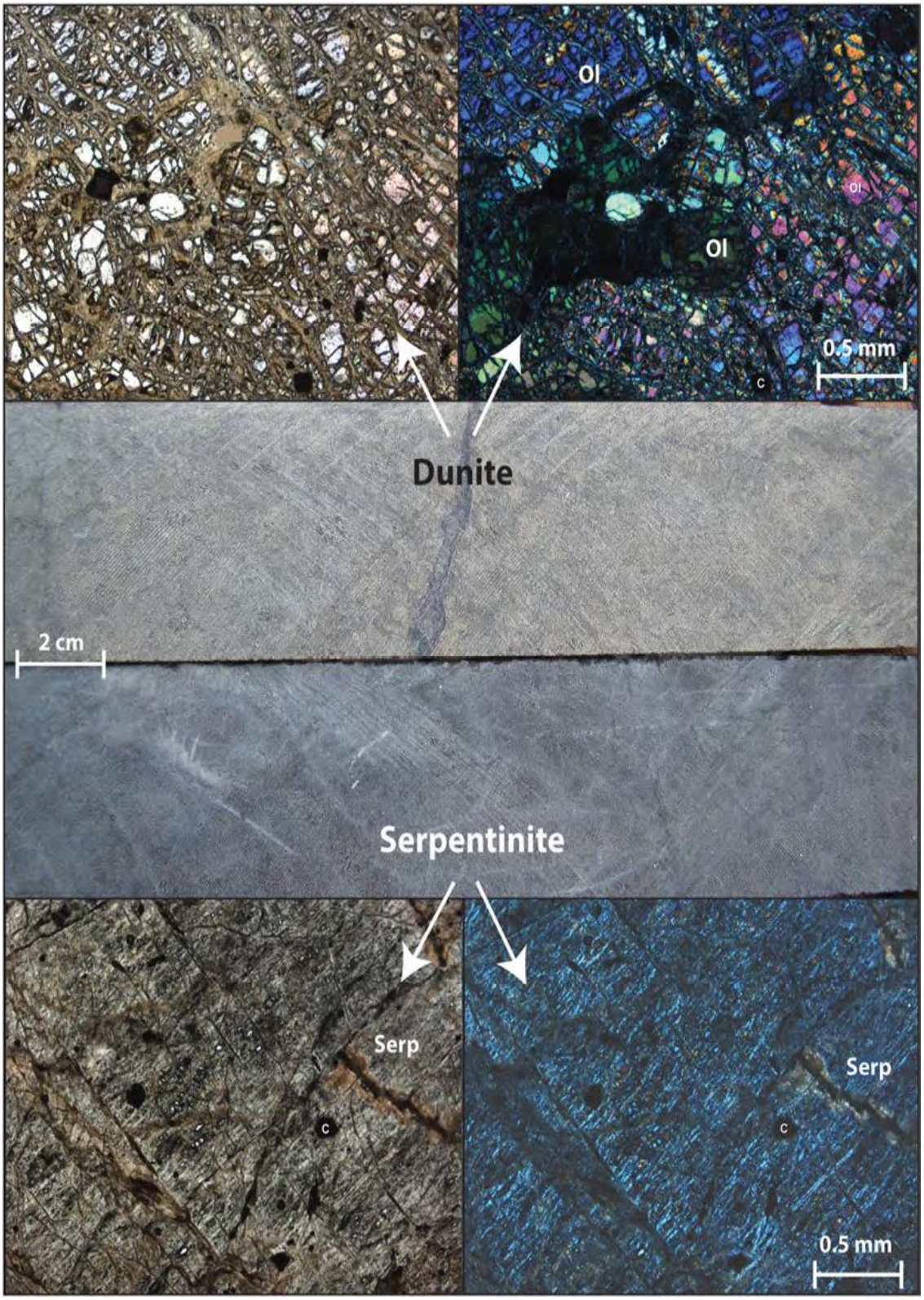

Figure 7. Photos and photomicrographs of variably serpentinized dunite of the Morro Sem Boné intrusion. The photo of the upper core (light color) and related photomicrographs are representative of partially serpentinized dunite. The photo of the lower core (dark gray color) and related photomicrographs are typical serpentinite with olivine (Ol) pseudomorphs pervasively replaced by serpentine (Serp) and magnetite (opaques along olivine fractures). Chromite (C) occurs as fine-grained euhedral opaque minerals that show up in the left hand side microphotographs (parallel polarizers).

Sulfide mineralization also occurs in several thick intersections in drill holes (e.g., FD-06 with ~88 m at 1–10% sulfides) in the southern portion of the MSB (Fig. 5). The sulfide-rich interval of FD-06 (Fig. 5 Section D and Fig. 6b) includes one intersection with 12 m at 0.4 wt% Ni and 0.1 wt% Cu, and another with 9 m at 0.3 wt% Ni and 0.1 wt% Cu. The sulfide assemblage and textures of mineralized zones in the MSB are typical of magmatic sulfides segregated as immiscible sulfide liquids from mafic-ultramafic magmas (Naldrett, 2004). Disseminated interstitial sulfide predominates (>95 vol%), with minor associated net-textured and massive intervals. Disseminated sulfides form typical interstitial blebs within dunite (Fig. 9c and e), harzburgite (Fig. 9c) and orthopyroxenite (Fig. 9g). The blebs are predominantly small (<1 mm), poorly interconnected (based on 2-D observation in drill core and thin sections) and isolated at olivine and/or orthopyroxene grain boundaries (Fig. 9g). Massive and net-textured sulfides occur in thin intersections (<0.2 m thick) within domains of disseminated sulfides (Fig. 10d). Contacts of massive sulfides with disseminated domains are commonly sharp, but gradational transitions from massive to network, and to interstitial blebs also occur (Fig. 9d). The mineralogy and texture of sulfides are the same for different ultramafic rocks (i.e., dunite, harzburgite, orthopyroxenite) in the MSB. Primary sulfides consist mainly of pyrrhotite (>90 vol%) with minor proportions of variable amounts of pentlandite, chalcopyrite and pyrite. Although the pyrrhotite-rich assemblage is the most common in sulfide-rich zones, minor to moderate low-temperature alteration of sulfides, illustrated by pyrrhotite replaced by marcasite, magnetite and/or Fe-hydroxide also occur (Fig. 9f). The low-temperature alteration is highly heterogeneous, and sulfide blebs from one core sample may display a continuum from aggregates of unaltered pyrrhotite to those pervasively altered.

The contents of S throughout drill holes are consistent with the abundance of disseminated sulfides in the MSB, as illustrated by the FD- 01 and FD-06 strip logs (Fig. 6). Although S contents between 1 and 3 wt % occur in thick intersections in both drill holes, results for Ni, Cu, Pt and Pd do not show the strong positive correlation with S commonly observed in Ni–Cu-PGE sulfide deposits with similar amounts of sulfides (e.g., Santa Rita: Barnes et al., 2011; Limoeiro: Mota-e-Silva et al., 2013; Caboclo dos Mangueiros: Matos and Ferreira Filho, 2018). The plots of S–Ni, S–Cu, and S–Pt + Pd (Fig. 10) highlight the low Ni–Cu–Pt–Pd contents in the sulfide-rich zones and the variable but commonly weak correlation of these metals with S. These plots include just analyses of rocks with cumulate textures, thus excluding weathered samples, rocks from sheared and/or altered zones, as well as country rocks. The correlation of Ni and Cu with S

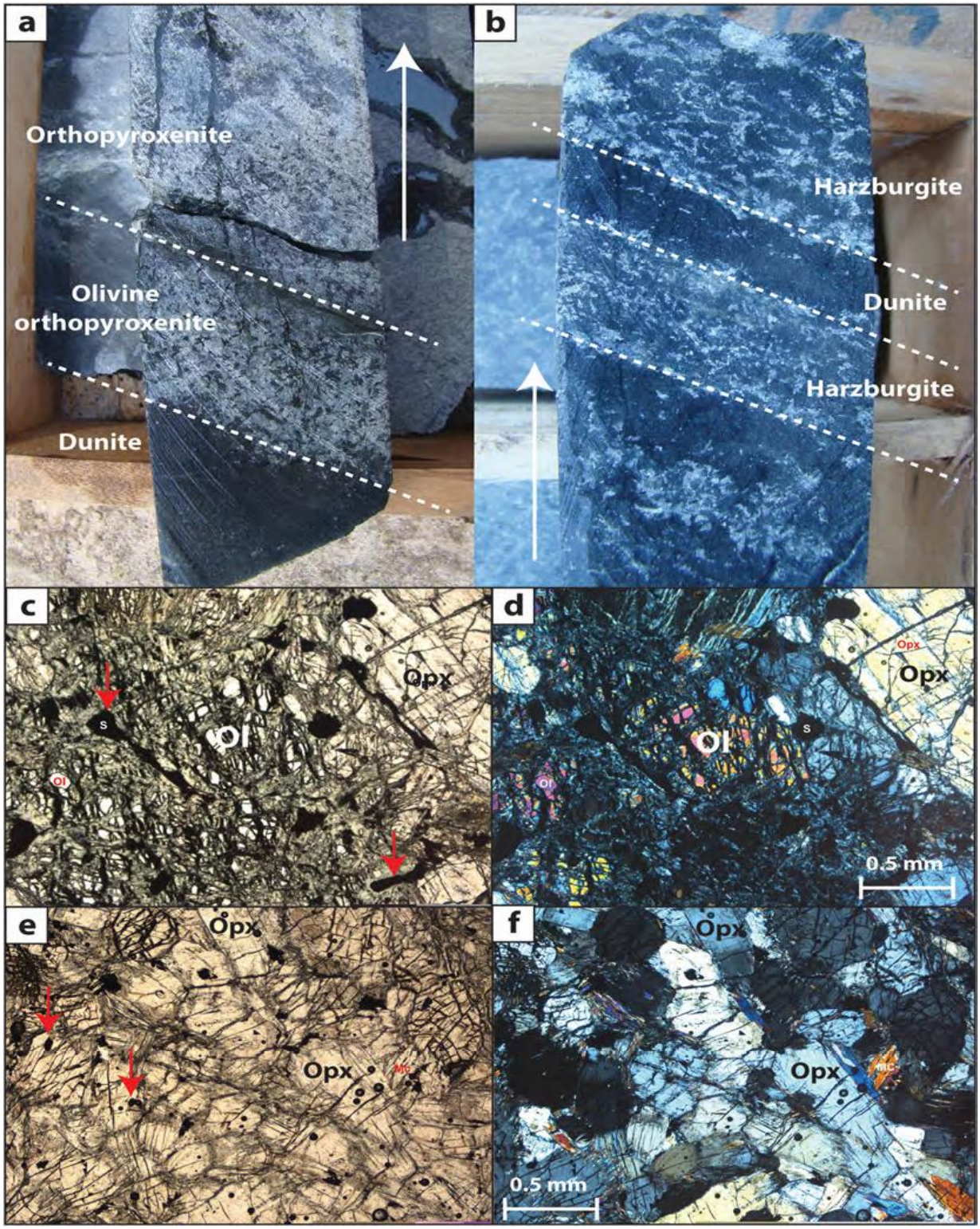

Figure 8. Photos and photomicrographs of layered ultramafic cumulates of the Morro Sem Boné intrusion. a) Drill core sample of layered dunite, olivine orthopyroxenite and orthopyroxenite. Photos and photomicrographs of layered ultramafic cumulates of the Morro Sem Boné intrusion. a) Drill core sample of layered dunite, olivine orthopyroxenite and orthopyroxenite. b) Drill core sample of layered dunite and harzburgite. Both core samples are 4.5 cm wide, and arrows point to the top of the drill core. c) Photomicrograph of a harzburgite consisting of partially serpentinized olivine (Ol) and orthopyroxene (Opx). Opaque minerals include sulfides (e.g., elongated blebs indicated by red arrows), chromite (tiny euhedral crystals) and magnetite (e.g., irregular elongated crystals along serpentinized olivine fractures). d) Same as “c" with crossed polars. e) Photomicrograph of an orthopyroxenite with adcumulate texture. Opaque minerals include sulfides (e.g., rounded blebs) and euhedral chromite crystals (e.g., see crystals included in Opx indicated by red arrows). f) Same as “e" with crossed polars.

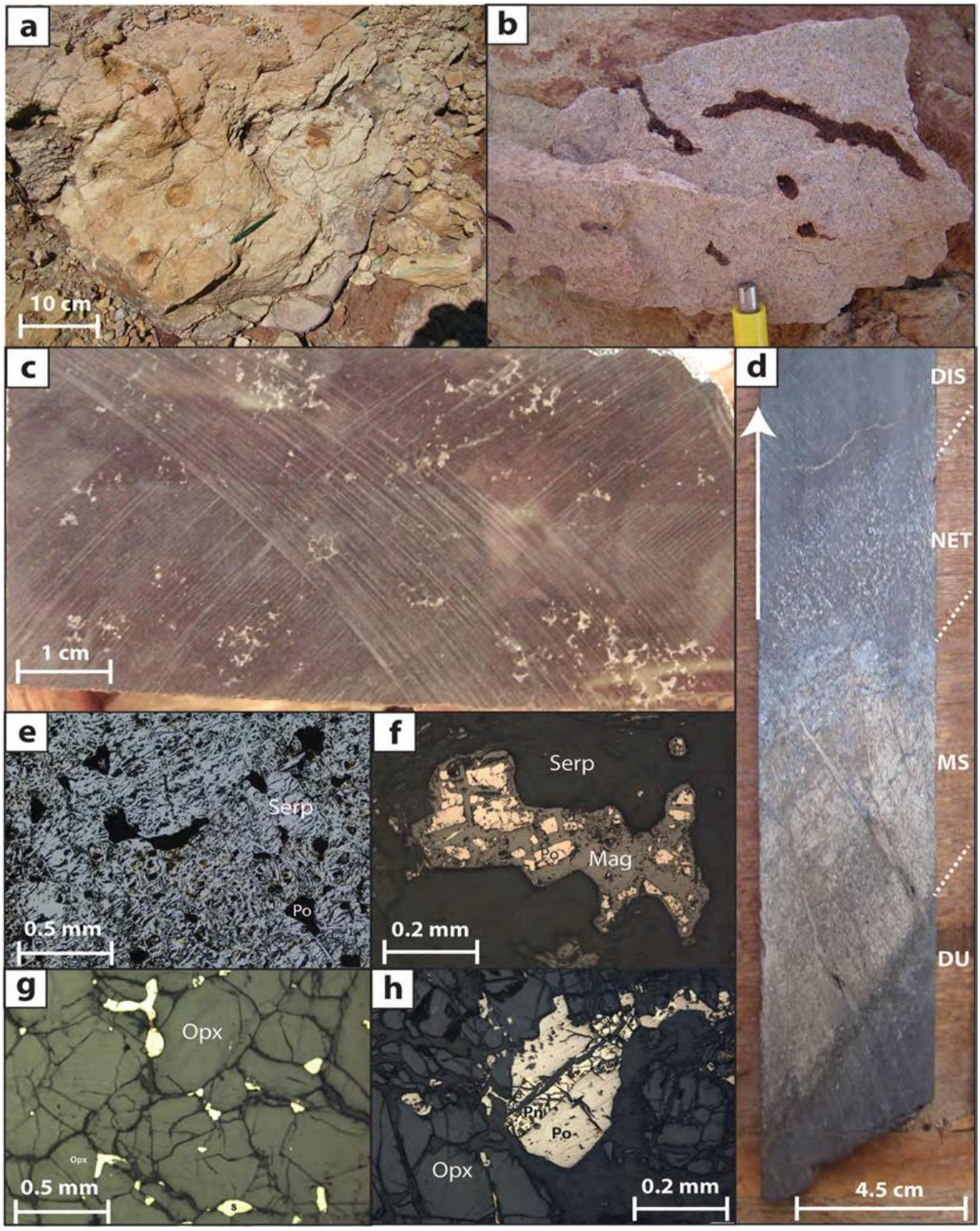

Figure 9. Photos and photomicrographs of sulfide mineralization of the Morro Sem Boné intrusion. a) Outcrop of weathered dunite. Photos and photomicrographs of sulfide mineralization of the Morro Sem Boné intrusion. a) Outcrop of weathered dunite. Rusted brownish spots indicate weathered rounded sulfide blebs. b) Boulder of weathered dunite with elongated weathered sulfide blebs. c) Drill core sample typical dunite with disseminated interstitial sulfide blebs. d) Drill core sample showing the transition from massive (MS) to net-textured (NET) and disseminated (DIS) sulfide. Note sharp contact with dunite at the bottom of the photo. e) Photomicrograph of serpentinized dunite with interstitial sulfide blebs (opaque minerals) consisting of pyrrhotite (Po). f) Photomicrograph of sulfide bleb in serpentinized dunite. Note euhedral olivine pseudomorphs at the contact. Sulfide is pyrrhotite (Po) partially replaced my magnetite (Mag). g) Photomicrograph of adcumulate orthopyroxenite with interstitial sulfide blebs. H) Detail of sulfide bleb consisting of pyrrhotite (Po) and pentlandite (Pn; yellowish color).

in drill holes FD-01 and FD-06 is remarkably distinct. The weak negative linear correlation in S–Ni plot in FD-01 (r = □ 0.57) contrasts with a distinctively positive correlation in FD-06 (r = 0.49). The negative S–Ni correlation in FD-01 results from very low Ni tenors combined with variable contents of Ni in cumulate rocks (i.e., ~0.2 wt% Ni in dunite and <0.05 wt% Ni in orthopyroxenite; see Fig. 6a) within a sequence where higher S contents predominate in intervals of orthopyroxenite and interlayered dunite/harzburgite and orthopyroxenite (i.e, contents > 0.1 wt% S; see Fig. 6a). In short, the content of Ni in samples from drill hole FD-01 is mostly contained in silicates with minor contribution from sulfides. On the other hand, the positive correlation in S–Ni plot of FD-06 indicates that S contained in sulfides become significant for samples with S contents >1.0 wt% (Fig. 10). Higher Cu contents in sulfides in samples from FD-06 than those from FD-01 are evident in S–Cu plots (Fig. 10). While samples from FD-01 have a very weak positive correlation of S–Cu plot (r = 0.22), the S–Cu plot for FD-06 show strong positive correlation (r = 0.70) that allows the calculation of an approximate Cu tenor (~2.2 wt%) by linear regression. It is assumed for linear regression calculation that 100 vol% of sulfides would produce a rock with 35 wt% S, which is approximately the expected grade for a rock containing 100 vol% of magmatic sulfides (e.g., Barnes et al., 2011). The plots of Pt + Pd with S for drill holes FD-01 and FD-06 indicate that they are mostly uncorrelated (r ~ zero; Fig. 10). The contents of Pt and Pt in core samples have very high positive correlations (r = 0.96 and 0.97 for FD-06 and FD-01, respectively) and Pt/Pd ratios close to 1. The distribution of Pt and Pd in both drill holes (Fig. 6) consists mostly of low contents (Pt + Pd < 0.1 ppm) with scattered values > 0.2 ppm (up to 2.1 ppm in one sample in FD-01, out of scale in Fig. 6a). The lower portion of drill hole FD-06, from 234 to 301 m, has distinctively higher Pt + Pd contents (Fig. 6b), including several intersections with values > 0.2 ppm (e.g., 8 m at 0.4 ppm Pt+ Pd; 2 m at 0.6 ppm Pt+ Pd).

5.3 Mamão Intrusion

Several mafic-ultramafic bodies covered by sediments of the Guaporé Basin were identified in the region of this study. A few of these bodies, commonly associated with MAG anomalies, were investigated by drilling during the exploration program. These covered or poorly exposed mafic-ultramafic occurrences, designated as satellite intrusions, consist mainly of ultramafic rocks similar to those described in the larger MSB and Morro do Leme intrusion. The Mamão intrusion (Fig. 2) is described here as an example of Ni–Cu sulfide mineralized satellite intrusion.

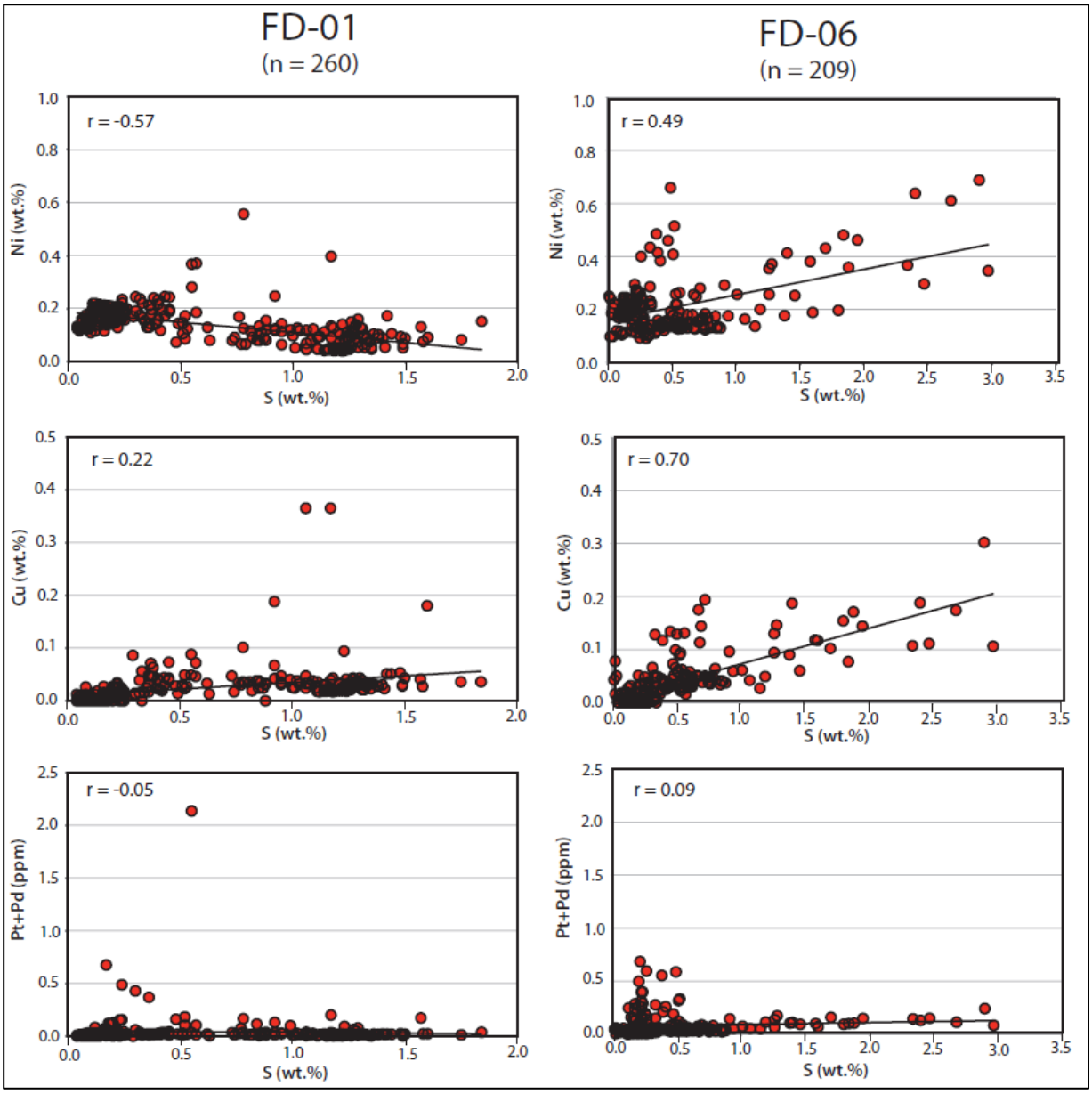

Figure 10. Plots of Ni, Cu and Pt + Pd vs S for samples of unweathered cumulate rocks from drill holes FD-01 and FD-06 of the Morro Sem Boné intrusion. Plots of Ni, Cu and Pt + Pd vs S for samples of unweathered cumulate rocks from drill holes FD-01 and FD-06 of the Morro Sem Boné intrusion. Trend lines correspond to the linear correlation. Data from Anglo American internal reports. See Figs. 3 and 5 for location of drill holes, and Fig. 6 for the strip log and distribution of geochemical results.

The Mamão intrusion is associated with a ~8 km long EW trending magnetic anomaly (Fig. 11a). Although covered by up to 50 m of sediments of the Guaporé Basin, several drill holes intersected ultramafic rocks over 4 km along the EW trending magnetic anomaly (Fig. 11a). A geological section based on drill core logs across the magnetic anomaly (Fig. 11b) indicates a ~140 m thick ultramafic intrusion hosted within biotite schist. The magmatic layering dips ~40◦ to the south and consists of dunite with interlayered harzburgite and minor orthopyroxenite. This intrusion consists of a central portion where dunite predominates, with a complex border zone

consisting of variably textured orthopyroxenite and harzburgite associated with fine-grained ultramafic rocks in both margins (Fig. 11b). Country rocks consist of fine-to medium-grained plagioclase-biotite-quartz schists. The petrography of the ultramafic rocks is very similar to those described in the MSB. They consist mainly of medium-to coarse-grained olivine (dunite) and olivine + Opx (harzburgite) cumulates, with minor interlayered Opx cumulate (orthopyroxenite). Dunite, harzburgite and orthopyroxenite have accessory (2–4 vol%) euhedral chromite as an additional cumulus mineral. The contact between cumulate rocks and biotite schist consists of a thin zone (<3 m) of fine-grained granoblastic ultramafic rocks with abundant amphiboles, that may occur close to partially assimilated country rocks. Sulfides are abundant just in the contact zone, consisting mainly of fine-grained disseminated blebs (<5 vol%) but up to 10 vol% in few meters long intersections. The sulfide zone is mainly contained within the ultramafic intrusion, but disseminated sulfides also occur in biotite schist in the drilled country rocks close to the contact. Sulfides in the ultramafic intrusion consist of pyrrhotite (>90 vol%) and minor pentlandite and chalcopyrite, while those hosted within biotite schist consist mainly of pyrrhotite and pyrite.

Figure. 12 summarizes the assay results from the exploration database for a representative drill core from the Mamão intrusion (FD-15). Results for each cumulate rock (i.e., dunite, harzburgite and orthopyroxenite) are very similar to those reported for the MSB. Significant distinctive features of the Mamão intrusion includes: (1) the lack of intersections with very high MgO contents (~40 wt%) characteristic of adcumulate dunite in the MSB; (2) a progressive decrease in MgO content and increase in SiO2, CaO and Al2O3 contents toward the margins of the intrusion; (3) the highest Cr contents are located in the marginal zone of the intrusion; (4) sulfide zones located at the margin of the intrusion. The symmetric fractionation is a remarkable feature of the Mamão intrusion and will be discussed in subsection 6.2 of this study.

The distribution of S throughout the Mamão intrusion, illustrated by drill hole FD-15 (Fig. 12), is consistent with sulfides being concentrated at the margins of the intrusion (Fig. 11). Sulfide mineralization occurs as thin intersections with modest metals contents (e.g., 4 m at 0.32 wt% Ni and 0.11 wt% Cu in FD-15; 6 m at 0.5 wt% Ni and 0.13% Cu in FD-17), and show strong positive correlation of S with Ni, Cu and Pt + Pd (Fig. 12). The plots of S–Ni, S–Cu, and S–Pt + Pd (Fig. 13) highlight the low Ni, Cu, and Pt + Pd contents in the sulfide-rich zones and the variable but commonly strong positive correlation of these metals with S. Chemical analyses plotted in Fig. 13 cover the entire interval of sulfide-rich rocks at the lower contact of the intrusion, including both sulfide-bearing ultramafics and biotite schists from drill holes FD-15

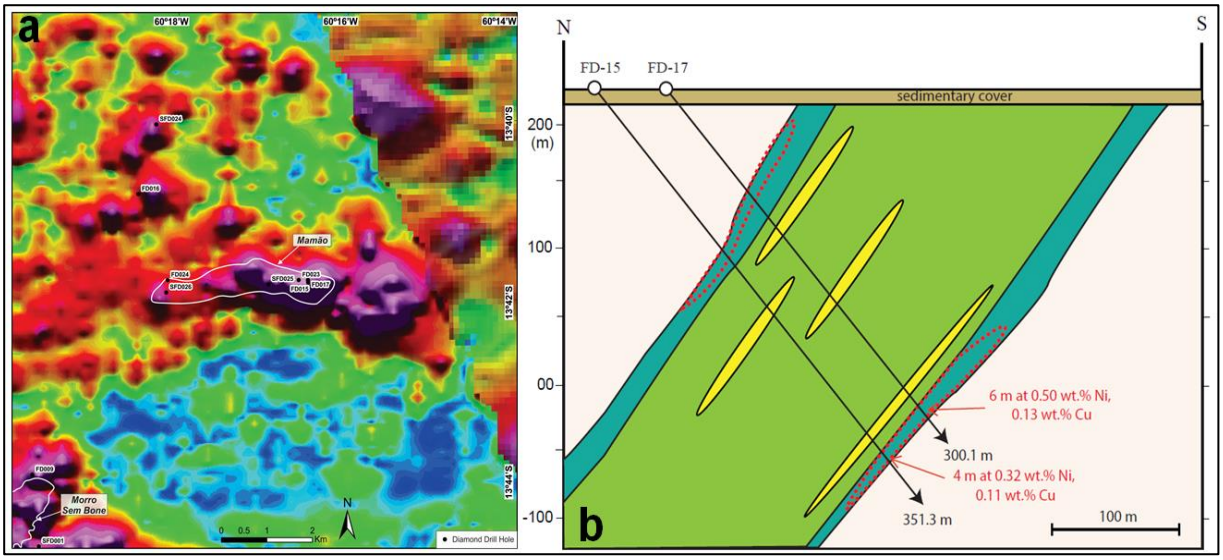

Figure 11. The Mamão ultramafic intrusion. a) Aeromagnetic map showing the analytical signal amplitude (nT/m) associated with the Mamão intrusion. The location of drill holes reported in this study is indicated. The area delineated in white color includes mafic-ultramafic rocks intersected by drilling. b) Geological section of the Mamão intrusion (FD-15 and FD-17). See Fig. 5 for captions. Modified from Anglo American internal reports.

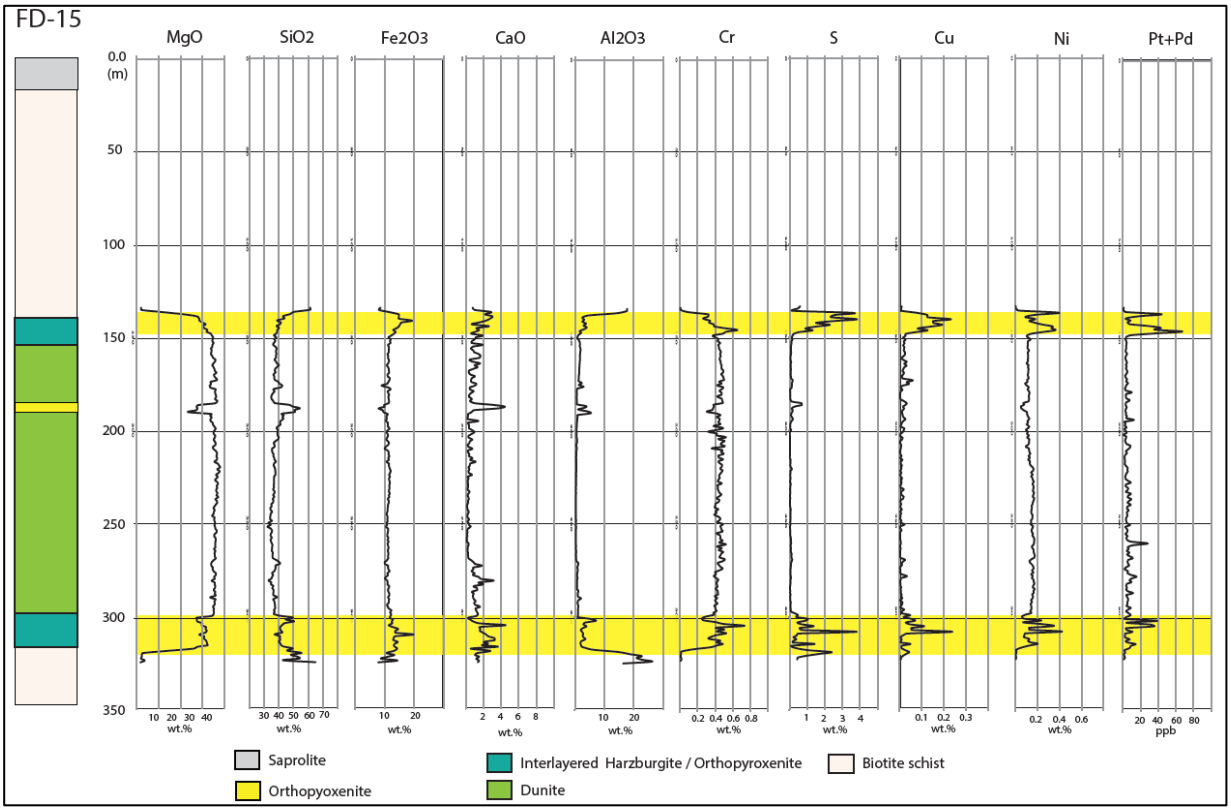

Figure 12. Strip log of drill hole FD-15 of the Mamão intrusion and its MgO, SiO2, Fe2O3, CaO, Al2O3, Cr, S, Cu, Ni and Pt + Pd geochemical results. Strip log of drill hole FD-15 of the Mamão intrusion and its MgO, SiO2, Fe2O3, CaO, Al2O3, Cr, S, Cu, Ni and Pt + Pd geochemical results. Sulfide-rich zones are indicated by yellow shade. Data from Anglo American internal reports. See Fig. 11 for location of drill hole.

and FD- 17. Very low contents of Ni, Cu, Pt and Pd in sulfide-bearing samples of biotite schists contrast with results for sulfide-bearing ultramafic rocks (Fig. 13). In addition, with very low contents of Zn (<300 ppb) and Pb (<100 ppb) in the sulfide bearing country rocks, these results

are consistent with a sulfide assemblage consisting mainly of pyrrhotite and pyrite indicated by petrographic studies. Due to highly different metal contents between sulfide-bearing host rocks and ultramafic rocks, linear correlation is calculated just for samples from the intrusion (see Fig. 13). Strong positive correlations of Ni and Cu with S in drill holes FD-15 (r = 0.86 and 0.96, respectively) and FD-17 (r = 0.92 and 0.94, respectively) are characteristic of magmatic sulfides (e.g., Naldrett, 2004). The plots of Pt + Pd with S indicate a moderate positive correlation for drill hole FD-17 (r = 0.68) and a much weaker positive correlation for drill hole FD-15 (r = 0.27). The latter has very low Pt + Pd contents (<40 ppb) and results of Pt and Pd are commonly below or close to the detection limits of our methods of analyses. The contents of Pt and Pt in these core samples have very high positive correlations (r = 0.82 and 0.90 for FD-15 and FD-17, respectively) and Pt/Pd ratios close to 1.

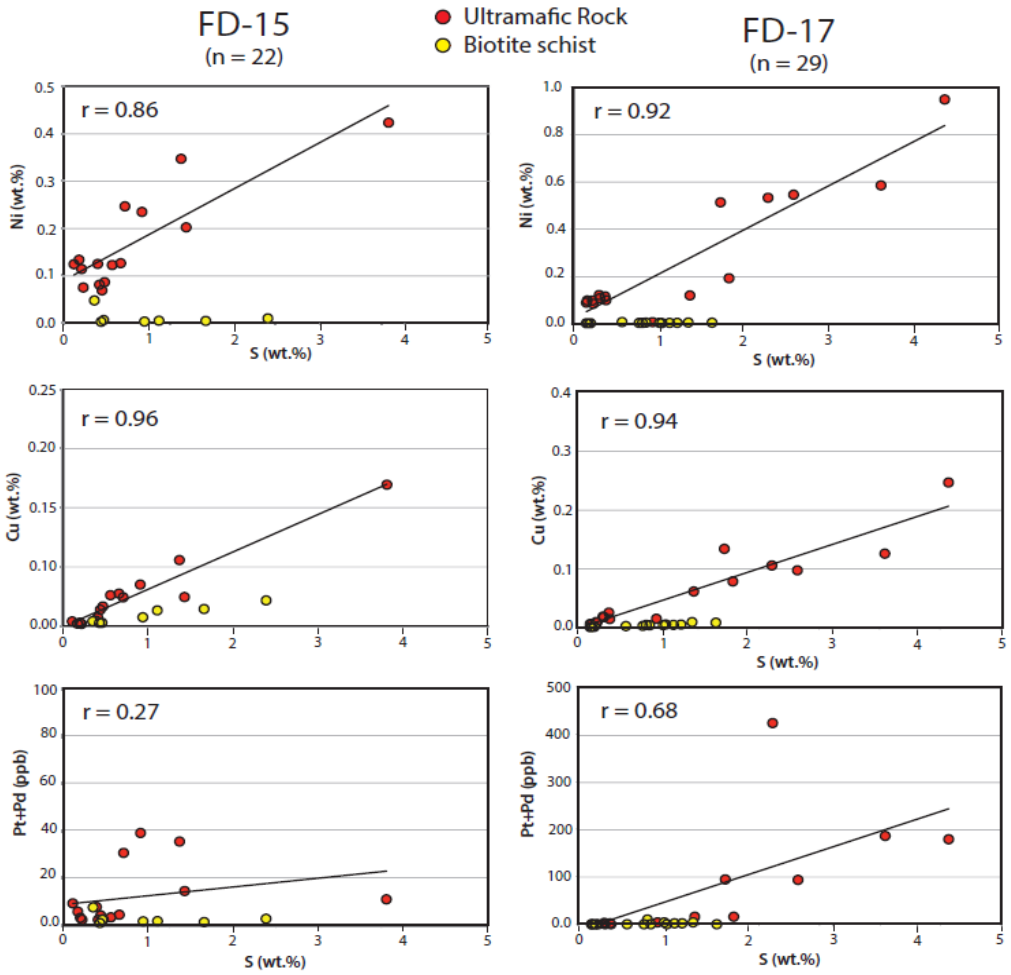

Figure 13. Plots of Ni, Cu and Pt + Pd vs S for samples of cumulate rocks from drill holes FD-15 and FD-17 of the Mamão intrusion. Trend lines correspond to the linear correlation for samples of ultramafic rocks. Data from Anglo American internal reports. See Fig. 11 for location of drill holes and Fig. 12 for the strip log and distribution of geochemical results.

5.4 Morro do Leme Intrusion

The Morro do Leme intrusion (ML) outcrops in three main bodies (Fig. 14a) consisting of extensively weathered olivine cumulates of the lateritic profile associated with Ni laterite resources. These bodies occur as isolated hills within a flat terrain, with the prominent Morro do Leme hill standing up to 200 m higher than the surrounding sedimentary covers (Fig. 15a). The largest outcrops of ultramafic rocks occur in the Morro do Leme hill and the southern body (Figs. 14a and 15a) where geological sections and drill holes selected for this study are located. The ML is associated with a broad magnetic anomaly (Fig. 14b) suggesting that the three mapped bodies may be part of a larger magmatic structure. Whether these bodies represent a tectonic disrupted intrusion, or a cluster of intrusions is an issue hard to be solved with the available density of drilling and outcrops. Similar to the MSB, the geology of the ML consists of domains of silica-rich laterite, typical of the upper portions of the weathered profile, and domains of saprolite from ultramafic rocks (Fig. 15b). The contact of the ultramafic intrusion with country rocks is covered by sediments of the Guaporé Basin, including ferrigenous soils and laterites developed nearby the hill where weathered ultramafic rocks occur (Fig. 14a). Country rocks occur as few domains of weathered metasedimentary rocks, including few outcrops of highly foliated mica schist and minor interlayered staurolite-garnet-mica schist along the Piolho creek (Fig. 15e). The predominance of primary igneous textures in the ultramafics rocks contrasts with the tectonic-metamorphic fabric of the metasedimentary country rocks. Besides the metasediments, massive to slightly foliated medium-grained tonalites are intersected in drill holes in the southern body of the ML. These tonalites are interpreted as part of the host rocks of the ultramafic intrusions.

Although outcropping rock is weathered relic magmatic textures are recognized and allow the identification of their protoliths throughout the ML. They consist of pseudomorphs of massive medium-grained olivine adcumulate (dunite) (Fig. 15c) and minor interlayered medium-to coarse-grained olivine + orthopyroxene cumulates (harzburgite) and orthopyroxene cumulates (orthopyroxenite) (Fig. 15d). Dunite, harzburgite and orthopyroxenite have cumulus chromite pseudomorphs (2–4 vol%) indicated by black fine-grained euhedral crystals located at the margins or enclosed in brownish weathered silicates. Similar to the MSB, discrete domains up to few meters thick of sheared ultramafic rocks occur within rocks with primary magmatic texture.

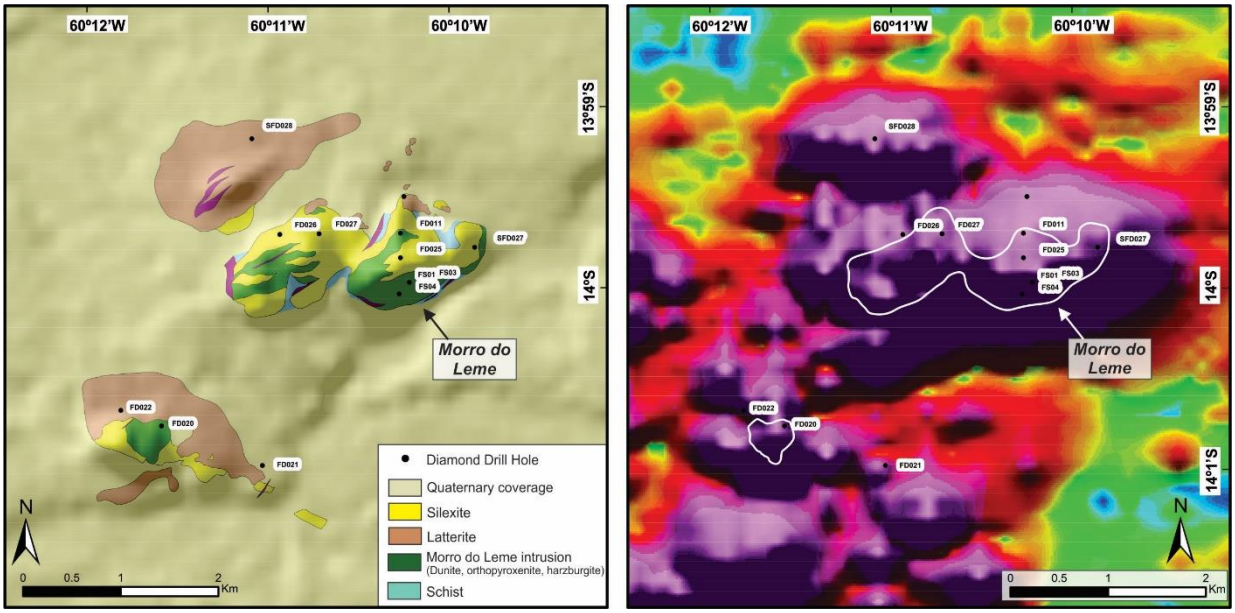

Figure 14. a) Geology of the Morro do Leme intrusion. b) Aeromagnetic map showing the analytical signal amplitude (nT/m) associated with the Morro do Leme intrusion. a) Geology of the Morro do Leme intrusion. b) Aeromagnetic map showing the analytical signal amplitude (nT/m) associated with the Morro do Leme intrusion. The location of drill holes and geological sections reported in this study is indicated. Modified from Anglo American internal reports.

5.4.1 Ultramafic Rocks and Associated Ni–Cu-PGE Mineralization

Dunite with associated harzburgite and orthopyroxenite are the ultramafic rocks intersected in several drill holes in the ML. Drill holes FD- 19 from the central ultramafic body and FD-22 from the southern body (Figs. 14 and 16) were selected to illustrate petrographic, stratigraphic and geochemical features of the layered rocks of the ML. Drill Hole FD- 19 consists mainly of dunite (Fig. 16 Section A and Fig. 17a), whereas drill hole FD-22 intersected dunite with interlayered harzburgite and orthopyroxenite close to the contact with metasedimentary host rocks (Fig. 16 Section B and Fig. 17b). Dunite is variably serpentinized with olivine replacement by serpentine varying from pervasive to moderate (~30 vol%). Chromite occurs as fine-grained euhedral crystals with 3–5 modal% commonly located at the contacts between olivine crystals. Petrographic features of dunite, harzburgite and orthopyroxenite of the ML are identical to those described for the MSB, and a detailed description will not be repeated in here.

The intersection of homogeneous dunite in drill hole FD-19 has the expected chemical composition of an olivine adcumulate (Fig. 17a), as indicated by high MgO (~40 wt%), low SiO2 (~35 wt%) and Fe2O3 (~7.5 wt% in samples with low S contents), together with very low Al2O3 (<0.15 wt%) and CaO (<0.15 wt%) contents. Chromium contents between 0.3 and 0.8 wt% in dunite are consistent with disseminated chromite described throughout the intersection. This intersection of homogeneous dunite hosts several zones of up to 5 vol% disseminated

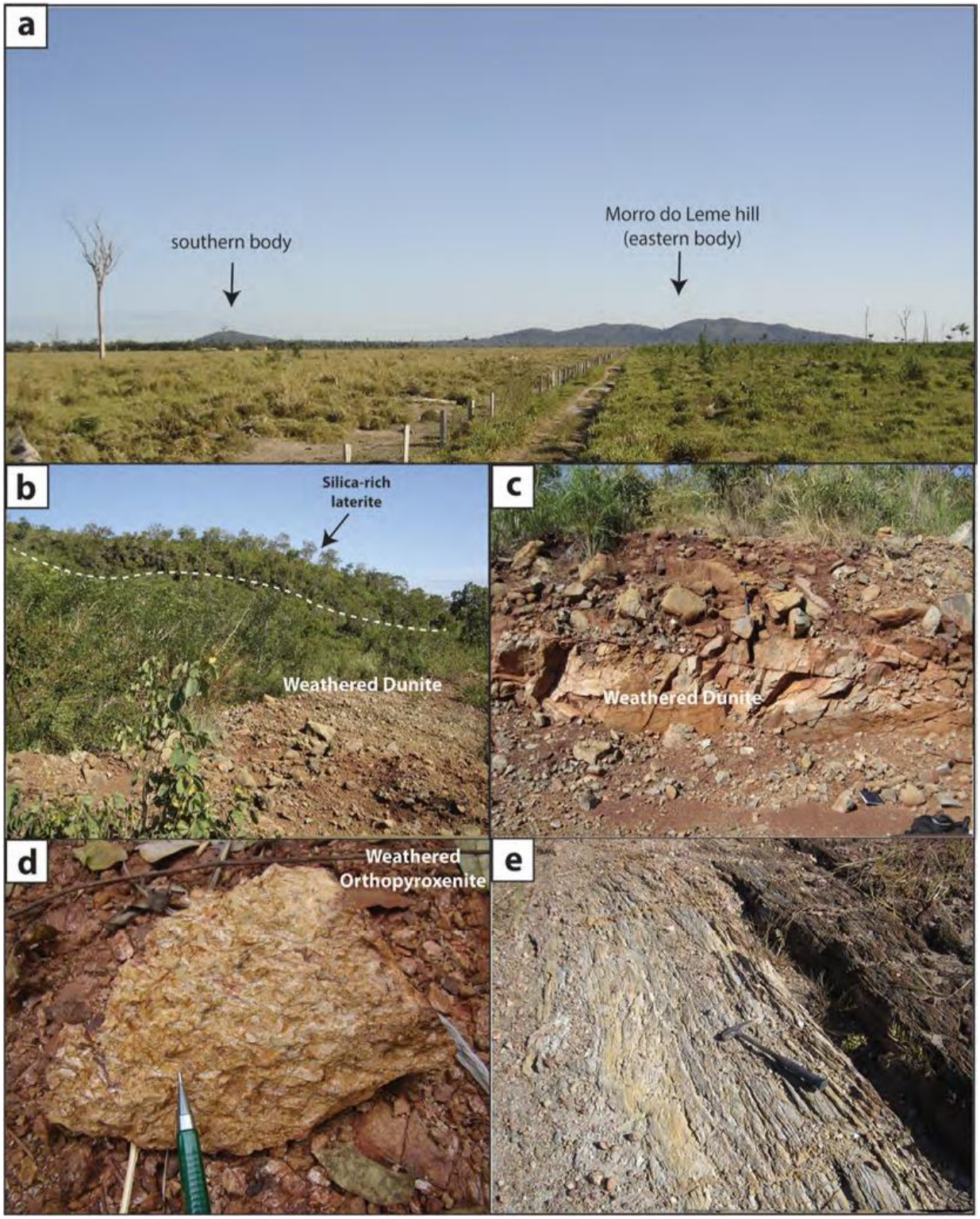

Figure 15. Photos of outcrops and rocks of the Morro do Leme intrusion. a) View from S to N of the Morro do Leme intrusion. Photos of outcrops and rocks of the Morro do Leme intrusion. a) View from S to N of the Morro do Leme intrusion. See Fig. 14 for location of the eastern and southern ultramafic bodies. b) Outcrops of weathered dunite and silica-rich laterite. c) Outcrop of weathered massive medium-grained dunite. d) Block of weathered coarse-grained orthopyroxenite. e) Outcrop of highly foliated mica schist with interlayered staurolite-garnet mica schist. Outcrop located in the Piolho creek close to the covered contact between metasedimentary host rocks and the southern ultramafic body.

sulfides, including one mineralized intersection with 20 m at 0.5 wt% Ni, 0.1 wt% Cu, and 0.5 ppm Pt+ Pd (i.e., 128–148 m in Fig. 17a; see also Section A in Fig. 16). Apart from variable proportions of disseminated sulfides, mineralized and barren dunite in drill hole FD-19 have the same mineralogical and textural features. The sulfide assemblage and textures of mineralized dunites are similar to those described in the MSB, consisting of interstitial fine-grained sulfide blebs at olivine grain boundaries. Primary sulfides consist mainly of pyrrhotite (>90 vol%) with minor proportions of variable amounts of pentlandite and chalcopyrite. The plots of Ni, Cu and Pt + Pd with S (Fig. 18) indicate weak to moderate positive correlations in the mineralized intersection (r = 0.35, 0.76, and 0.21, respectively). The contents of Pt and Pt in these core samples have very high positive correlations (r = 0.97) and Pt/Pd ratios close to 1 (average = 1.14).

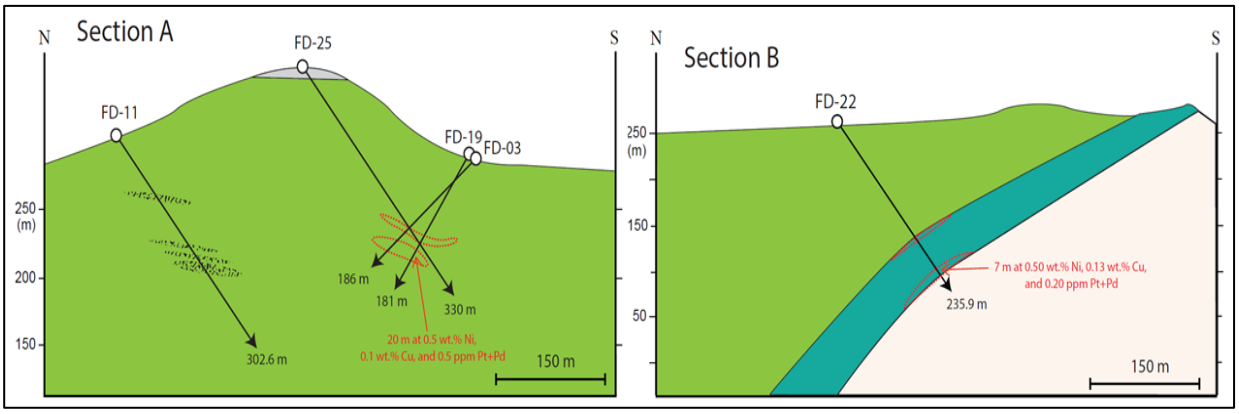

Figure 16. Geological sections of the Morro do Leme intrusion. See Fig. 14 for location of drill holes and sections. See Fig. 5 for captions. Modified from Anglo American internal reports.

The drill hole FD-22 (see Section B in Figs. 16 and 17b) intersected homogeneous dunite with contents of MgO (~40 wt%), SiO2 (~35 wt %), Fe2O3 (~10 wt%), Al2O3 (<0.15 wt%), CaO (<0.15 wt%) and Cr (between 0.3 and 0.6 wt%) very similar to those from drill hole FD-19. The compositional features of this intersection of homogeneous olivine cumulates are consistent with an olivine adcumulate. In contrast, the ~60 m intersection of interlayered dunite, harzburgite and orthopyroxenite located at the lower portion of drill hole FD-22, has variable contents of MgO (between 30 and 40 wt%) and SiO2 (between 30 and 50 wt%) resulting from samples with variable amounts of olivine and orthopyroxene. The thin intersection with distinctively higher contents of Al2O3 and CaO corresponds to sheared ultramafic rocks (Fig. 17b; from 158 to 161 m). Sulfides occur throughout the lower portion of FD- 22 drill hole, including the entire interval of interlayered dunite, harzburgite and orthopyroxenite and the

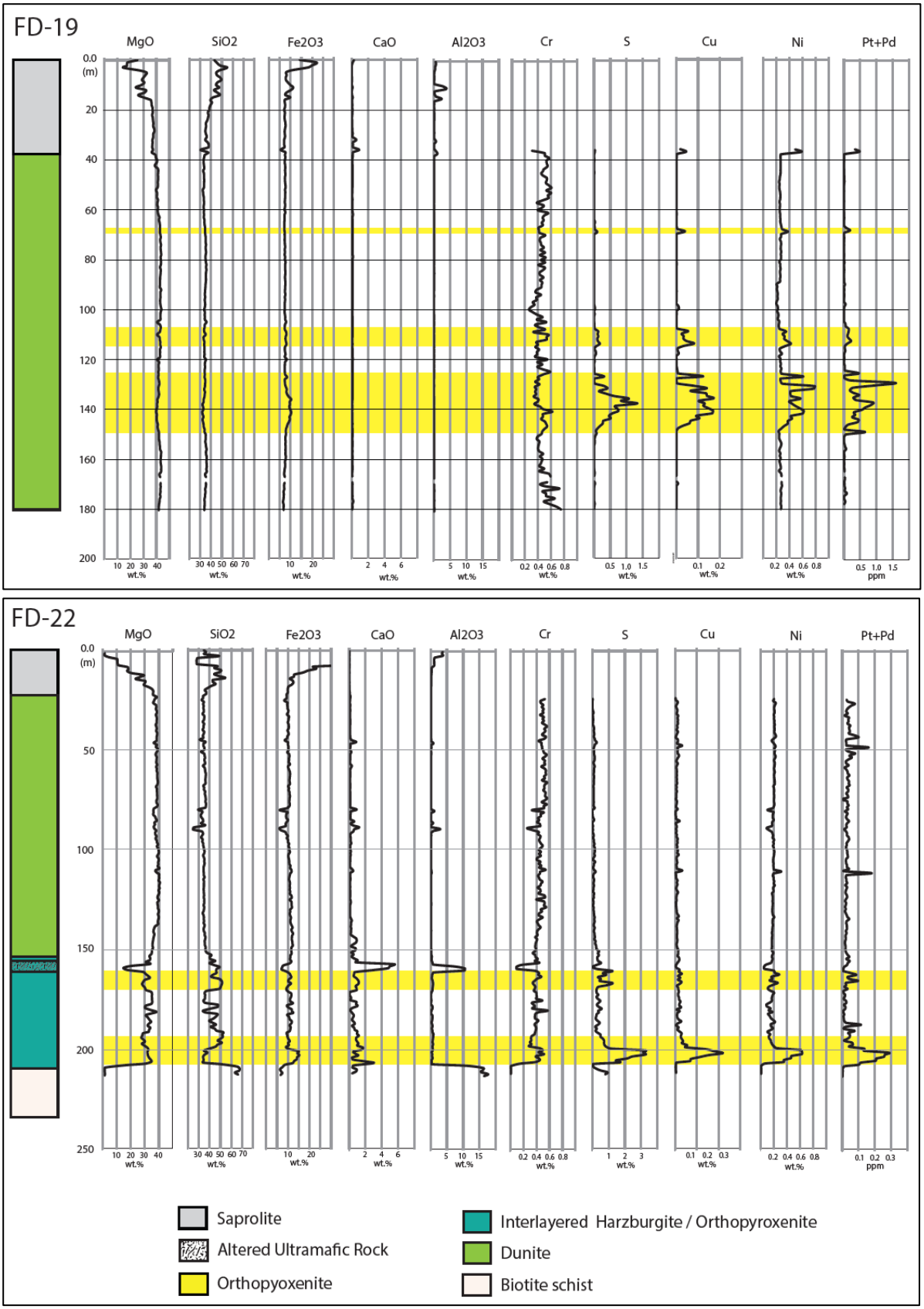

Figure 17. Strip logs of drill holes FD-19 and FD-22 of the Morro do Leme intrusion and its MgO, SiO2, Fe2O3, CaO, Al2O3, Cr, S, Cu, Ni and Pt + Pd geochemical results. Sulfide-rich zones are indicated by yellow shade. Data from Anglo American internal reports. See Figs. 14 and 16 for location of drill holes.

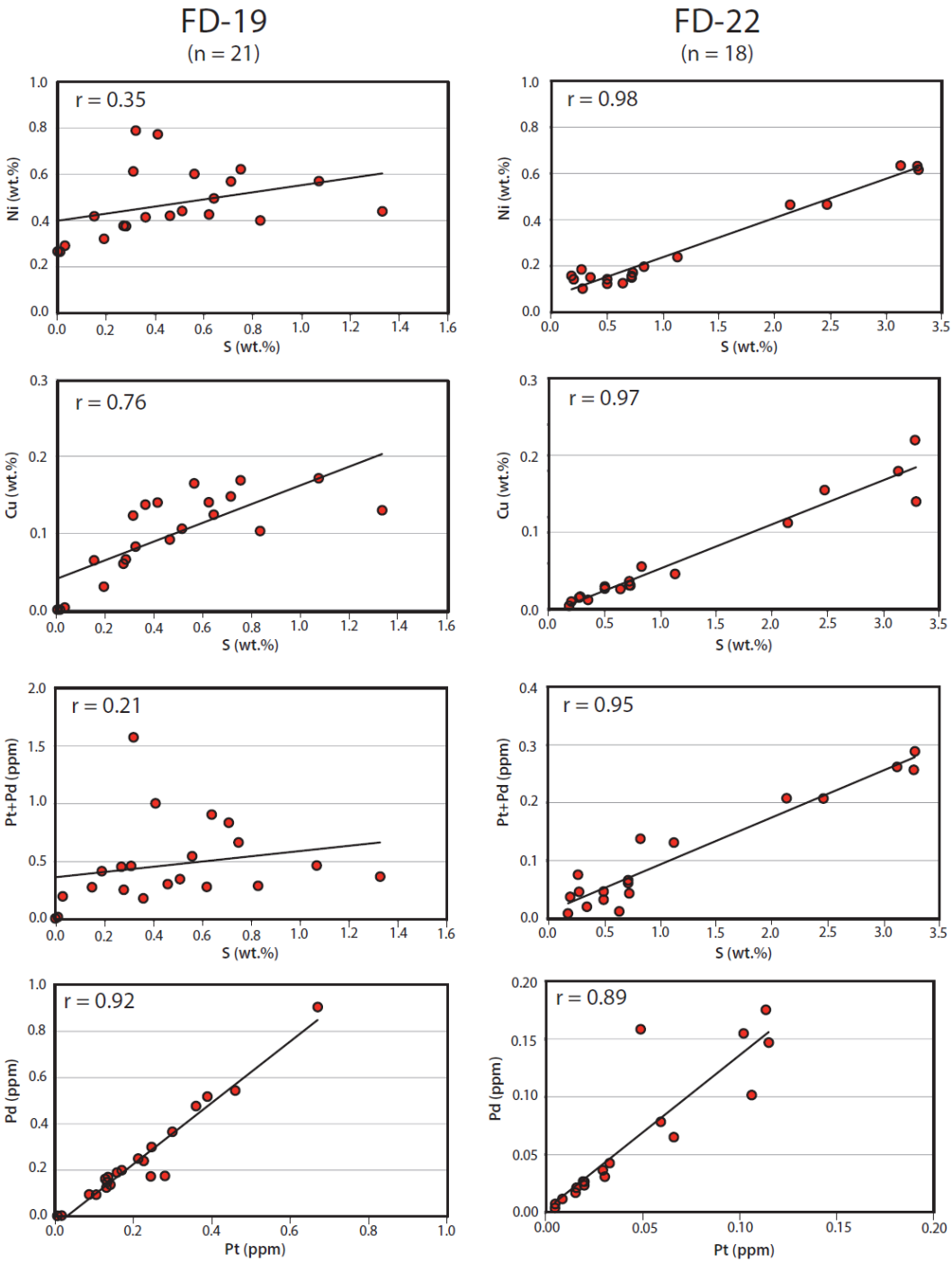

Figure 18. Plots of Ni, Cu and Pt + Pd vs S for samples of cumulate rocks from drill holes FD-19 and FD-22 of the Morro do Leme intrusion. Trend lines correspond to the linear correlation for samples of ultramafic rocks. Data from Anglo American internal reports. See Fig. 16 for location of drill holes, and Fig. 17 for the strip log and distribution of geochemical results.

lowermost dunite (Fig. 17b). This sulfide zone hosts a mineralized intersection with 17 m at 0.28 wt% Ni, 0.06 wt% Cu, and 0.11 ppm Pt+ Pd (i.e., 190–208 m in Fig. 17b). This mineralized intersection includes a sulfide-rich portion (~5–10 vol% sulfides) at the lower contact of the sulfide zone, with 7 m at 0.50 wt% Ni, 0.13 wt% Cu, and 0.20 ppm Pt+ Pd (see Section B in

Fig. 16). The sulfide assemblage and textures of the mineralized intersection are similar to those described in the FD-19, consisting of interstitial to net-textured sulfide blebs at olivine and/or orthopyroxene grain boundaries. Primary sulfides consist mainly of pyrrhotite (>90 vol%) with minor proportions of variable amounts of pentlandite and chalcopyrite. The plots of Ni, Cu and Pt + Pd with S (Fig. 18) indicate strong positive correlations in the mineralized intersection (r = 0.98, 0.97, and 0.95, respectively). These strong positive correlations of S–Ni, S–Cu and S–Pt + Pd plots allow the calculation of approximate tenors for Ni (~6.5 wt %), Cu (~2.0 wt%) and Pt + Pd (~3 ppm) by linear regression. The contents of Pt and Pt in these core samples have high positive correlation (r = 0.89) and Pt/Pd ratios close to 1 (average = 0.78).

5.4.2 Olivine Composition

Analyses of olivine were acquired in unweathered drill core samples of olivine cumulates from the Morro do Leme eastern body and from a satellite body associated with a magnetic anomaly (see Table 1 for representative analyses).

Olivine was analyzed in 10 samples of adcumulate dunites from drill holes FS01 (7 samples; 43 analyses) and FS03 (3 samples; 22 analyses) in the Morro do Leme intrusion. These samples, selected after petrographic studies of 22 samples, are moderately serpentinized dunite with domains of well-preserved olivine crystals. Olivine has primitive compositions (i.e., high Fo content) and minor compositional variations in samples from both drill holes, ranging from Fo 91.6 to Fo93.4 and Fo91.2 to Fo91.9 in FS01 and FS03 drill holes, respectively (Fig. 19). Nickel and Fo contents are positively correlated in both drill holes, with nickel contents ranging from 0.30 to 0.37 wt% and 0.26 to 0.33 wt% in FS01 and FS03 drill holes, respectively (Fig. 19). A systematic evaluation of cryptic variation of olivine is hampered by the restricted distribution of olivine preserved from serpentinization throughout these drill holes.

Analyses of olivine were carried out in drill core samples (6 samples; 63 analyses) of partially serpentinized dunite from a covered ultramafic body located to the south of the Morro do Leme intrusion. Although not investigated in detail, these adcumulate dunites are associated with a magnetic anomaly interpreted as a satellite intrusion. Olivine has moderately primitive compositions ranging from Fo82.5 to Fo87.9, low nickel contents ranging from <0.01 wt% (i.e., below detection limit of our analyses) up to 0.16 wt% and has poorly correlated Ni and Fo contents (Fig. 19). Olivine compositions for individual samples of the satellite intrusion have relatively large range (see ellipses in Fig. 19).

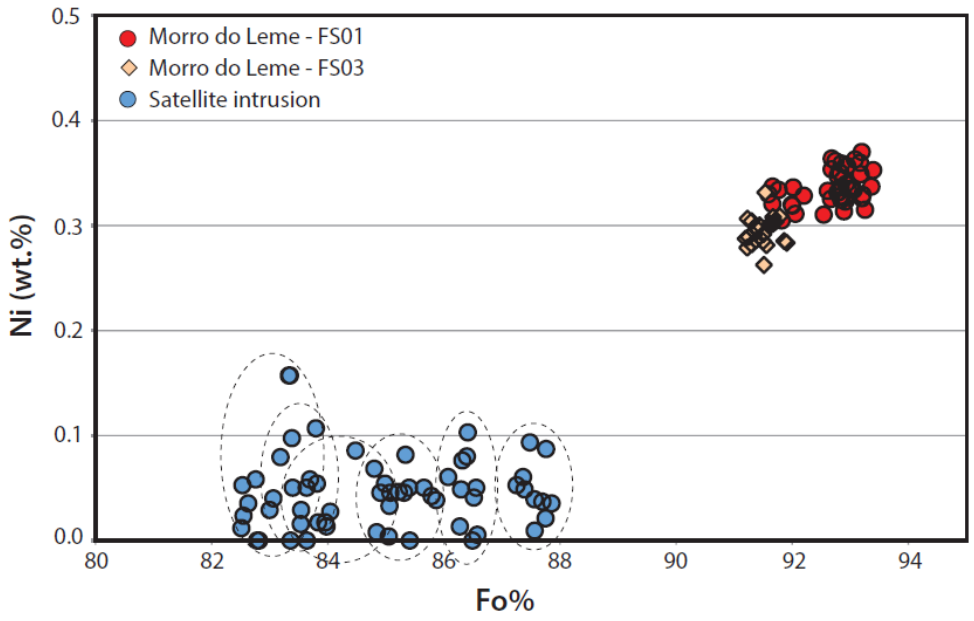

Figure 19. Plot of Fo versus Ni content of olivine for drill core samples of dunite from the Morro do Leme intrusion and satellite body. Dashed ellipses indicate compositions for each sample of the satellite intrusion.

Table 1. Representative analyses of olivine of the Morro do Leme intrusion and satellite body.

Sample		81232	81233	81234	81235	81238	81239	81240	ML03-55	ML03-58	ML03-63	MLST-15	MLST-14	MLST-12	MLST-6	MLST-5
Intrusion		ML	ML	ML	ML	ML	ML	ML	ML	ML	ML	ST	ST	ST	ST	ST
Drill hole		FS01	FS01	FS01	FS01	FS01	FS01	FS01	FS03	FS03	FS03	NA	NA	NA	NA	NA
Depth		29.5	42.0	51.5	60.5	183.5	188.0	195.0	55.2	58.5	63.9	NA	NA	NA	NA	NA
Rock		Dunite	Dunite	Dunite	Dunite	Dunite	Dunite	Dunite	Dunite	Dunite	Dunite	Dunite	Dunite	Dunite	Dunite	Dunite
SiO2	wt.%	41.41	41.79	41.86	41.88	41.76	41.74	41.69	41.82	41.07	41.35	40.22	40.05	39.68	39.86	40.97
Cr2O3	wt.%	0.03	<0.01	<0.01	<0.01	0.06	0.04	0.01	<0.01	0.12	<0.01	<0.01	0.02	<0.01	0.04	0.01
FeO	wt.%	7.99	7.71	6.90	6.66	6.82	6.74	6.96	8.32	8.38	8.08	13.89	15.23	15.98	15.34	11.91
MnO	wt.%	0.13	0.10	0.11	0.08	0.09	0.11	0.05	0.11	0.09	0.08	0.18	0.21	0.30	0.20	0.18
MgO	wt.%	49.66	50.52	51.07	50.74	50.90	50.41	50.74	50.11	49.28	50.42	45.88	44.77	43.87	45.15	47.00
NiO	wt.%	0.42	0.43	0.46	0.43	0.43	0.41	0.45	0.38	0.37	0.38	0.10	0.14	<0.01	0.01	0.12
Total	wt.%	99.65	100.55	100.39	99.79	100.06	99.45	99.89	100.74	99.31	100.32	100.27	100.41	99.82	100.59	100.18
Normalization based on four oxygens																
Si	apfu	1.010	1.008	1.008	1.013	1.009	1.013	1.009	1.010	1.007	1.003	0.991	0.992	0.992	0.986	0.999
Cr	apfu	0.001	<0.001	<0.001	<0.001	0.001	0.001	<0.001	<0.001	0.002	<0.001	<0.001	<0.001	<0.001	0.001	<0.001
Fe	apfu	0.163	0.156	0.139	0.135	0.138	0.137	0.141	0.168	0.172	0.164	0.286	0.315	0.334	0.317	0.243
Mn	apfu	0.003	0.002	0.002	0.002	0.002	0.002	0.001	0.002	0.002	0.002	0.004	0.004	0.006	0.004	0.004
Mg	apfu	1.805	1.817	1.833	1.829	1.833	1.824	1.830	1.803	1.801	1.822	1.685	1.652	1.635	1.664	1.708
Ni	apfu	0.008	0.008	0.009	0.008	0.008	0.008	0.009	0.007	0.007	0.007	0.002	0.003	<0.001	<0.001	0.002
Total	apfu	2.990	2.991	2.991	2.987	2.991	2.985	2.990	2.990	2.991	2.998	2.968	2.966	2.967	2.972	2.956
Fo	%	91.59	92.02	92.85	93.06	92.92	92.91	92.81	91.38	91.20	91.67	85.34	83.80	82.78	83.84	87.48
Ni	wt.%	0.33	0.34	0.36	0.33	0.34	0.32	0.35	0.30	0.29	0.30	0.08	0.11	<0.01	0.01	0.09

Code: ML = Morro do Leme intrusion; ST = satellite body; NA = not available.

5.5 Bulk Rock Lithogeochemistry

Whole-rock chemical compositions were obtained from 13 drill core samples representative of ultramafic rocks of the Morro Sem Boné intrusion (Table 2). The compositional variations of major elements and compatible trace elements (e.g., Ni, Cr) are consistent with those from the larger dataset of drill core assays previously presented for each intrusion. The plot of MgO vs

FeO of these samples and the compositional range of assays of ultramafic rocks from drill hole FD-01 (Fig. 20) are consistent with rocks consisting of variable proportions of cumulus olivine and orthopyroxene (i.e., dunite, harzburgite and orthopyroxenite). Dunites have very high MgO contents, with compositions normalized to 100% on an anhydrous base ranging from 45.9 to 48.3 wt %, and Mg# from 0.78 to 0.84. These compositions are close to the compositions of olivines from dunites of the Morro do Leme (Fig. 20; note the compositional shift of dunite compositions recalculated to 100% on an anhydrous base). Higher contents of FeO and higher Mg# in dunites compared with olivine compositions may result in part from the presence of disseminated sulfides and chromite in these rocks. The contents of incompatible major and trace elements are very low for the analyzed ultramafic rocks (Table 2), with values commonly below or close to their lower detection limits in the analyses. Very low contents of incompatible trace elements (e.g., REE, Zr, Th, Nb), an expected result for olivine adcumulates, compromise their use for petrological studies.

Analyses of trace elements throughout the entire drill hole FD-15 show their distributions in the Mamão intrusion, including ultramafic and country rocks. Representative whole rock analyses and the distribution of selected elements are shown in Table 2 and Fig. 21, respectively. The distribution of incompatible trace elements (e.g., Th, Ce, Zr, Yb) follows the symmetrically zoned distribution of rock types and major elements in the Mamão intrusion (Fig. 11), consisting of very low contents in the central dunitic zone and progressively higher contents toward the contacts with country rocks, where harzburgite and orthopyroxenite predominate. Bulk rock analyses of dunites have incompatible trace element contents commonly below or close to their lower detection limits in the analyses, similar to results obtained for dunite in the Morro Sem Boné intrusion (Table 2). Incompatible trace element contents in the country rocks are much higher than those from ultramafic rocks, as indicated by analyses of biotite schists close to the lower contact of FD-15 (Fig. 21). The distribution of Cr indicates the sharp contact between chromite-bearing ultramafic rocks (Cr > 0.35 wt% through the interval close to the contact) and biotite schists of the country rocks (Cr < 0.02 wt%). One sample in the contact zone includes both ultramafic and country rocks and has an intermediate Cr content (see the location of the lower contact in Fig. 21). The plots of Cr vs selected incompatible elements for samples located in the contact zone (Fig. 21) illustrate the sharp difference in incompatible trace elements between ultramafic cumulates and country rocks, with contents in the country rocks in the range of 1–2 orders of magnitude higher.

Chondrite-normalized REE patterns of ultramafic rocks and biotite schists emphasize the higher contents of incompatible trace elements in the country rocks (Fig. 22a and b). On the other hand, REE patterns of ultramafic cumulates (Fig. 22a) and biotite schists (Fig. 22b) are similar, with positive slope for LREE (average chondrite-normalized La/Sm = 2.22 for ultramafic rocks and 2.60 for biotite schists), positive slope for HREE (average chondrite-normalized Gd/Yb = 1.70 and 1.32, respectively) and distinctively negative anomaly of Eu. Apart from highly distinct whole rock contents, mantle-normalized incompatible trace element patterns of ultramafic rocks (Fig. 22c) and biotite schists (Fig. 22d) are remarkably similar. They all have fractionated patters indicated by relative enrichment in LREE, U and Th and pronounced Nb and Ta negative anomalies, as well as distinctively negative anomalies of Sr, Eu and Ti.

6. Discussion

6.1 Relative Timing of Ultramafic Magmatism and Regional Tectonism and Metamorphism

The tectonic emplacement of the ultramafic bodies of the Morro Sem Boné, Morro do Leme and satellite intrusions as slices of ophiolites along the Guaporé Suture Zone, as suggested by Rizzotto and Hartmann (2012) for the Trincheira Complex, are not supported by field relations described in this study. The intrusion of mafic-ultramafic magmas into volcanic-sedimentary host rocks is indicated by partially assimilated country rocks in contact zones, as well as consistent inward sequence of ultramafic cumulates. These field relations are so far restricted to the ultramafic intrusions investigated in this study and, therefore, they do not apply to the mafic-ultramafic ophiolites of the Trincheira Complex described elsewhere by Rizzotto and Hartmann (2012). Considering the broad consensus on the need to incorporate crustal S to generate Ni–Cu–PGE deposits (e.g., Barnes and Robertson, 2019; Lesher, 2019), and the abundance of sulfides in the country rocks, primary intrusive contacts between the ultramafic rocks and metasediments are critical to support the following discussions regarding the origin of Ni–Cu-PGE mineralization of the ultramafic intrusions and their potential to host economic deposits.

On the other hand, the relative timing of ultramafic intrusions and regional tectonism remains somewhat contentious due to poor outcropping and limited drilling. Detailed structural studies of country rocks and ultramafic bodies are hampered by widespread sedimentary covers.

Table 2. Chemical composition of representative drill core samples of the ultramafic intrusions.

Intrusion		MSB	MSB	MSB	MSB	MSB	MSB	MSB	MSB	MSB	MSB	MSB	MSB	MSB	Mamão	Mamão	Mamão	Mamão	Mamão	Mamão	Mamão	CR	CR	CR	CR
Drill Hole		FD001	FD001	FD001	FD001	FD001	FD001	FD001	FD001	FD001	FD001	FD001	FD001	FD001	FD015	FD015	FD015	FD015	FD015	FD015	FD015	FD015	FD015	FD015	FD015
Depth	(m)	150.4	156.8	166.2	185.4	227.3	246	299.6	352	249.4	272.4	334.3	392.75	400.3	302	312	313	314	315	315.8	316.6	320	321	322	323
Rock		Dunite	Dunite	Dunite	Dunite	Dunite	Dunite	Dunite	Dunite	Opxt	Opxt	Opxt	Opxt	Hzb	UM	UM	UM	UM	UM	UM	UM	XT	XT	XT	XT
SiO2	wt.%	35.39	32.24	34.49	34.55	32.55	33.24	33.33	33.51	49.95	52.19	51.32	51.00	43.20	43.71	39.72	40.09	39.00	40.26	40.55	42.41	54.49	47.30	51.69	53.24
Al2O3	wt.%	0.57	0.06	0.07	0.07	0.11	0.04	0.08	0.06	0.62	0.44	0.60	0.51	0.31	7.15	3.55	2.10	1.84	2.07	2.16	3.51	18.79	22.72	20.99	22.91
Fe2O3	wt.%	8.21	9.25	8.83	9.12	9.02	12.20	10.63	10.50	12.45	10.90	12.14	12.93	13.24	12.79	13.05	12.90	14.43	13.38	13.09	13.47	10.63	13.28	10.99	8.74
MgO	wt.%	38.38	39.74	41.03	39.94	38.87	39.21	39.33	39.87	28.93	31.15	29.40	30.17	33.04	27.36	30.45	31.36	31.85	31.99	32.30	27.65	2.73	2.38	2.31	2.02
CaO	wt.%	0.43	0.30	0.10	0.05	0.08	0.13	0.14	0.06	0.60	0.81	0.88	0.74	0.43	0.51	3.25	3.29	2.05	2.51	1.85	3.62	1.29	1.02	1.50	1.17
Na2O	wt.%	< 0.01	< 0.01	< 0.01	< 0.01	< 0.01	< 0.01	< 0.01	< 0.01	0.05	0.04	0.03	0.02	0.02	0.09	0.03	0.02	0.02	0.02	0.02	0.07	5.55	3.77	4.96	3.96
K2O	wt.%	< 0.01	< 0.01	< 0.01	< 0.01	< 0.01	< 0.01	< 0.01	< 0.01	0.09	0.05	0.05	0.03	< 0.01	0.06	0.01	<0.01	<0.01	<0.01	<0.01	0.04	3.23	5.20	3.69	4.06
TiO2	wt.%	0.03	0.01	0.01	0.01	0.01	0.01	0.01	0.01	0.07	0.05	0.06	0.06	0.04	0.51	0.23	0.11	0.11	0.13	0.13	0.18	1.26	1.31	1.08	1.13
P2O5	wt.%	0.03	0.02	0.02	0.02	0.02	0.03	0.03	0.02	0.01	< 0.01	< 0.01	0.01	0.01	0.14	0.07	0.02	0.02	0.03	0.04	0.07	0.05	0.15	0.16	0.08
MnO	wt.%	0.09	0.14	0.09	0.10	0.15	0.09	0.10	0.13	0.18	0.19	0.21	0.24	0.21	0.11	0.17	0.17	0.14	0.15	0.14	0.16	0.08	0.07	0.06	0.06
Cr2O3	wt.%	0.44	0.43	0.35	0.37	0.75	0.33	0.29	0.31	0.40	0.37	0.41	0.42	0.37	0.36	0.51	0.47	0.67	0.61	0.71	0.62	0.02	0.02	0.01	0.01
LOI	wt.%	15.50	16.70	14.10	14.90	17.60	13.90	15.10	14.60	6.00	3.10	4.00	3.20	8.50	6.60	8.30	8.80	9.10	8.10	8.30	7.40	1.60	2.30	2.20	2.30
Total	wt.%	99.12	98.89	99.09	99.14	99.17	99.18	99.04	99.08	99.35	99.30	99.11	99.33	99.37	99.39	99.34	99.33	99.23	99.25	99.29	99.20	99.72	99.52	99.64	99.68
C	wt.%	1.05	0.68	0.22	0.53	1.49	0.33	0.2	0.13	0.11	0.13	0.05	0.01	0.06	0.12	0.23	0.36	0.11	0.22	0.15	0.21	0.04	0.37	0.42	0.25
S	wt.%	0.2	0.41	0.06	0.08	0.19	0.98	0.5	0.11	1.21	0.83	1.44	1.36	1.02	0.38	0.41	0.22	0.39	0.20	0.17	1.43	1.11	2.39	1.66	0.94
Ba	ppm	13	<1	<1	<1	<1	<1	1	<1	6	3	2	3	<1	4	2	1	<1	1	<1	5	661	2172	1259	1410
Sr	ppm	15.8	11.6	1.9	1.5	2.1	2.9	1.5	1	10.4	7.7	3.7	3.1	1.4	47.4	94.1	75.7	50	66.5	42.4	76.5	231.1	226.7	318.2	340
Zr	ppm	1.9	0.6	0.1	0.2	0.2	0.6	0.7	0.1	0.7	0.3	0.6	0.6	0.2	38.8	29	16.9	20.2	26.8	22.9	27.4	249.7	246.8	252.9	307.2
Y	ppm	0.9	0.1	0.1	<0.1	0.1	<0.1	0.2	<0.1	0.8	0.4	0.8	0.6	0.3	9.7	14.8	6.1	5.7	8.7	6.2	7.3	46.6	47.7	42.5	44.5
Nb	ppm	0.5	0.3	0.2	<0.1	<0.1	<0.1	<0.1	<0.1	<0.1	<0.1	<0.1	<0.1	<0.1	2.3	2.1	0.7	0.7	0.9	1.0	1.3	17.3	15.3	13.0	14.5
Sc	ppm	5	2	2	2	2	2	2	3	12	7	10	10	8	29	18	15	13	15	12	14	35	31	25	28
Cs	ppm	0.4	<0.1	<0.1	<0.1	<0.1	<0.1	<0.1	<0.1	3.1	1.5	0.9	0.9	<0.1	0.8	0.2	0.3	0.1	0.2	0.3	1.1	21.4	16.2	12.3	6.6
Ga	ppm	1.3	<0.5	<0.5	<0.5	<0.5	<0.5	<0.5	<0.5	1.6	1.1	1.5	1.5	1	11	4.1	2.7	1.9	2.4	2.6	3.7	15.9	24.4	22.2	25.7
Hf	ppm	<0.1	<0.1	<0.1	<0.1	<0.1	<0.1	<0.1	<0.1	<0.1	<0.1	<0.1	<0.1	<0.1	1.2	1.2	0.6	0.7	1.2	0.9	0.9	7.3	7.7	7.3	9.3
Rb	ppm	1.5	0.1	<0.1	<0.1	0.1	<0.1	0.3	<0.1	7.3	3.8	2.7	3.4	<0.1	3.2	0.5	0.7	0.4	0.5	0.8	2.6	136.6	150.9	112.2	96.3
Sn	ppm	<1	<1	<1	<1	<1	<1	<1	<1	<1	<1	<1	<1	<1	<1	<1	<1	<1	<1	<1	<1	2	2	2	2
Ta	ppm	0.2	0.2	0.05	0.05	0.05	0.05	0.05	0.05	0.05	0.05	0.05	0.05	0.05	0.1	0.2	0.1	<0.1	<0.1	0.1	0.1	1.2	1.1	0.8	0.9
Th	ppm	0.1	0.1	0.1	0.1	0.1	0.1	0.1	0.1	0.1	0.1	0.1	0.1	0.1	1.4	1.8	0.7	0.5	0.5	0.5	0.8	10.3	13.7	13.3	13.4
U	ppm	<0.1	<0.1	<0.1	<0.1	<0.1	<0.1	<0.1	<0.1	<0.1	<0.1	<0.1	<0.1	<0.1	0.6	0.6	0.3	0.2	0.2	0.3	0.5	2.8	4.5	4.1	4.2
V	ppm	18	4	4	4	8	4	4	4	35	17	26	25	16	180	60	47	48	43	43	63	155	188	138	136
W	ppm	27.0	9.9	8.3	9.6	7.6	6.6	11.4	17.5	23.2	63.3	34.2	46.9	19.0	1.1	1.4	1.2	1.0	1.1	0.8	1.1	2.6	1.6	1.3	1.2
La	ppm	0.7	0.1	0.1	0.1	<0.1	<0.1	0.2	<0.1	0.1	0.2	0.1	<0.1	<0.1	8.5	10.8	4.2	4.7	6	5.1	5.7	30.8	40.9	39.7	41.9
Ce	ppm	1.5	0.1	0.1	0.1	<0.1	<0.1	0.2	0.1	0.2	0.3	0.2	<0.1	<0.1	22	27.2	9.4	10.3	13.7	11.7	14	67.1	94.7	88.3	98.6
Pr	ppm	0.19	0.03	<0.02	<0.02	<0.02	<0.02	0.02	<0.02	<0.02	0.03	<0.02	<0.02	<0.02	2.96	3.62	1.16	1.24	1.66	1.4	1.73	7.97	11.24	10.77	11.6
Nd	ppm	0.5	<0.3	<0.3	<0.3	<0.3	<0.3	<0.3	<0.3	<0.3	<0.3	<0.3	<0.3	<0.3	13.5	16.2	4.7	4.6	6.4	5.6	6.7	30.9	43.5	42.5	45.1
Sm	ppm	0.2	<0.05	<0.05	<0.05	<0.05	<0.05	<0.05	<0.05	<0.05	<0.05	<0.05	<0.05	<0.05	2.78	3.82	1.15	1.24	1.63	1.37	1.73	8.17	10.11	9.7	9.96
Eu	ppm	0.05	<0.02	<0.02	<0.02	<0.02	<0.02	0.02	<0.02	<0.02	0.02	<0.02	<0.02	<0.02	0.29	0.43	0.29	0.27	0.34	0.26	0.25	1.20	1.69	1.63	1.90
Gd	ppm	0.21	<0.05	<0.05	<0.05	<0.05	<0.05	<0.05	<0.05	0.05	<0.05	<0.05	<0.05	<0.05	2.56	3.05	1.1	1.05	1.57	1.16	1.49	7.81	8.84	8.18	8.28
Tb	ppm	0.04	<0.01	<0.01	<0.01	<0.01	<0.01	<0.01	<0.01	0.01	<0.01	0.02	<0.01	<0.01	0.38	0.52	0.2	0.2	0.29	0.2	0.24	1.47	1.55	1.42	1.47
Dy	ppm	0.14	<0.05	<0.05	<0.05	<0.05	<0.05	<0.05	<0.05	0.12	<0.05	0.1	<0.05	0.05	1.98	2.84	1.08	1.07	1.61	1.11	1.55	8.84	9.06	8.06	8.53
Ho	ppm	0.03	<0.02	<0.02	<0.02	<0.02	<0.02	0.02	<0.02	0.03	<0.02	0.03	<0.02	<0.02	0.41	0.54	0.23	0.2	0.31	0.22	0.25	1.82	1.83	1.57	1.68
Er	ppm	0.15	<0.03	0.04	<0.03	<0.03	<0.03	<0.03	<0.03	0.16	0.08	0.11	0.08	0.08	1.15	1.53	0.61	0.65	0.96	0.65	0.79	5.56	5.56	4.42	5.05
Tm	ppm	0.03	<0.01	<0.01	<0.01	<0.01	<0.01	<0.01	<0.01	0.02	0.005	0.02	0.01	<0.01	0.15	0.24	0.09	0.09	0.14	0.1	0.12	0.92	0.86	0.72	0.81
Yb	ppm	0.09	<0.05	<0.05	<0.05	<0.05	<0.05	<0.05	<0.05	0.15	0.08	0.14	<0.05	0.1	0.92	1.35	0.58	0.59	0.89	0.64	0.71	5.98	5.37	4.43	5.19
Lu	ppm	0.03	<0.01	0.01	<0.01	0.01	<0.01	<0.01	<0.01	0.03	0.02	0.03	0.02	0.01	0.14	0.19	0.09	0.09	0.13	0.08	0.12	0.90	0.86	0.70	0.81
Ni	ppm	1601	1728	1549	1116	1334	1059	2108	1441	466	710	2003	817	679	716	903	844	1296	1216	1453	2210	58	110	55	39

Code: Opxt = orthopyroxenite; Hzb = harzburgite; UM = utramafic rock; XT = biotite schist.

Nevertheless, the ultramafic intrusions show remarkably well preserved primary magmatic layering and textures (Figs. 4 and 7–9). Except for minor discrete shear zones, the ultramafic rocks have primary textures and minerals largely preserved, contrasting with highly foliated biotite schists in the country rocks (Fig. 15e). The contrast in deformation between mafic-ultramafic intrusions and metapelitic country rocks is common in metamorphic terrains (e.g., Mota-e-Silva et al., 2013; Matos and Ferreira Filho, 2018) and results from their distinct rheological properties (e.g., Passchier et al., 1990). The deformation observed in the ultramafic intrusions, largely taken up on discrete shear zones crosscutting the intrusions or located at their margins, indicates that they are affected by the regional tectonism. In addition, fine-grained ultramafic rocks at the intrusions margins or within shear zones have metamorphic assemblages consisting mainly of amphiboles (hornblende + cummingtonite), indicating their recrystallization under amphibolite facies of regional metamorphism, which is consistent with metamorphic parageneses described in country rocks metapelites (i.e., staurolite + garnet + biotite + muscovite + quartz). Therefore, the available results suggest that both country rocks and the ultramafic intrusions were deformed and metamorphosed during the regional accretional-collisional orogeny (Rizzotto and Hartmann, 2012; Rizzotto et al., 2013).

6.2 Magmatic Structure

Several ultramafic bodies were discovered during exploration work carried out in the investigated region. Results point out that they consist of very similar rock types that occur in magmatic structures with distinct size and morphology, as illustrated by the three ultramafic intrusions detailed in our study. A remarkable common feature of these ultramafic intrusions is that they are composed mainly of olivine cumulates. A detailed study of these magmatic structure is limited by (1) poor outcropping due regional sedimentary cover; (2) thick weathering and laterization of the exposed intrusions; (3) limited drilling; (4) possible tectonic disruptions of the original magmatic structure; (5) the erosion level. Keeping in mind these limitations, our results provide important constraints for the magmatic structure of three ultramafic intrusions.

The MSB forms an elongated 6 km long by ~1 km wide intrusion with poorly constrained but predominantly sub-horizontal layering (Figs. 3 and 5). The exposed and drilled portion of the MSB is weakly differentiated and composed mainly of dunite with minor harzburgite and orthopyroxenite, resembling komatiitic channelized facies (e.g., Mt Keith and Perseverance in Western Australia; Lesher, 2019) or the ultramafic intrusions of the Thompson Nickel Belt in Manitoba, Canada (Layton-Matthews et al., 2010). These olivine-rich bodies are interpreted as

the result of olivine accumulation in volcanic or intrusive flow-through magma channels (e.g., Lesher, 2019). One should keep in mind that we are describing the remnants of MSB at the actual erosional level, such that an overlying sequence of more fractionated rocks may have existed in the original magmatic structure. In this context, the thick pile of olivine cumulates of the MSB may also represents the basal portion of a layered intrusion, as exemplified by the lower zones of several medium- (e.g., Mirabela Complex; Barnes et al., 2011) to large-sized (e.g., Great Dyke: Wilson, 1982; Niquelândia Complex: Ferreira Filho et al., 1992, 2010) intrusions. Because the lower portions of this elongated structure (i.e., length > width) with likely sub-horizontal axis is not constrained, it may be interpreted as an elongated funnel or a boat-shaped body (see schematic magmatic structures in Barnes et al., 2016).

The magmatic structure of the Morro do Leme intrusion, which consists of three mapped bodies associated with a large magnetic anomaly (Fig. 14), is poorly constrained. The exposed and drilled portions of the three mapped intrusions are very similar to the MSB, consisting of weakly differentiated sequences of ultramafic rocks composed mainly of dunite with minor harzburgite and orthopyroxenite. The basal contact of the southern ultramafic body of the Morro do Leme intrusion exhibits an upward variation characterized by a ~60 m basal zone of interlayered dunite, harzburgite and orthopyroxenite that grades into homogeneous dunite (Figs. 16 and 17). Similar variation of rock types and whole-rock compositional trends have been observed in preserved contact zones of the MSB and other satellite intrusions, suggesting that a consistent inward increase in the amount of cumulus olivine is a primary characteristic of their contact zones.

The covered Mamão intrusion consists of a thin (~140 m thick) ultramafic body associated with a ~5 km long magnetic anomaly (Fig. 11a). The magmatic structure delineated by drill core logs indicates a 40◦ dipping ultramafic body hosted by biotite schists (Fig. 11b). The intrusion is symmetrically differentiated consisting mainly of dunite with interlayered harzburgite and orthopyroxenite in the upper and lower border zones (Fig. 12). The rock types and differentiation trend observed in these border zones are analogous to what is described in the basal portion of the Morro do Leme intrusion (see Section B in Fig. 16; and FD-22 in Fig. 17). The progressive decrease in MgO content and increase in SiO2, CaO and Al2O3 contents toward the margins of mafic-ultramafic intrusions (Figs. 12 and 16) is commonly ascribed to processes linked to the effect of cooler country rocks and/or flow differentiation in magma conduits (e.g., Latypov, 2003; Barnes and Robertson, 2019). The very high MgO contents (~40 wt%) characteristic of adcumulate dunite in the MSB and Morro do Leme intrusions do not occur in the Mamão

intrusion, which is characterized by maximum MgO contents of ~35 wt%. This compositional difference is consistent with a smaller intrusion (i.e., compared with MSB and Morro do Leme) where the conditions for the development of olivine adcumulates with very high Fo contents are less favored. Because the Mamão intrusion was intersected just by few deep drill holes, the exact ratio of width and height of this elongated (i.e., length ≫ than width and height) is not constrained. Therefore, this symmetrically zoned elongated structure may correspond to tube-like conduits or chonoliths like the Limoeiro (Mota-e-Silva et al., 2013) and Nebo-Babel (Seat et al., 2007) intrusions, or channelized sills (i.e., width ≫ height) like those from the Cape Smith belt (e.g., Lesher, 2007).

Independent of the exact geometry of the magmatic structures, very similar sequences of ultramafic cumulates support the interpretation that the MSB, Morro do Leme, and satellite intrusions belong to a complex magma transport network of primitive magma through the crust. The Mamão and other satellite intrusions may represent the magma conduits of this system, while larger bodies the staging magma chambers.

6.3 Constraints for the Parental Magma of the Ultramafic Intrusions

The abundance of ultramafic cumulates with high MgO contents is a distinctive feature of the Morro Sem Boné, Morro do Leme and satellite intrusions. All the intrusions investigated in this study consist of olivine and orthopyroxene cumulates, without plagioclase-bearing fractionated rocks. Although the predominance of ultramafic cumulates may be biased by exploration focused on outcropping nickel laterite deposits and/or covered intrusions associated with high magnetic anomalies typical of ultramafic rocks, the rare occurrence of plagioclase-bearing rocks in this large area with abundant ultramafic intrusions is remarkable. Clusters of intrusions with the predominance of ultramafic cumulates are commonly associated with primitive parental magmas. Very high MgO contents and Mg# of dunites of the ultramafic intrusions, up to 45.9 wt% and 0.84 respectively (Fig. 20), are consistent with the very high forsterite content of olivines from dunites of the Morro do Leme intrusion (up to Fo93; Fig. 19). The composition of the most primitive olivine in the Morro do Leme intrusion ranks among the highest values reported in intrusions from different parts of the world, comparable with those reported for the Bushveld Complex (Fo91; Wilson, 2012), Great Dyke (Fo92; Wilson, 1982), ultramafic intrusions of Thompson Belt (Fo93; Lesher and Barnes, 2008), Ipueira-Medrado sill (Fo93; Marques and Ferreira Filho, 2003), Niquelândia Complex (Fo93; Ferreira Filho et al.,

2010) and layered intrusions in the Carajás Mineral Province (Fo91-93; Mansur and Ferreira Filho, 2016; Siepierski and Ferreira Filho, 2020). All these intrusions are considered to have high-MgO parental magmas originated from high-temperature mantle melting, as suggested for the intrusions of the Thompson belt (i.e., 22–23 wt% MgO; Lesher and Barnes, 2008). The Fo content of the most primitive olivine and the estimated range of MgO content for the parental magma of these intrusions are within the range of picrite and low-Mg komatiites, and higher than typical arc tholeiite magmas.

The broad composition of the parental magma of the ultramafic intrusions is also constrained by the crystallization sequence of the cumulate rocks. Cumulus minerals indicate that the sequence of crystallization consists of olivine + chromite, olivine + orthopyroxene + chromite, and orthopyroxene + chromite. Crystallization sequences dominated by orthopyroxene are characteristic of large PGE mineralized intrusions (e.g., Bushveld, Great Dyke, Stillwater; Eales and Cawthorn, 1996), and interpreted as the result of SiO2 enrichment of high-MgO magmas by assimilation of crustal rocks (Campbell, 1985). High-temperature primitive magmas facilitate the assimilation of pelitic to psamitic wall rocks (e.g., Williams et al., 1998), a process also recognized as the mechanism by which sulfur is transferred from country rocks to mafic-ultramafic magmas (e.g., Barnes et al., 2016; Lesher, 2017).

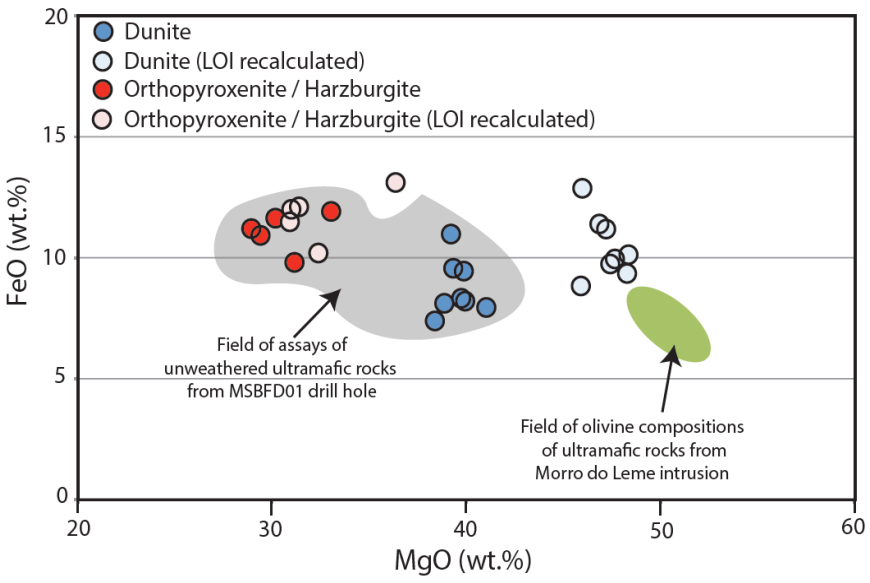

Figure 20. Plot of MgO vs FeO for samples of cumulate rocks from drill holes FD-01 of the Morro Sem Boné intrusion. The plot includes whole rock analyses from Table 2 and these results recalculated to 100% on an anhydrous base (LOI recalculated). Whole rock analyses are appropriate for comparison with the exploration results (where values for LOI are not available), while those recalculated to 100% on an anhydrous base provide a comparison with olivine compositions. The shaded area shows the compositional field of ultramafic rocks of FD-01 based on whole rock exploration analyses. The field of olivine compositions from the Morro do Leme intrusion is also indicated (see Table 1 and Fig. 19).

The assimilation of country rocks during the ascent and/or emplacement of the parental magma of the ultramafic intrusions is also suggested by lithogeochemical results. The REE and incompatible trace element patterns for the border zone of the Mamão intrusion and their country rocks have similar enough patterns (Fig. 22) to imply a significant contamination of the parental magma. Biotite schist, the common host rock of the ultramafic intrusions, has significantly higher content of incompatible elements than the ultramafic intrusions (Fig. 21). The content of trace elements in cumulate rocks may be modeled as the result of combined content of cumulate minerals and trapped intercumulus liquid (Barnes, 1986). The symmetric distribution of incompatible trace elements in the Mamão intrusion may be explained by the predominance of adcumulates in the central portions of the intrusion and progressively higher amounts of trapped intercumulus liquid toward the borders. Because REE and incompatible trace element patterns in the border zone of the Mamão intrusion and their country rocks are very similar (Fig. 22), we suggest that the content of incompatible trace elements in the parental magma largely results from assimilation of country rocks. The lack of data representative of the composition of the parental magma (e.g., chilled margins, melt inclusions) limit the attempt of modeling the assimilation process, a subject beyond the scope of this paper. Nevertheless, the ratios of some incompatible elements are consistent with contamination of the parental magma with country rocks. The plot of Nb/Yb versus Th/Yb, a commonly used discriminant diagram for arc-related magmas (Pearce, 2008), indicates a large overlap of incompatible trace element ratios between country rocks and ultramafic rocks (Fig. 23). Although our data may be used to suggest the contamination of the high-MgO parental magma with sedimentary country rocks, alternative interpretation should not be ruled out with currently available data. Considering the location of the intrusions in a craton margin (Rizzotto et al., 2013), our lithogeochemical data may also be interpreted as the result of an enriched subcontinental mantle lithosphere source. Cratonic margins may be affected by surrounding subduction and/or collision events, and the subcontinental lithospheric mantle could be refertilized (e.g., Tang et al., 2013).

6.4 Origin of Ni–Cu-PGE Sulfide Mineralization

Magmatic Ni–Cu-PGE sulfide deposits form by the accumulation of immiscible sulfide liquid from coexisting silicate magmas (e.g., Naldrett, 2004; Barnes and Lightfoot, 2005; Barnes et al., 2016). The bulk of sulfide mineralization in the ultramafic intrusions in this study comprises typical magmatic sulfides associated with cumulate rocks, consisting of interstitial (<5 vol%) to net-textured (5–10 vol%) sulfides hosted by dunite, harzburgite or orthopyroxenite.

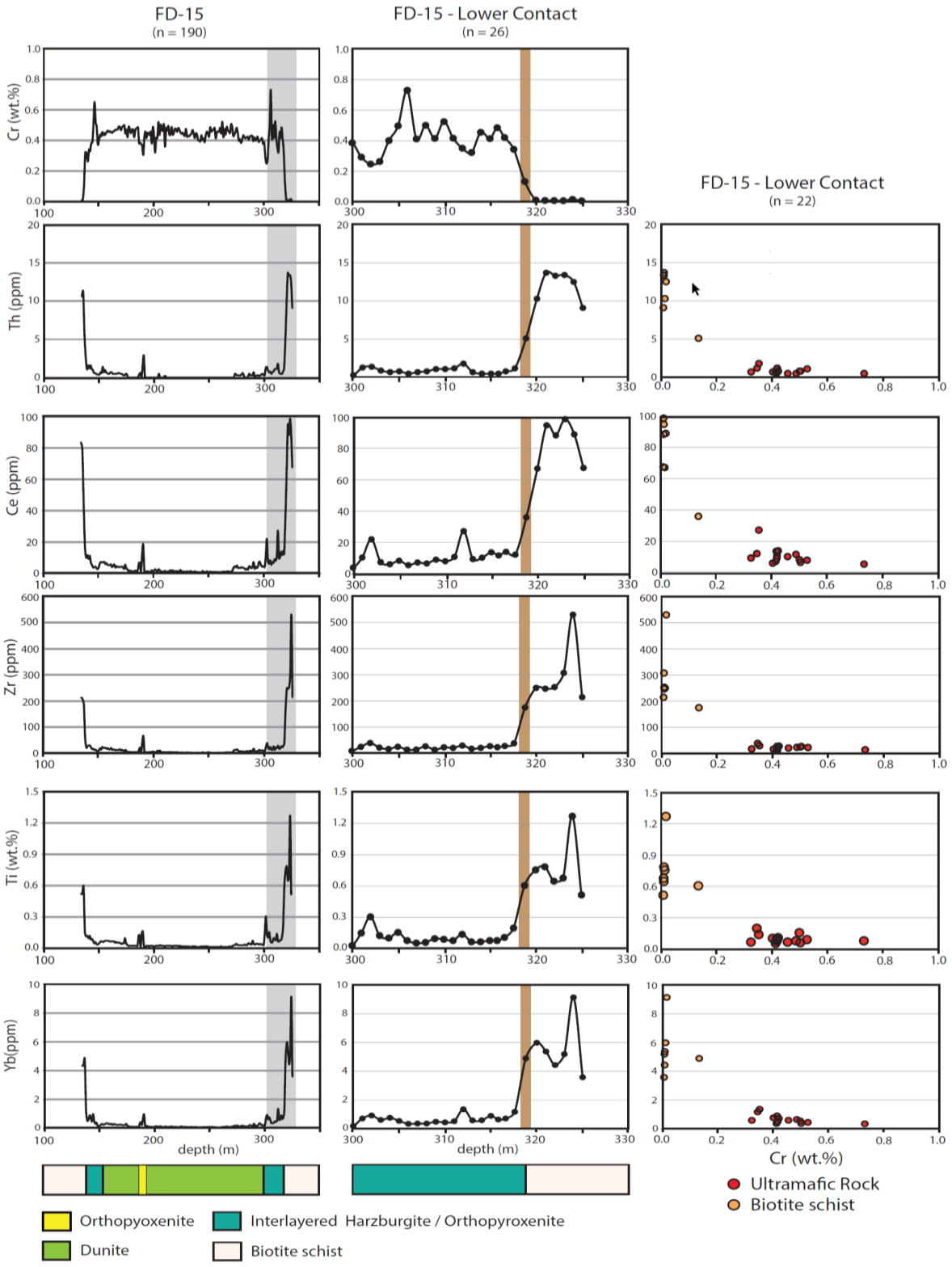

Figure 21. Selected trace elements in drill hole FD-15 of the Mamão intrusion. The left side diagrams show the strip log of the drill hole and its Cr, Th, Ce, Zr, Ti and Yb geochemical results, while the central plot shows a detail of the lower contact zone of the drill hole (lower 25 analyses). The gray shaded area in the left diagrams show the location of the interval detailed in the central diagrams. The brown shaded heavy lines in the central diagrams show the location of the contact between the ultramafic intrusion and country rocks. The plots of Cr vs Th, Ce, Zr, Ti and Yb are shown in the right-side diagrams for samples of the lower contact zone (lower 22 analyses). Data from Anglo American internal reports. See Table 2 for representative whole rock analyses of ultramafic rocks and biotite schists from the Mamão intrusion.

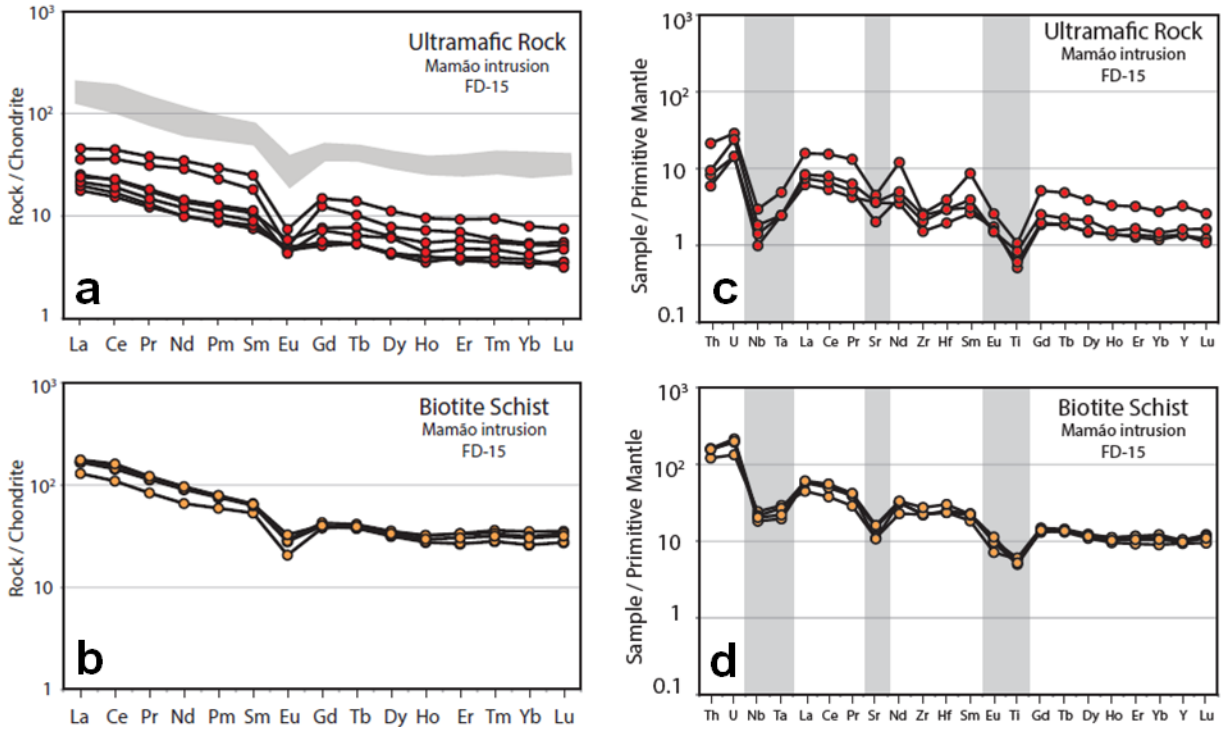

Figure 22. Trace element patterns for rocks of the drill hole FD-15 of the Mamão intrusion. a) and b) chondrite normalized REE patterns. c) and d) Primitive mantle-normalized incompatible element patterns See Table 2 for whole rock analyses. Normalization data from Sun and McDonough (1989).

Different styles of magmatic Ni–Cu-PGE sulfide mineralization occur in the Morro Sem Boné, Morro do Leme and satellite intrusions. They are grouped into three main styles: (1) contact-type; (2) stratabound-type; and (3) conduit-hosted, represented in simplified conceptual geological models in Fig. 24.

Contact-type or basal stratabound mineralization (Fig. 24a) is illustrated by Ni–Cu sulfides intersected in the Morro do Leme intrusion at the lower contact of the ultramafic intrusion with country rocks (Section B in Figs. 16 and 17). Disseminated sulfide mineralization occurs through 50 m of the lower contact zone, including a ~7 m net-textured zone at the contact with biotite schist host rocks. Contact-type Ni–Cu- PGE mineralization is a common feature of many mafic-ultramafic intrusions including those associated with the Duluth Complex, USA (see Ripley, 2014, and references therein), the East Bull Lake, Canada (e.g., Peck et al., 2001) and Platreef, South Africa (e.g., McDonald and Holwell, 2011). The location of sulfide mineralization at or near the basal contact of the host unit suggests that the sulfides were emplaced at an early stage in the crystallization of the host mafic-ultramafic intrusion. In addition, the increase in the amount of sulfides toward the base is interpreted as the result of gravitational settling of a dense immiscible sulfide liquid, possibly during the flow of the mafic-ultramafic magma at the lower portion of the intrusion (e.g., Lesher, 2019).

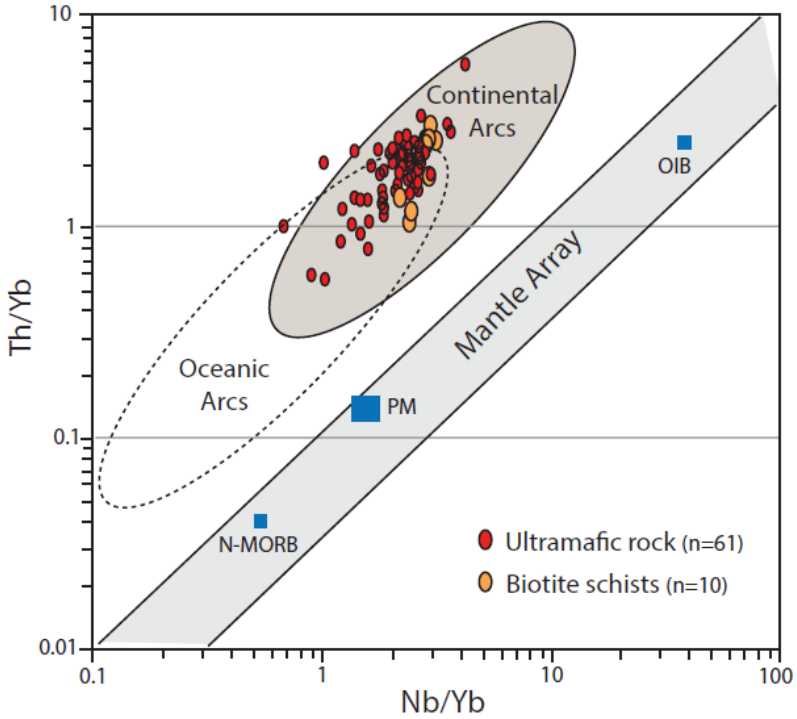

Figure 23. Plot of Nb/Yb versus Th/Yb for samples of ultramafic rocks and country rocks from the Mamão intrusion (drill hole FD-15). The plot includes all analyzed samples of biotite schist country rocks (n = 10) and samples of ultramafic rocks with higher contents of Nb, Yb and Th (≫ lower detection limits). The fields for continental arcs, oceanic arcs, normal mid-ocean ridge basalts (N-MORB), ocean-island basalt (OIB), primitive mantle composition (PM) and mantle array are included (after Pearce, 2008).

Stratabound-type mineralization (Fig. 24b) is illustrated by Ni–Cu sulfides intersected within the cumulate pile in the Morro do Leme (Section A in Figs. 16 and 17) and MSB (Figs. 5 and 6b) intrusions. Disseminated sulfides with very minor (i.e., few cm thick) net-textured and massive intersections occur through 80 m of mainly homogeneous dunite in drill hole FD-06 in the MSB, as well as disseminated sulfides through 20 m of homogeneous dunite in drill hole FD-19 in the Morro do Leme intrusion. Barren and mineralized dunites have the same mineralogy and texture in both intrusions, without any distinctive feature associated with the onset of sulfide mineralization. Stratabound mineralization within the internal portion of intrusions indicate that the sulfides were emplaced at an intermediate stage in the crystallization of the host unit. Stratabound-type mineralization is common in mafic-ultramafic intrusions including the Santa Rita deposit in the Mirabela Complex in Brazil (Barnes et al., 2011), the Dumont Sill in Canada (e.g., Brugmann et al., 1990) and the Luanga Complex in Brazil (e.g., Mansur et al., 2020). Although economic Ni–Cu sulfide deposits rarely occur as stratabound zones located within the main cumulus sequence in mafic-ultramafic intrusions, the Santa Rita deposit provides a high-tonnage example of this style of mineralization.

Conduit-hosted mineralization (Fig. 24c) is illustrated by Ni–Cu sulfides intersected in the thin (~140 m thick) and very elongated Mamão intrusion (Figs. 11b and 12) in this study, interpreted as a magma conduit. Disseminated sulfides occur as thin intersections (<5 m thick) located at the upper and lower margins of the conduit, following the symmetrically zoned elongated structure. Analogous rock types and differentiation trend observed in the contact zone of the interpreted conduit-hosted Mamão intrusion, and the contact-type basal portion of the Morro do Leme intrusion suggests that they are both linked to similar differentiation processes and parental magmas. Sulfide mineralization restricted to the margins suggests that sulfides were emplaced at an early stage in the evolution of the conduit system. This suggestion favors a model for sulfide liquid saturation, possibly due to assimilation of sulfide-bearing country rocks, at the initial stages of magmas flowing in the conduit followed by their concentration along the conduit margins. There is a consensus of the preferential localization of Ni–Cu-PGE deposits within magma conduit systems (e.g., Barnes and Robertson, 2019; Lesher, 2019), with the spectrum of conduit geometries associated with large and high-grade deposits summarized by Barnes et al. (2016). Prolonged or multiple events of magma flow within magma conduits provides a favorable environment for assimilation of sulfur-bearing country rocks, for reaction of transported sulfide melts with large volumes of magma leading to high ore tenors, as well as physical traps for concentration of sulfide melts (e.g., Barnes et al., 2016). The majority of the large and high-grade intrusion-hosted Ni–Cu-PGE deposits occur in magma conduits, including the deposits in the Noril'sk-Talnakh field, Russia, Jinchuan, China and Voisey's Bay, Canada (Barnes et al., 2016; and references therein). Although not all conduit systems are mineralized or host high-grade deposits (e.g., Limoeiro deposit consists mainly of disseminated sulfides within one specific conduit that belongs to a system of multiple magma pathways; Mota-e-Silva et al., 2013; 2015), the interpretation of a mineralized conduit closely associated with mineralized larger intrusions provides further evidence for a complex transport network of primitive magma through the crust in the region investigated in this study.

The generation of Ni–Cu-PGE sulfide deposits is dependent on the host magma becoming sulfide saturated and segregating a large amount of immiscible sulfides. Although sulfide saturation can be attained by several processes, it is now accepted that externally derived sulfur has been involved in the formation of many Ni–Cu-PGE sulfide deposits (e. g., Ripley and Li, 2013; Lesher, 2017). The abundance of disseminated and massive sulfides hosted within country rocks of the ultramafic intrusions, together with geochemical evidence for assimilation of crustal rocks by their high-MgO parental magma, suggest an external source of sulfur. The country rock

sulfides are composed mainly of pyrrhotite and pyrite, consistent with the negligible amounts of Ni, Cu, Zn and PGE in their whole-rock composition (e.g., Fig. 13). Because the solubility of sulfide in silicate melts is very low, the assimilation of abundant sulfide-rich country rocks should have generated an initially Ni–Cu-PGE-poor and Fe-rich sulfide xenomelt (Lesher, 2017), that may become enriched in Ni, Cu and PGE through reaction with the mafic-ultramafic magma. The extremely low contents of Ni, Cu, Pt and Pd of the sulfide mineralization in the southernmost tip of the MSB intrusion (Fig. 10; drill hole FD-01) is likely to represent compositions close to sulfide xenomelts. On the other hand, sulfide mineralization with relatively higher contents of Ni, Cu, Pt and Pd intersected toward the interior of the MSB (Fig. 10; drill hole FD-06) would indicate xenomelts that were upgraded through interaction with the mafic-ultramafic magma. The model of an immiscible sulfide xenomelts resulting from melting sulfide-rich country rocks followed by dynamic upgrading through interaction with the magma (e.g., Lesher and Campbell, 1993; Lesher, 2017) is consistent with our results. Sulfur isotope data of sulfides from the ultramafic intrusions and country rocks may be used to test this model in future studies.

The Ni–Cu-PGE sulfide mineralization of the ultramafic intrusions in this study are mainly disseminated without significant zones of massive sulfides. In addition, low contents of Ni, Cu and PGE indicate generally low tenors. These features indicate that optimal conditions for dynamic upgrade of metal contents (i.e., high R factors) and mechanical concentration of sulfides (i.e., high sulfide/silicate ratios) were not attained in the sulfide mineralization so far intersected in the ultramafic intrusions. Preliminary estimates of Ni, Cu and Pt + Pd tenors for contact-type sulfide mineralization of the Morro do Leme intrusion are 6.5 wt%, 2.0 wt% and 3 ppm, respectively. These values were calculated by linear regression (Fig. 18, drill hole FD-22) and provide the current estimate for metal tenors of the ultramafic intrusions. These range of values, the highest among the sulfide mineralization intersected in the ultramafic intrusions, indicate moderate tenors comparable with those from some world-class Ni–Cu-PGE deposits (e.g., Barnes and Lightfoot, 2005). Although the calculated Ni tenor is slightly overestimated due to an additional amount of Ni hosted in silicates in our whole-rock analyses, the high Ni/Cu ratio (~3.2) is consistent with a high-MgO parental magma (e.g., Barnes and Lightfoot, 2005). The Pt/Pd ratios of different styles of sulfide mineralization from the three investigated intrusions are ~1, consistent with their origin from parental magmas with close compositions.

Our results indicate that high-MgO ultramafic intrusions emplaced into a stratigraphic level with abundant S-rich sediments (Fig. 24), providing a scenario where mantle-derived magmas flowing from conduits to staging magma chambers have plenty of opportunity to interact and

assimilate crustal sulfur. This scenario is consistent with the abundance of different styles of Ni–Cu-PGE mineralization with variable tenors. The wide range of tenors, from moderate to values close to the expected sulfide xenomelt (i.e., very low Ni, Cu and PGE), may result from varying efficiency of equilibration of sulfides incorporated from the country rocks. Satellite intrusions with Ni depleted olivines is also consistent with a interconnected networks of conduits, sills and staging chambers, indicating that sulfides removed Ni-(Cu-PGE) during magma transport through the crust.

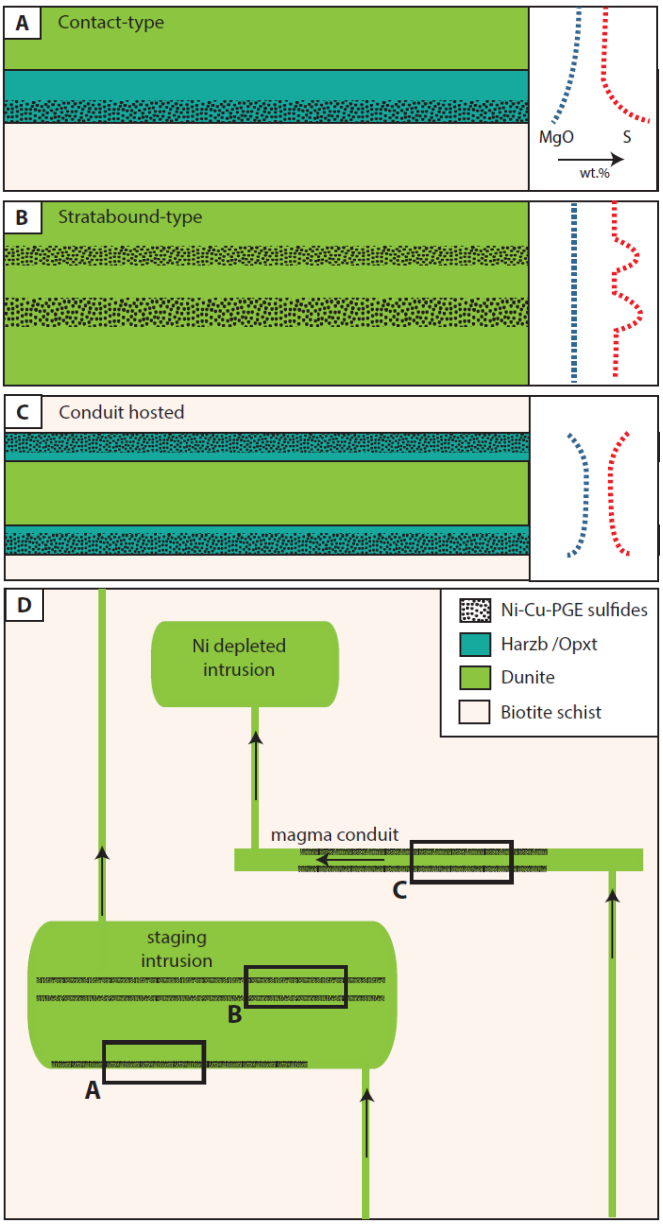

Figure 24. Schematic model for the different styles of Ni–Cu-PGE sulfide mineralization and the emplacement of the ultramafic intrusions. a) Contact-type based on mineralized intersection in drill hole FD-22 (Figs. 15 and 16). b) Stratabound-type based on mineralized intersections in drill holes FD-06 (Figs. 4 and 5) and FD-19 (Figs. 15 and 16). c) Conduit hosted based on mineralized intersections in drill holes FD-15 and FD-17 (Figs. 11 and 12). d) Sketch model for the emplacement of staging magma chambers (e.g., MSB and Morro do Leme intrusions), conduits (e.g., Mamão intrusion) and nickel depleted intrusions.

6.5 Tectonic setting and implications for exploration

The recognition of the close spatial association of Ni–Cu-PGE sulfide deposits and the margins of ancient Archean cratons (e.g., Begg et al., 2010; Maier and Groves, 2011; Barnes et al., 2016), together with the indication that orogenic settings of different ages host magmatic nickel sulfides (e.g., Li et al., 2012; Song et al., 2011; Maier et al., 2016), are important recent developments for regional targeting criterion. This suggests that several orogenic belts and/or craton margins may be more prospective than previously thought. Recent discoveries of Ni–Cu-PGE sulfide deposits closely associated with craton margins and/or orogenic settings in Brazil (e.g., Santa Rita deposit; Barnes et al., 2011; Limoeiro deposit; Mota-e-Silva et al., 2013; Caboclo dos Mangueiros deposit; Matos and Ferreira Filho, 2018; Luanga deposit; Mansur et al., 2020) provide further support for this suggestion.

The MSB, Morro do Leme, and satellite intrusions are located in the Guaporé Suture Zone, a Mesoproterozoic paleo-plate boundary in the southwestern margin of the Amazonian craton (e.g., Rizzotto et al., 2013). This suture is interpreted as the result of an accretional-collisional orogeny by oceanic plate subduction between 1.47-1.43 Ga. (Rizzotto and Hartmann, 2012; Rizzotto et al., 2013). Previous studies considered the Morro Sem Boné, and Morro do Leme intrusions as part of an ophiolitic sequence obducted during the collision (Rizzotto and Hartmann, 2012). As previously discussed in this study, field relations rule out the tectonic emplacement of the ultramafic intrusions as tectonic slices of ophiolites. In addition, field and geochemical evidence indicate that high-MgO magmas intruded into a volcanic-sedimentary sequence. Although the absolute age of the ultramafic intrusions is not known, a relative age is constrained by field relation of dated granitoides (Anglo American internal reports). The ultramafics are intrusive into synorogenic tonalites in the Morro do Leme intrusion (U–Pb zircon ages of 1454 ± 11 Ma and 1452 ± 2.9 Ma) and crosscut by granitic plutons in the Morro Sem Boné intrusion (U–Pb zircon ages of 1449 ± 7.4 Ma and 1436 ± 7 Ma), indicating a relatively short time span for mafic-ultramafic and granitic-tonalitic magmatism. These ages are consistent with the timeframe of the orogeny associated with the Guaporé suture zone indicated by Rizzotto and Hartmann (2012) and Rizzotto et al. (2013).

Although age does not appear to be an important control on the genesis of Ni–Cu-PGE deposits (e.g., Lesher, 2019), and deposits originated throughout most of the geological time (Naldrett, 2010; Maier et al., 2011), major deposits cluster at specific ages: ~2.7 Ga (Neoarchean komatiites in various continents), 2.0–1.8 Ga (Pechenga, Thompson, Raglan, Santa Rita), 1.4–

1.3 Ga (Kabanga, Voisey's Bay), 1.1 Ga (Duluth, Eagle, Nebo-Babel), 0.82 Ga (Jinchuan) and 0.3–0.25 Ga (Noril'sk, NW China) (partially based on Maier and Groves, 2011). The relative age of the ultramafic intrusions (~1.45 Ga) is close to the age of the 26 Mt at 2.6% Ni Kabanga deposit in Tanzania (1403 ± 14 Ma; Maier et al., 2011), both of them associated with abundant mafic-ultramafic intrusions within orogenic belts.

The Morro Sem Boné, Morro do Leme, and satellite intrusions share several compositional features suggesting that they belong to a cogenetic belt of mafic-ultramafic intrusions. Important common characteristics include: (1) abundance of olivine + chromite cumulates, (2) the same crystallization sequence dominated by olivine, orthopyroxene and chromite cumulates, (3) dunites with very high MgO content and Mg#, (4) the same styles of Ni–Cu-PGE sulfide mineralization with similar Pt/ Pd ratios (~1). The belt of ultramafic intrusions extends for at least 50 km (Fig. 2), and possibly more than 200 km considering the NNW and SSE extension of covered magnetic anomalies and scattered occurrences of mafic-ultramafic rocks beyond the area investigated in this study (Fig. 1).

7. Conclusions

Our study characterizes a large belt of Ni–Cu-PGE sulfide mineralized ultramafic intrusions in the southwestern margin of the Amazonian Craton. Contrary to what was previously suggested, field relations and geochemical results suggest that these ultramafic bodies are not tectonic slices of ophiolites. They are interpreted as intrusions of high-MgO magmas into a volcanic-sedimentary sequence emplaced along a suture zone during a Mesoproterozoic orogeny. This study suggests that ultramafic intrusions belong to a complex magma transport network of primitive magma through the crust, where larger intrusions (e.g., Morro Sem Boné, Morro do Leme) represent the staging magma chambers, while smaller intrusions (e.g., Mamão) the magma conduits of this system. These ultramafic intrusions have several features commonly used as guidelines for regional exploration for Ni–Cu-(PGE) magmatic deposits, including:

(1) abundant olivine- and chromite-rich mafic-ultramafic rocks.
(2) primitive MgO-rich parental magmas.
(3) variable magmatic structures indicative of dynamic magmatic systems.
(4) regional association with a major crustal scale structure (suture zone).
(5) emplacement into sulfide bearing country rocks.
(6) field and lithogeochemical evidence of assimilation of country rocks.

(7) different styles and abundance of Ni–Cu-PGE sulfide mineralization.
(8) depleted Ni contents of olivines.

This up to 200 km belt of poorly outcropping and underexplored mafic-ultramafic intrusions provides an additional opportunity for exploration for Ni–Cu-PGE sulfides in cratonic margins in Brazil. Potential exists for high-grade massive sulfide deposits in unexposed small magma conduits.

Funding

This study was financed in part by the Coordenação de Aperfeiçoamento de Pessoal de Nível Superior - Brasil (CAPES) - Finance Code 001.

This study was supported and funded by Anglo American. Analytical facilities at the Instituto de Geociências of the University of Brasília (UnB) provided additional support for this research.

Authors' contributions

Jomar Stabili Farias: Conceptualization, Investigation, Methodology, Formal analysis, Visualization, Writing – original draft.

Cesar F. Ferreira Filho: Conceptualization, Supervision, Investigation, Methodology, Formal analysis, Visualization, Writing – review & editing.

Declaration of competing interest

The authors declare that they have no known competing financial interests or personal relationships that could have appeared to influence the work reported in this paper.

Acknowledgements

This study was financed in part by the Coordenação de Aperfeiçoamento de Pessoal de Nível Superior - Brasil (CAPES) - Finance Code 001. This study was also supported and funded by Anglo American. We are grateful to Romero Souza Queiroz (Country Manager Exploration Brazil) and Geraldo Sarquis Dias (Geoscience Manager) for permission to publish this study. Analytical facilities at the Instituto de Geociências of the University of Brasília (UnB) provided

additional support for this research. Cesar F. Ferreira Filho is a Research Fellow of CNPq (Conselho Nacional de Desenvolvimento Científico e Tecnológico - Processo 302465/2019-7) and acknowledges the continuous support through research grants and scholarships for the “Metalogênese de Depósitos Associados ao Magmatismo Máfico-Ultramáficos" Research Group since 1996. This study was financed in part by the Coordenação de Aperfeiçoamento de Pessoal de Nível Superior – Brasil (CAPES). Also, a special thanks goes to the Anglo American team (geologists and support staff) for their successful exploration for Ni–Cu-PGE deposits in the Guaporé region in the last 30 years. Special acknowledgement goes to Vanderlei Farias (Anglo American exploration geologist) for his enthusiasm and dedication to this project. This study is part of the first author’s (Jomar Stabili de Farias) M.Sc. project at the Instituto de Geociências (UnB). The authors thank two anonymous reviewers for their constructive and helpful reviews, and Editor-in-Chief Dr. Andres Folguera for carefully handling the manuscript.

Appendix A. Supplementary data

Supplementary data to this article can be found online at
https://doi.org/10.1016/j.jsames.2021.103240

References

Barnes, S.J., 1986. The effect of trapped liquid crystallization on cumulus mineral compositions in layered intrusions. Contrib. Mineral. Petrol. 93, 524–531.

Barnes, S.J., Cruden, A.R., Arndt, N., Saumur, B.R., 2016. The mineral system approach applied to magmatic Ni–Cu–PGE sulphide deposits. Ore Geol. Rev. 76, 296–316.

Barnes, S.J., Osborne, G.A., Cook, D., Barnes, L., Maier, W.D., Godel, B., 2011. The Santa Rita nickel sulfide deposit in the Fazenda Mirabela intrusion, Bahia, Brazil: geology, sulfide geochemistry, and genesis. Econ. Geol. 106, 1083–1110.

Barnes, S.J., Robertson, J.C., 2019. Time scales and length scales in magma flow pathways and the origin of magmatic Ni–Cu–PGE ore deposits. Geoscience Frontiers 10 (1), 77–87.

Barnes, S.-J., Lightfoot, P.C., 2005. Formation of magmatic nickel-sulfide ore deposits and processes affecting their copper and platinum-group element contents. In: Hedenquist, J.W., Thompson, J.F.H., Goldfarb, R.J., Richards, J.P. (Eds.), Economic Geology 100th Anniversary, ume, pp. 179–213.

Begg, G.C., Hronsky, J.A.M., Arndt, N.T., Griffin, W.L., O'Reilly, S.Y., Hayward, N., 2010. Lithospheric, cratonic and geodynamic setting of Ni–Cu–PGE sulfide deposits. Econ. Geol. 105, 1057–1070.

Bettencourt, J.S., Tosdal, R.M., Leite, W.B., Payolla, B.L., 1999. Mesoproterozoic rapakivi granites of the Rondônia Tin Province, southwestern border of the Amazonian craton, Brazil — I . Reconnaissance U-Pb geochronology and regional implications. Precambrian Res. 95, 41–67.

Brugmann, G.E., Naldrett, A.J., Duke, J.M., 1990. The platinum-group element distribution in the Dumont sill, Quebec. Implications for the formation of Ni-sulfide mineralization. Mineral. Petrol. 42, 97–119.

Bucher, K., Grapes, R., 2011. Petrogenesis of Metamorphic Rocks, eighth ed. Springer, Berlin, p. 428.

Campbell, I.H., 1985. The difference between oceanic and continental tholeiites: a fluid dynamic explanation. Contrib. Mineral. Petrol. 91, 37–43.

Eales, H.V., Cawthorn, R.G., 1996. The Bushveld complex. In: Cawthorn, R.G. (Ed.), Layered Intrusions (Developments in Petrology 15). Elsevier, Amsterdam, The Netherlands, pp. 181–229.

Ferreira Filho, C.F., Nilson, A.A., Naldrett, A.J., 1992. The Niquelândia Mafic–Ultramafic Complex, Goias, Brazil: a contribution to the ophiolite X stratiform controversy based on new geological and structural data. Precambrian Res. 59, 125–143.

Ferreira Filho, C.F., Pimentel, M.M., Araujo, S.M., Laux, J.H., 2010. Layered intrusions and volcanic sequences in Central Brazil: geological and geochronological constraints for Mesoproterozoic (1.25 Ga) and Neoproterozoic (0.79 Ga) igneous associations. Precambrian Res. 183, 617–634.

Latypov, R.M., 2003. The origin of basic-ultrabasic sills with S-, D-, and I-shaped compositional profiles by in situ crystallization of a single input of phenocryst poor parental magma. J. Petrol. 44 (9), 1619–1656.

Layton-Matthews, D., Lesher, C.M., Burnham, O.M., Hulbert, L., Peck, D.C., Golightly, J. P., et al., 2010. In: Exploration for Komatiite-Associated Ni–Cu–(PGE) Mineralization in the Thompson Nickel Belt, Manitoba, vol. 15. Special Publication Society of Economic Geologists (U.S.), pp. 513–538.

Lesher, C.M., 2007. In: Ni-Cu-(PGE) Deposits in the Raglan Area, Cape Smith Belt, New Quebec, vol. 5. Geological Survey of Canada and Mineral Deposits Division of the Geological Association of Canada, Special Publication, pp. 351–386.

Lesher, C.M., 2017. Roles of residues/skarns, xenoliths, xenocrysts, xenomelts, and xenovolatiles in the genesis, transport, and localization of magmatic Fe-Ni-Cu-PGE sulfides and chromite. Ore Geol. Rev. 90, 465–484.

Lesher, C.M., 2019. Up, down, or sideways: emplacement of magmatic Fe–Ni–Cu–PGE sulfide melts in large igneous provinces. Can. J. Earth Sci. 56, 756–773.

Lesher, C.M., Barnes, S.J., 2008. Komatiite-associated Ni-Cu-PGE deposits. In: Arndt, N. T. (Ed.), Komatiite: Cambridge. Cambridge University Press, pp. 295–327.

Lesher, C.M., Campbell, I.H., 1993. Geochemical and fluid dynamic modeling of compositional variations in Archean komatiite-hosted nickel sulfide ores in Western Australia. Econ. Geol. 88, 804–816.

Li, C.S., Zhang, M.J., Fu, P., Qian, Z., Hu, P.Q., Ripley, E.M., 2012. The Kalatongke magmatic Ni-Cu deposits in the Central Asian orogenic belt, NW China: product of slab window magmatism? Miner. Deposita 47, 51–67.

Maier, W.D., Groves, D.I., 2011. Temporal and spatial controls on the formation of magmatic PGE and Ni–Cu deposits. Miner. Deposita 46, 841–857.

Maier, W.D., Peltonen, P., Livesey, T., 2011. The ages of the Kabanga North and Kapalagulu intrusions, western Tanzania: a reconnaissance study. Econ. Geol. 102, 47–154.

Maier, W.D., Smithies, R.H., Spaggiari, C., Barnes, S.-J., Kirkland, C., Yang, S., Lahaye, Y., Kiddie, O., Macrae, C., 2016. Petrogenesis and Ni–Cu sulphide potential of mafic–ultramafic rocks in the mesoproterozoic fraser zone within the albany–fraser orogen, western Australia. Precambrian Res. 281, 27–46.

McDonald, I., Holwell, D.A., 2011. Geology of the northern Bushveld Complex and the setting and genesis of the Platreef Ni–Cu–PGE deposit. In: Li, C., Ripley, E.M. (Eds.), Magmatic Ni–Cu and PGE Deposits: Geology, Geochemistry, and Genesis, vol. 17, pp. 297–327.

Mansur, E.T., Ferreira Filho, C.F., 2016. Magmatic structure and geochemistry of the Luanga Mafic-Ultramafic Complex: further constraints for the PGE-mineralized magmatism in Carajas, Brazil. Lithos 266, 28–43.

Mansur, E.T., Ferreira Filho, C.F., Oliveira, D.P.L., 2020. The Luanga deposit, Carajás Mineral Province, Brazil: different styles of PGE mineralization hosted in a medium size layered intrusion. Ore Geol. Rev. 118 https://doi.org/10.1016/j. oregeorev.2020.103340.

Marques, J.C., Ferreira Filho, C.F., 2003. The chromite deposits of the ipueira-medrado sill, Bahia, Brazil. Econ. Geol. 98, 87–108.

Matos, V.B.M., Ferreira Filho, C.F., 2018. The Caboclo dos Mangueiros deposit: Ni-Cu sulfide mineralization hosted by an ultramafic intrusion in the northern edge of the São Francisco craton, Brazil. Econ. Geol. 113, 1525–1552.

Matos, R., Teixeira, W., Geraldes, M.C., Bettencourt, J.S., 2009. Geochemistry and Nd-Sr isotopic signatures of the pensamiento granitoid complex, Rondonian-San Ignacio province, eastern precambrian shield of Bolivia: petrogenetic constraints for a mesoproterozoic magmatic arc setting. Geol. Usp. S´erie Científica 9 (2), 89–117.

Mota-e-Silva, J., Ferreira Filho, C.F., Della Giustina, M.E.S., 2013. The Limoeiro deposit: Ni–Cu–PGE sulfide mineralization hosted within an ultramafic tubular magma conduit in the Borborema Province: Northeast Brazil. Econ. Geol. 108, 1753–1771.

Mota-e-Silva, J., Prichard, H.M., Ferreira Filho, C.F., Fisher, P.C., McDonald, I., 2015. Platinum-group minerals in the Limoeiro Ni–Cu–(PGE) sulfide deposit, Brazil: the effect of magmatic and upper amphibolite to granulite metamorphic processes on PGM formation. Miner. Deposita 50 (8), 1007–1029.

Naldrett, A.J., 2004. Magmatic Sulphide Deposits: Geology, Geochemistry and Exploration. Springer-Verlag, Berlin, p. 728.

Naldrett, A.J., 2010. Secular variation of magmatic sulfide deposits and their source magmas. Econ. Geol. 105, 669–688.

Naldrett, A.J., Cabri, L.J., 1976. Ultramafic and related mafic rocks: their classification and genesis with special reference to the concentration of nickel sulfides and platinum-group elements. Econ. Geol. 71, 1131–1158.

Passchier, C.W., Myers, J.S., Kroner, A., 1990. Field Geology of High Grade Gneiss Terrains. Springer, Berlin, p. 150.

Pearce, J.A., 2008. Geochemical fingerprinting of oceanic basalts with applications to ophiolite classification and the search for Archean oceanic crust. Lithos 100, 4–48.

Peck, D.C., Keays, R.R., James, R.S., Chubb, P.T., Reeves, S.J., 2001. Controls on the formation of contact-type platinum-group element mineralization in the East Bull Lake intrusion. Econ. Geol. 96, 559–581.

Pedreira, A.J., Bahia, R.N.C., 2000. Sedimentary Basins of Rondônia state, Brazil: response to the geotectonic evolution of the Amazonic craton. Rev. Bras. Geociencias 30, 477–480.

Ripley, E.M., 2014. Ni-Cu-PGE mineralization in the partridge river, south Kawishiwi, and Eagle intrusions: a review of contrasting styles of sulfide-rich occurrences in the midcontinent rift system. Econ. Geol. 109, 309–324.

Ripley, E.M., Li, C., 2013. Sulfide saturation in mafic magmas is external sulfur required for magmatic Ni–Cu–(PGE) ore genesis? Econ. Geol. 108, 45–58.

Rizzotto, G.J., 2010. Geologia e Recursos Minerais da Folha Pimenteiras (SD.20-X-D). Sistema de Informação Geográfica-SIG. CPRM, Rondônia, Brazil, p. 136.

Rizzotto, G.J., Bettencourt, J.S., Teixeira, W., Pacca, I.G., D'Agrella-Filho, M.S., Vasconcelos, P.M., Basei, M.A.S., Onoe, A.T., Passarelli, C.R., 2002. Geologia e geocronologia da Suite Metamórfica Colorado e suas encaixantes, SE de Rondônia: implicaç˜oes para a evoluç˜ao Mesoproterozóico do SW do Craton Amazônico. Revista do Instituto de Geociências USP, S´erie Científica 2, 41–55.

Rizzotto, G.J., Hartmann, L.A., 2012. Geological and geochemical evolution of the Trincheira Complex, a Mesoproterozoic ophiolite in the southwestern Amazon craton, Brazil. Lithos 148, 277–295.

Rizzotto, G.J., Santos, J.O.S., Hartmann, L.A., Tohver, E., Pimentel, M.M., McNaughton, N.J., 2013. The Mesoproterozoic Guapor´e suture in the SW Amazonian Craton: geotectonic implications based on field geology, zircon geochronology and Nd-Sr isotope geochemistry. J. S. Am. Earth Sci. 48, 271–295.

Ruiz, A.S., 2005. Evoluç˜ao Geol´ogica Do Sudoeste Do Cr´aton Amazˆonico, Região Limítrofe Brasil-Bolívia-Mato Grosso. Unpublished PhD Thesis, Universidade Estadual Paulista (Brazil), p. 299.

Santos, S., Hartmann, L.A., Gaudette, H.E., Groves, D.I., Mcnaughton, N.J., Fletcher, I.R., 2000. A new understanding of provinces of the amazon craton based on integration of filed mapping and U-Pb geochronology and Sm-Nd geochronology. Gondwana Res. 3, 453–488.

Santos, J.O.S., Rizzotto, G.J., Potter, P.E., McNaughton, N.J., Matos, R.S., Hartmann, L. A., Chemale, F., Quadros, M.E.S., 2008. Age and autochthonous evolution of the Sunsás orogen in West amazon craton based on mapping and U-Pb geochronology. Precambrian Res. 165, 120–152.

Scandolara, J.E., Amorim, J.L., Rizzotto, G.J., Quadros, M.L.E.S., Bahia, R.B.C., 1999. Compartimentação tectônica-estratigráfica pré-cambriana de Rondônia: subsídios para os modelos evolutivos. In: Simpósio de Geologia da Amazônia, vol. 6. Boletim de Resumos Expandidos.

Scandolara, J.E., Correa, R.T., Fuck, R.A., Souza, V.S., Rodrigues, J.B., Ribeiro, P.S.E., Frasca, A.A.S., Saboia, A.M., Lacerda Filho, J.V., 2017. Paleo-Mesoproterozoic arcaccretion along the southwestern margin of the Amazonian craton: the Juruena accretionary orogen and possible implications for Columbia supercontinent. J. S. Am. Earth Sci. 73, 223–247.

Seat, Z., Beresford, S.W., Grguric, B.A., Waugh, R.S., Hronsky, J.M.A., Gee, M.A.M., Groves, D.I., Mathison, C.I., 2007. Architecture and emplacement of the Nebo-Babel gabbronorite-hosted magmatic Ni-Cu-PGE sulphide deposit, West Musgrave, Western Australia. Miner. Deposita 42, 551–581.

Siepierski, L., Ferreira Filho, C.F., 2020. Magmatic structure and petrology of the Vermelho complex, Caraj´as mineral province, Brazil: evidence for magmatic processes at the lower portion of a mafic-ultramafic intrusion. J. S. Am. Earth Sci. 102 https://doi.org/10.1016/j.jsames.2020.102700.

Song, X., Xie, W., Deng, Y., Crawford, A.J., Zheng, W., Zhou, G., Deng, G., Cheng, S., Li, J., 2011. Slab break-off and the formation of Permian mafic-ultramafic intrusions in southern margin of central Asian orogenic belt, Xinjiang, NW China. Lithos 127, 128–143.

Sun, S.S., McDonough, W.F., 1989. Chemical and isotopic systematics of oceanic basalts: implications for mantle composition and processes. In: Saunders, A.D., Norry, M.J. (Eds.), Magmatism in Oceanic Basins, vol. 42. Geological Society of London Special Publication, pp. 313–345.

Tang, Y.J., Zhang, H.F., Ying, J.F., Su, B.X., 2013. Widespread refertilization of cratonic and circum-cratonic lithospheric mantle. Earth Sci. Rev. 118, 45–68.

Williams, D.A., Kerr, R.C., Lesher, C.M., 1998. Emplacement and erosion by Archean komatiite lava flows at Kambalda: revisited. J. Geophys. Res., Solid Earth 103, 27533–27549.

Wilson, A.H., 1982. The geology of the Great ‘Dyke’, Zimbabwe: the ultramafic rocks. J. Petrol. 23, 240–292.

Wilson, A.H., 2012. A chill sequence to the Bushveld complex: insight into the first stage of emplacement and implications for the parental magmas. J. Petrol. 53, 1123–1168.